WARWICK
THE UNIVERSITY OF WARWICK

A Thesis Submitted for the Degree of PhD at the University of Warwick

Permanent WRAP URL:
http://wrap.warwick.ac.uk/92352

Copyright and reuse:
This thesis is made available online and is protected by original copyright.
Please scroll down to view the document itself.
Please refer to the repository record for this item for information to help you to cite it.
Our policy information is available from the repository home page.

For more information, please contact the WRAP Team at: wrap@warwick.ac.uk

warwick.ac.uk/lib-publications

Polymersome Modification and Functionalisation via Particle-Bilayer Interactions

by

Rong Chen

A thesis submitted in partial fulfilment of the requirements for the degree of Doctor of Philosophy in Chemistry

University of Warwick, Department of Chemistry

Chapter 1 A review of vesicle functionalisation: Amphiphiles self-assembly, production techniques, bilayer modification and reinforcement

1.1 Self-assembly of amphiphiles in solution

Amphiphiles are often described as molecules that possess a dual hydrophobic-hydrophilic character. The hydrophobic tail is often one or two long alkyl chains, while the hydrophilic part is known to be ionic and commonly referred to as head group of the molecular structure. Amphiphiles come in a variety of forms, both naturally occurring phospholipids, such as phosphatidyl choline, which is the major component of biological membranes and can be obtained from a variety of readily available source, e.g. Soybeans or egg yolk, and the fully synthetic such as sodium dodecyl sulphate (SDS) or cetyltrimethylammonium bromide (CTAB), which has been widely used in commercial products, such as hair conditioner and facial cleanser. Amphiphilic molecules have gained considerable interest among scientists for not only its use as surfactants but also the potential applications and their microscopic morphologies in bulk and in aqueous solutions, which motivates the studies including those on self-assembly principles, theories, structures and functionalisation of the amphiphilic molecules. In aqueous solution amphiphiles undergo self-assembly in order to minimise energetically unfavourable hydrophobe/water interactions, which results in various morphologies. The factors that determine the nanostructures of these assemblies are influenced by the packing parameter, which is dependent on the dimensions of amphiphilic molecules.

Taking sodium dodecyl sulphate (SDS), one of the most widely used amphiphiles as an example, when this surfactant is dispersed in water, the SDS molecules aggregate into a globular structure, which the hydrophilic heads are in contact with the water, while the hydrophobic tails are shielded from the water to form a hydrophobic core; thus a so called micelles structure is formed with approximately 2-3 nm and contains around 100 molecules. The reverse structure is achievable when a non-polar solvent is

used instead of water, which hydrophilic heads gather in the centre of the structure and hydrophobic tails spread into the solvent.

However, micelle structure is only one of the nanostructures that amphiphilic molecules can assemble in solution. In order to study the self-assembly behaviour and its principle, a dimensionless "packing parameter", p, is defined in equation (1.1)[1]:

$$p = \frac{v}{a_o l_c}$$

Where v is the volume of the hydrophobic chains, a_o is the optimal area of the hydrophilic group, and l_c is the length of the hydrophobic tail. Therefore, the self-assembled morphology of a given molecule in a particular solvent can usually be predicted by the packing parameter. Generally, spherical micelles are favoured structure when p<1/3, whereas when the p is between 1/3 and 1/2 then the cylindrical rods can be expected. Enclosed membrane structures also known as vesicles, are formed when p is between 1/2 and 1. (Figure 1.1)[1, 2]

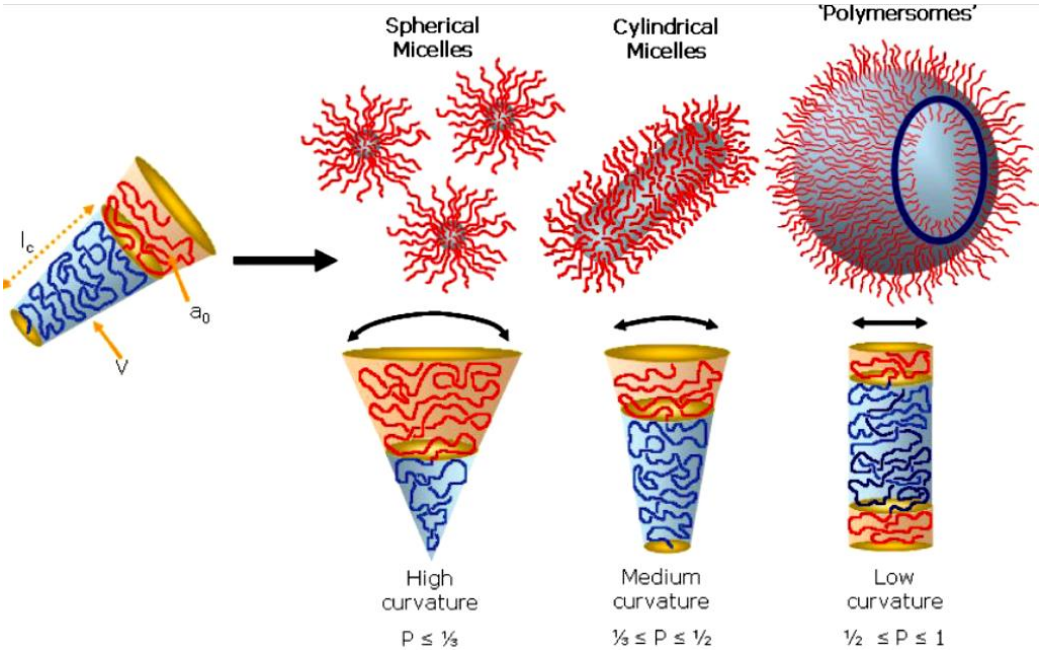

Figure 1.1 Various self-assembled structures formed by amphiphilic block copolymers in a block-selective solvent. The type of structure formed is due to the inherent curvature of the molecule, which can be estimated through calculation of its dimensionless packing parameter, p. [2]

1.2 Lipids vesicles

Vesicles that are formed from mainly phospholipids molecules, also known as liposomes, are arguably the most dominant and important structures that are present in nature because the arrangement of molecules that a bilayer forms are the fundament of all cell membranes. Despite the fact that the size and properties of membrane varied due to the differences of the membrane composition and the presence of functionalised molecules, biological membranes are generally composed of phospholipids, glycolipids, proteins, glycoproteins and cholesterol. In the early stage of the scientific research history, phospholipids were obtained from natural sources, such as egg or brain tissue. However, in present, scientists have developed a range of synthetic ways to obtain these molecules, which have the advantages of higher purity and productivities. Today, there is still much research continuing using phospholipids as a reliable and biocompatible system. Due to the relatively high fluidity and the structure of phospholipids, these amphiphilic molecules have high mobility in aqueous and self-assemble in a rapid rate, therefore bilayer aggregates and vesicles form spontaneously in aqueous conditions once the critical concentration has been reached. However, because of the specialised structure and the low molecular weight (less than 1 kilodalton) of phospholipids, liposomes are sensitive to change in concentration and pH and usually have a soft and flexible surface at ambient temperature. When using liposomes as nanocarriers, the thin bilayer shell can easily be broken by external forces, which results in unintended release of the inner content; or in other cases, the encapsulated substances can gradually diffuse across the bilayer as a result of high permeability for small molecules which caused by the low thickness and high fluidity of the lipid film.

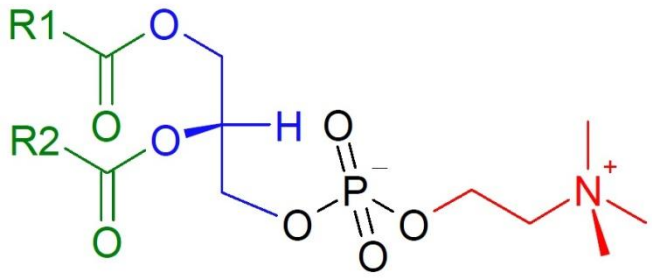

Figure 1.2. Phosphatidyl choline an example of a phosphoglyceride.

1.3 Polymer vesicles and self-assembly of block copolymers

Different structures can be obtained via self-assembly of amphiphilic polymeric molecules such as micelles, rods and vesicles, which are the result of hydrophilic and hydrophobic domains of molecules interacting with a given solvent, e.g. water, in a similar way as phospholipids. During the last two decades, chemists have designed more advanced molecules with amphiphilic properties, which can respond to changes including but not limited to solvent type, temperature, oxidant, pH, light or magnetic field adding a further dimension to the molecules, which expand the potential application of the assembled structures.

1.3.1 Polymeric micelles

A simple spherical micelle structure is formed when the hydrophilic part of the polymer molecule occupies much larger space than the hydrophobic part in aqueous media due to the fact that, with a packing parameter value less than a third, the curvature of the outer shell of each section formed by a polymer molecule limits the space for other molecules to occupy, which results in a core shell spherical structure with a spherical hydrophobic core surrounded by hydrophilic coronal chains.[3, 4] The size of spherical micelles is relatively smaller than other type of self-assembled aggregates due to the fact that the radius of the core cannot exceed the chain length in their planar zigzag configuration. [5] The spherical micelles can be considered as the starting morphology for other aggregates when preparing cylinder or vesicle solutions via solvent addition method. The hydrophilic coronas provide the solubility to the

micelles, while the hydrophobic cores provide a possible location for encapsulation of hydrophobic drugs [6-8] or fluorescence probes [8], and a range of other substances such as DNA or enzymes.[5, 7, 8] Therefore, spherical micelles have been studied extensively for application in drug delivery system and biological imaging.[5, 7] Moreover, complex micelles such as schizophrenic diblock copolymer micelles,[9] Janus micelles with two chemically distinct hemispheres,[10-12] and multicompartmental ‘hamburger’ micelles[13] have been developed and reported.

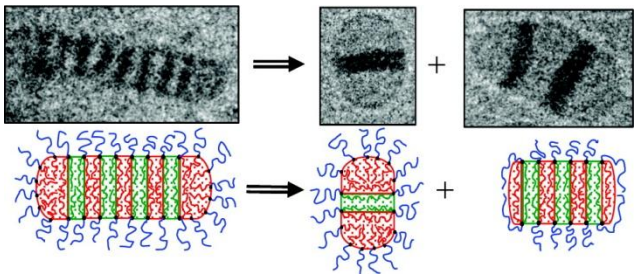

Figure 1.3 Schematic and Transmission electron micrographs of ‘hamburger’ micelles

1.3.2 Block copolymer cylindrical micelles (rods)

Worm-like micelles, formed from block copolymers, have been widely reported. Infinitely long cylinders are energetically favourable relative to shortened cylinders with incorporated end-defects. The packing parameter of this self-assembled structure has a very narrow window, which means that the polydispersity of the block copolymer that made for this structure plays an important role in the formation of defects such as end caps (more energetically favourable) and branch points (less favourable).[14] Literature reports of giant[15] and short worms,[16, 17] y-junction and end cap defects[18, 19], and even worm-like micellar networks demonstrate the increasing complexity associated with amphiphilic block copolymer self-assemblies.[2] Discher *et. al.* reported giant and flexible worm micelles self-assembled from degradable copolymer poly(ethylene oxide)-*block*-polycaprolactone. Such worm micelles spontaneously shorten to generate spherical micelles, triggered by polycaprolactone hydrolysis,[20] which show a very delicate relationship between micelles and cylinders. Also, it has been

reported that the secondary self-assembly of ABC triblock copolymer spherical micelles can, in specific conditions form giant segmented worm-like micelles.[21] Moreover, there have been reports of the selective formation of segmented,[22] toroidal,[23] and helical[24] cylindrical micelles from the triblock copolymers.

1.3.3 Block copolymer vesicles

Block copolymers that mimic lipid amphiphilicity can self-assemble into vesicles in dilute solution, which have been given the name "polymersomes". The investigation and formation of vesicles and other aggregates from block copolymers was initially led by the groups of Eisenberg[4, 25], Hammer and Disher.[26] Unlike phospholipids or other classical synthetic amphiphiles, polymer molecules are considerably much larger ranging from thousands to millions of grams per mol, which can be orders of magnitude greater than those of lipids. The physical characterisation of block copolymer vesicles has shown that these structures are more robust than their naturally occurring counterparts, which is attributed to its significant higher molecular weight. Membrane "toughness" or cohesive energy density for polymersomes taken as the integral of the tension with respect to the areal strain as given by the formula:

$$E \approx \frac{1}{2} K_a \alpha_c^2$$

It has been reported with a value of 2.2 mJ/m^2 compared with phospholipids at 0.05 – 0.5 mJ/m^2. Moreover, the membrane permeability can be affected by the thickness of the bilayer as well as the porosity. It has been shown that the permeability of polymeric membranes is at least 10 times less than phospholipids as a result of significant increase in thickness.

The first synthesised vesicle forming amphiphiles used asymmetric A-B block copolymers [26, 27], however, it has also been reported using A-B-A[28-31], A-B-C[32, 33] and A-B-C-A.[34] Block copolymers composed of polylactide, polyethyleneoxide and polycaprolactones have also become a popular choice due to the biocompatibility [35, 36] of these molecules.

1.4 Vesicle production techniques

A significant number of techniques have been developed for vesicle preparation from both lipid and amphiphilic polymer molecules. It is worth noting that, not all amphiphiles spontaneously form vesicles when dispersed in aqueous media. Furthermore, even if vesicles form spontaneously upon dispersion, it usually gives a polydisperse system of uni and multilamellar vesicles. Further processing protocols are applied for vesicle dispersions to improve the homogeneity of solutions. Scientist have developed different techniques for different types of amphiphilic molecules to prepare vesicle solution and in some cases, as the hydrophobic part of the amphiphiles is rigid at desired temperature without organic solvent presence, more than one solvents are used to provide extra fluidity therefore stability to the bilayer.

1.4.1 Bangham Method

This classical procedure was used firstly by Alec Bangham in his research work with vesicles and is well known as film hydration method and is most commonly employed with liposomes preparation.[37] It yields a broad size distribution of vesicles, which can be used directly or subjected to homogenisation processing, such as extrusion or sonication. It has also been demonstrated with polymeric surfactants, which has a relatively low glass transition temperature.[38]

Typically, the amphiphiles are dissolved in chloroform/methanol and then cast onto the surface of a curved glass, for example a glass jar, by evaporation of organic solvent under nitrogen flow or vacuum. Aqueous buffer, water or a sucrose solution is added after the sample is dried. Gentle shaking or vibration is applied to yield vesicles, which form spontaneously. In some cases, mild heat can be also applied to increase the fluidity of the chemicals. The action of the solvent and osmotic forces then lift amphiphiles formed film from the glass surface, which then driven by spontaneous curvature of the molecules and the packing parameter to form vesicles. This technique works less efficient for most block copolymers due to their poor fluidity and higher

film thickness as a result of their high molecular weight and high glass transition temperature.

1.4.2 Templated film hydration

This technique was developed based on classical film hydration and gives much better control in both size distribution and structure complexity. Ryan and co-workers have firstly reported this method for giant unilamellar vesicles formation (GUV). In their work, a plasma-cleaned gold coated silicon wafers were treated with photolithography under a TEM grid mask in order to fabricate a micron sized square feature patterned substrate. Then a PEO-PBO copolymer with a molecular weight of 2.3k, which prepared by anionic polymerisation, was spin-cast to generate films several hundred nanometres thick, followed by spontaneous dewetting process, which result in a collection of vesicles with sizes corresponding to the original TEM grid used.[39]

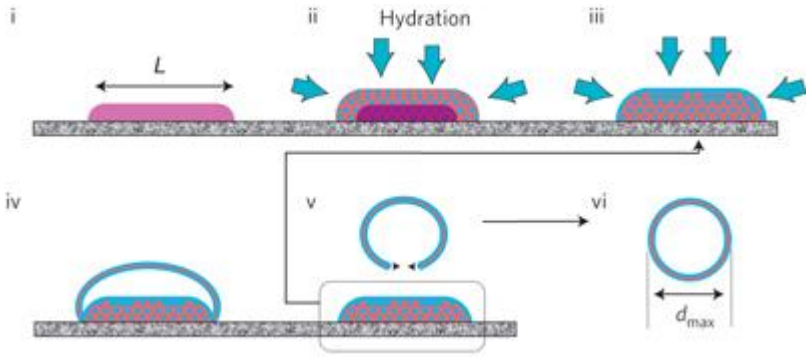

Figure1.4 Schematic representation of the controlled formation of vesicles: (i) Resulting drop profile following dewetting. (ii) Hydration resulting in microphase separation—hexagonal rod phase (blue: hydrophilic, red: hydrophobic). (iii) Further hydration at the surface resulting in surface lamellae and further internal phase separation. (iv) Expansion of exterior bilayer. (v) Detachment. (vi) Surface minimisation leading to closure and vesicle formation.[39]

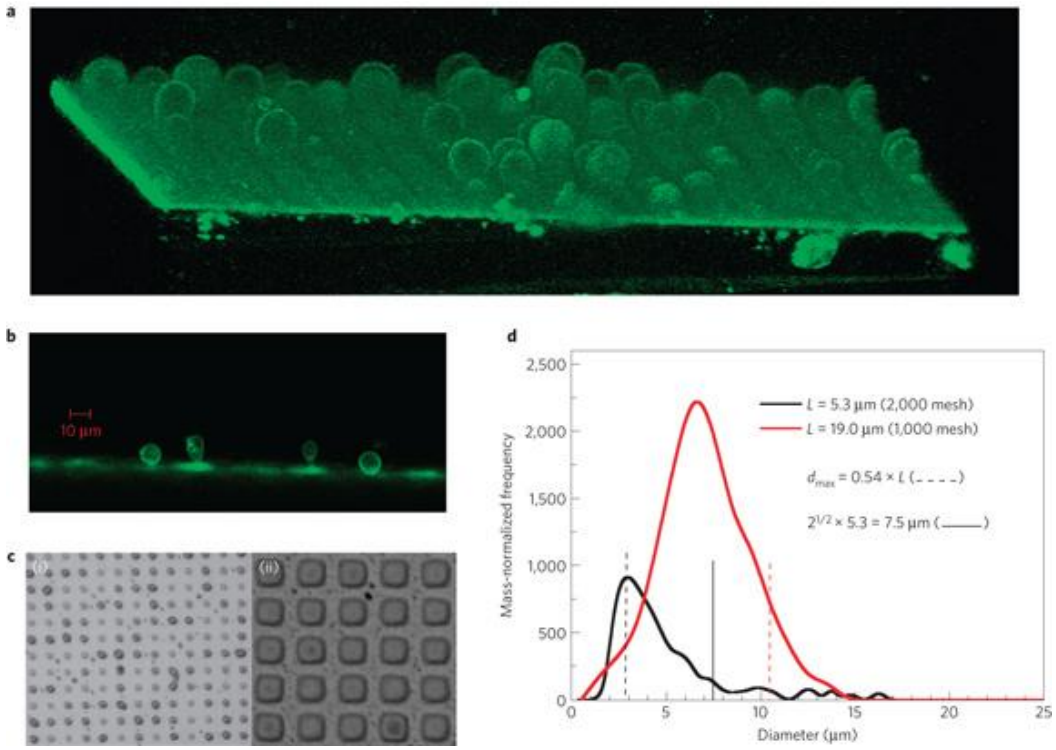

Figure 1.5. Images of the polymer islands, the vesicle formation process and vesicle size distributions. Image taken from ref [39]

1.4.3 Electroformation

One approach that has been proved to be successful in the production of giant vesicles with both phospholipids and block copolymers is the use of an AC current in the electroformation method. Firstly, two glass slides coated with a layer of semi-conductor, commonly indium tin oxide, also widely used in LCD panel, attached to a power supply[40]. One of the slides has an enclosed well, capable of taking small volumes of conducting liquid, usually salt aqueous solution or glucose/dextran. The same protocol is used as film hydration method to cast a thin lipid or polymer film on this slide. The well is then filled with a conducting liquid and then covered with the second slide, with the semi-conductor in contact with the water. The two slides are kept pressed together to prevent liquid from escaping and to ensure a good contact with the water to make a circuit. A typical 1-10 V at a frequency of 10 Hz is applied. Vesicle formation has been reported within a few seconds and is usually complete in

1-2 hours.

A modified version of this method involves the use of a PDMA stamp to pattern the ITO glass surface. Giant phospholipid vesicles were formed only from the squares which had direct contact with the glass at the time of printing.[41]

Instead of using ITO glass, there is a second version of electroformation method which involves two Pt [42, 43] or Au[31] wires spaced 2-3 mm apart, lipid film is casted on the electrodes and a well of liquid is also required to complete the circuit. Reported vesicles dimensions range from 0.1-300 μm[44]. Early reports of successful vesicle production by this method used charged phospholipids,[45] however, more and more recent work showed successful production of polymersomes, from nonionic block copolymers with low glass transition temperatures.

Both versions of the electroformation technique have shown that the electric field helps to gently shake the deposited lipids from surface of either the ITO glass or metal electrode. It is the osmotic pressures and electrostatic forces that drive phospholipids to form liposomes. Therefore, an upper concentration limit usually exist for solutes, since the increasing of solute concentration also increases osmotic pressure and represses the lipids film.

1.4.4 Homogenisation/extrusion

One of the best approaches to yield relatively narrow size distribution vesicles is to extrude the vesicles in a homogeniser. Commercial devices are available on the market, which all devices will subject the fluid to high shear, collision and cavitation by forcing it through tiny holes at high pressure, then a more homogenised dispersion is obtained. The high pressure that applied in the process disrupts the bilayer in large lamellae or spontaneously formed multilamellar vesicles. This leads to a reorganisation of the molecules into smaller unilamellar vesicles. After disruption of the bilayer in the homogeniser, the solution is then immediately passed through membranes with chosen porosity of desired size. Large objects will be separated from vesicles with sizes smaller than the filter. The populations formed tend to be near to

monodisperse, depending on the number of extrusion, pore size of the membrane and the applied pressure. [46, 47]

1.4.5 Sonication

This technique makes use of high energy in the form of ultrasonic waves, which play a role in disrupting the lamellar bilayers in large lamellae or multilamellar vesicles. It has been reported that this approach leads to the production of very small vesicles with variable population distributions. [48, 49]

There are a number of factors affecting the efficiency of this approach, including the processing time, power and type of ultrasound apparatus. However, this method cannot be applied to "hard" materials, which normally have a high glass transition temperature and large molecular weight. This is due to the fact that amphiphiles with rigid chains can hardly move and rearrange in the water without the aid of organic solvent, which results in a trapped thermodynamic state, therefore fail to self-assemble into vesicles.

1.4.6 Freeze-pump-thaw

This technique does not directly lead to the formation of vesicles; therefore it is commonly used with homognisation or sonication. By forming ice crystals, the bilayers that formed in the solution are disrupted into small pieces. The result is increased hydration of lipids upon thawing. The following reformulation to unilamellar vesicles can be achieved more easily by other homogenisation method.

1.4.7 Inkjet printing

This method has been first reported by Förster and coworkers in order to demonstrate how polymeric vesicles can be made via modified inkjet printer. Typically, the printer

cartridge is filled with a solution (0.1- 5 wt%) of the vesicle-forming amphiphiles in ethanol or other water miscible solvents such as THF or dioxane. Routinely, an experiment consists of printing three black pages with the highest print quality, which corresponds to the highest ink throughput[50]. Approximately 1-1.5 mL of the solution, depending on the cartridge type, is then "printed" into 10 ml of water under stirring. Monodisperse unilamellar vesicles in the diameter size range of 50-200 nm can be directly and reproducibly prepared. Modern inkjet printers produce droplets with volumes in the picoliter range with high reproducibility,[51, 52] which allows vesicle formation to be controlled with good precision.

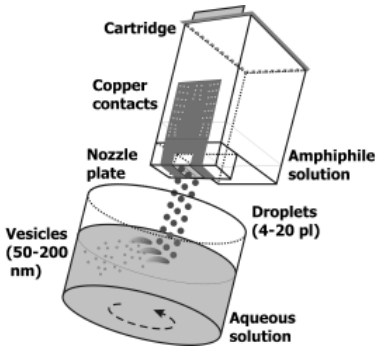

Figure 1.6 Scheme of the preparation of nanometer-sized vesicles using simple inkjet printing technology. A solution of a vesicle-forming amphiphile is filled into a cartridge and "printed" into a stirred aqueous solution, where the amphiphiles spontaneously assemble into vesicles. The printers are modified to hold the printhead in a fixed position. [50]

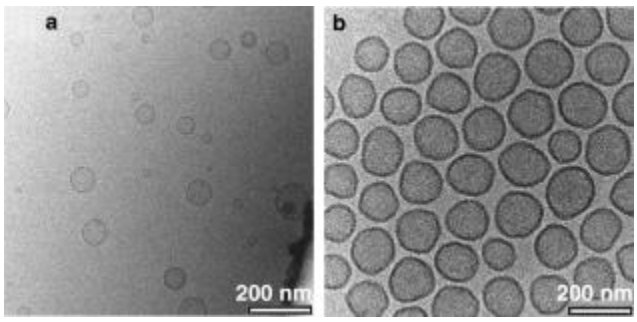

Figure 1.7 Cryo-TEM images of a) egg-PC vesicles prepared with a HP 695C printer and b) P2 VP_{29}-PEG_{15} vesicles prepared with a HP 890 printer. All vesicles are small and unilamellar with, in the case of the polymersomes, very narrow size distributions.[50]

1.4.8 Nanoparticle induce self-assembly

Park and co-workers have reported on how to control the self-assembly of magnetic nanoparticles and a prototypical amphiphilic block-copolymer into polymersomes, micelles and core-shell type micelles by controlling the solvent-nanoparticle and polymer nanoparticles interactions. Incorporation of nanoparticles drastically affects the self-assembly structure of block-copolymers by modifying the relative volume ratio between the hydrophobic block and the hydrophilic block.[53] As a consequence, the self-assembly of micelle-forming block-copolymers typically produces magneto-polymersomes instead of magneto-micelles. In this case, the packing parameter of the block copolymers is in the range of micelle formation. However, by adding oleic acid bond magnetic nanoparticles, the hydrophobic block can be considered extended, which results in the change of the effective volume ratio between two blocks.

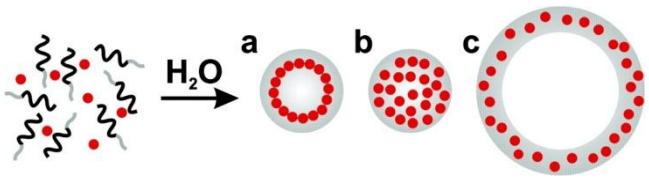

Figure 1.8. Self-assembly of nanoparticles and block copolymers. (a) Magneto-core shell assemblies formed when DMF/THF mixture (96.8% DMF) was used as the initial solvent for polymers and nanoparticles. (b) Magneto-micelles assembled in THF. (c) Magneto-polymersomes assembled in dioxane/THF (96.8% dioxane).[53]

1.4.9 Solvent addition

This technique was originally proposed for use with phospholipid vesicles, but now is commonly used with block copolymer amphiphiles, which are too hydrophobic to be directly suspended in aqueous systems. [54]

The idea of the solvent addition method is to firstly dissolve amphiphiles in a good solvent for both blocks. Then a second solvent is chosen, which is good solvent for one block but not the other and is also miscible with the first solvent. The result is that as the concentration of the second solvent increases, the amphiphiles arrange themselves into a range of three diamensional equilibrium structures to minimise the unfavourable hydrophobe-water interactions. Typically, block copolymers are dissolved in an organic solvent such as THF and then water is slowly added to the system with vigorous stirring. Dialysis is usually applied additionally, which can take days to weeks for the organic solvent to be removed completely. The addition of the second solvent is often required to be slow enough, so that the polymer chains in the solution can have enough time for relaxation and rearrangement. One of the advantages of this approach is that simply by stopping addition of the solvent, the structures formed for that solvent composition are frozen; the sample can be taken out for further study.

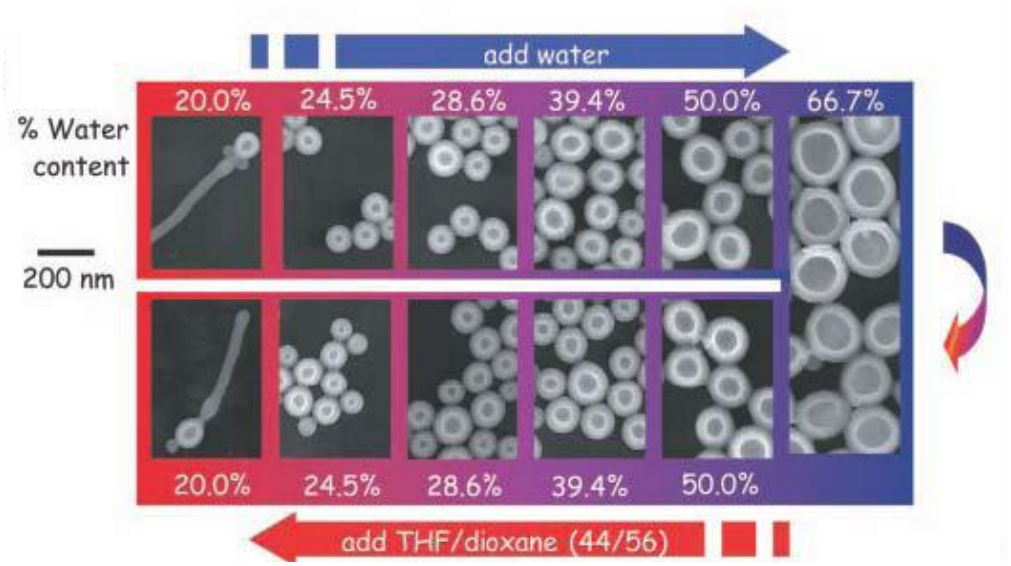

Figure 1.9 A diagram showing changing morphology and size with changing solvent environment, note the increase in vesicles size as water moves toward 66%.[55]

Besides typical structures such as micelles, rods and vesicles are formed, a range of intermediate and complex structures are often observed.[3]

1.4.10. Use of double emulsions and microfluidics.

This technique uses microfluidic devices to form water-in-oil-in-water double-emulsion droplets in aqueous.[56] Typically, an amphiphilic block copolymer is dissolved in the oil (organic phase), which is immiscible with water and capillary based device is used to generate droplet in the droplet structure. After the formation of the emulsion, the organic solvent is evaporated and the block copolymer chains adsorbs to the interfaces between the oil and water phases upon evaporation of the middle phase, then polymersome forms.

The Weitz group has developed a range of different types of microfluidic devices by using glass capillaries. These devices enable not only the possibility of which the monodisperse polymersomes can be made, but also the possibility to generate other core-shell or multicompartment structures.[57-59]

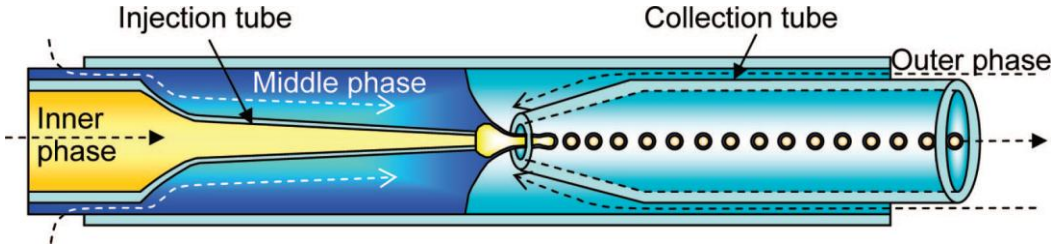

Figure 1.10. Schematic of the microcapillary geometry for generating double emulsions. The geometry requires the outer phase to be immiscible with the middle phase, which is in turn immiscible with the inner phase. However, the inner phase can be miscible with the outer phase.[60]

Polymersomes formed by this method have been used for a range of copolymers including PBA-PAA, PBMA-PDMAEMA, PS-PEO, PBD-PEO etc., indicating that the technique is a generally applicable on for polymers of varying glass transition temperatures. Reported diameters are in the range of 10-300 μm with bilyer (sometimes multiple bilayer) thicknesses of few micrometer, which can be controlled by the polymer concentration in the organic phase. In addition to thicker than average bilayers, the polymersomes can sometimes have one side or spot thicker than the rest part. This is attributed to a dewetting process of the organic phase when a less

compatible organic solvent is used as co-solvent.[61]

1.5 Reinforcement of block copolymer self-assembly aggregates

Efforts have been made to develop different ways of giving different functionalities to polymer molecules. For this reason, those aggregates that assembled from block copolymers can possess various physical and chemical properties, which arises from every single molecule in the structures. One of the directions is to increase the stability and mechanical properties of micelles, cylinders or vesicles to enable them suitable for special applications.

1.5.1 Shell crosslinked micelles

One of the fundamental problems with block copolymer micelles is that when the polymer concentration drops below its critical micelles concentration (CMC), spontaneous dissociation can happen. However, in 1996, Wooley's group [62] reported that cross-linking micelles coronas at high dilution led to the structure of robust nanoparticles know as Shell Cross-Linked micelles (SCL) (Figure 1.11)

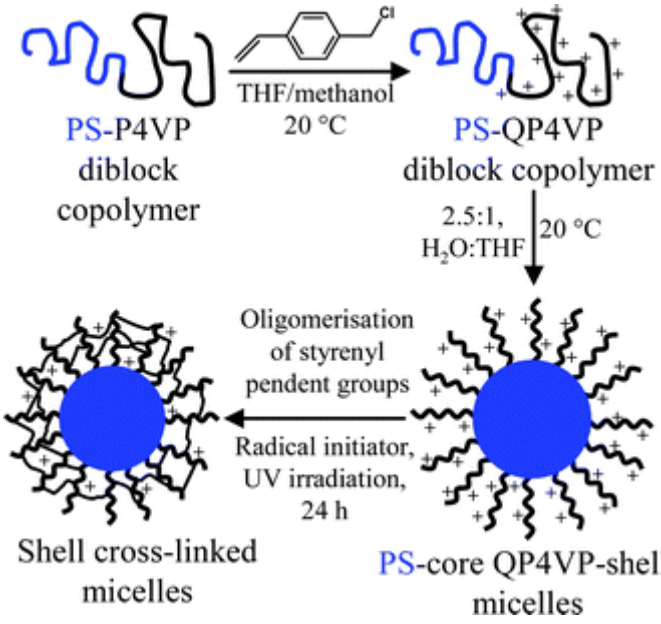

Figure 1.11 Schematic illustration of the first example of shell cross-linked micelles from PS-QP4VP diblock copolymer micelles.[62]

Unlike conventional micelles, these new covalently-stabilised SCL micelles were stable with respect to infinite dilution. Similar result can be achieved when cross-linking the micelles cores.[15, 63, 64] Moreover, it has been report not only for spherical micelles but also for cylindrical micelles, the combination of the two gives a new complex structure with extra stability. Amphiphilic block copolymers were micellised and shell-crosslinked in water to give cationic, spherical or anionic, cylindrical micelles.[65, 66] The differences in surface charge and particle shape result from the different polymers used to create these assemblies. The shell crosslinked cylinder were assembled from polyamidoethylamine$_{128}$-b-polystyrene$_{40}$, while the nanocylinders were assembled from poly(acrylic acid)$_{96}$-b-polystyrene$_{49}$. Upon mixing, the cationic spheres assembled on the nanoscopic curved surfaces of the nanocylinders and form a close-packed dense layer.[67]

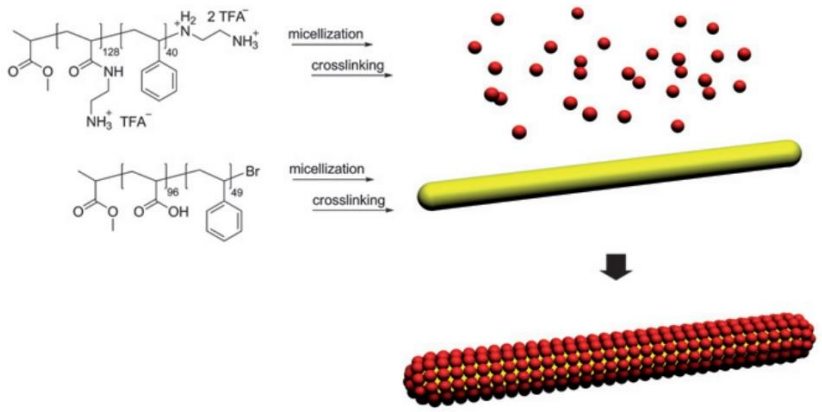

Figure 1.12 Formation of shell-crosslinked nanoparticles of spherical and cylindrical shapes, and the templated self-assembly of the spheres on the surface of a cylinder.[67]

1.5.2 Interaction of nanoparticles with polymersomes.

Polymersomes as synthetic analogues to liposomes have gain great interests due to their increased thickness, rigidity and stability. [55, 68] The interaction of nanoparticles and block copolymer vesicles has been shown by either segregating

nanoparticles into a favourably interaction polymer domain or at the interface between two polymers [69, 70]. Morphological changes of block copolymer assemblies can be induced by the incorporation of nanoparticles, which play an active role in the self-assembly of the block copolymer into membranes [53, 71]. Eisenberg and Mai[72] showed that nanoparticles can selectively be incorporated into the central part of block copolymer vesicle bilayer walls by simply coating the particles with similar structure diblock copolymers, which enabled the particles to be localised in the central part of the bilayer.

Duan and coworkers have reported a new class of plasmonic vesicular nanostructures assembled from amphiphilic gold nanocrystals with mixed polymer brush coatings. Instead of decorating polymersomes, gold nanoparticles have been incorporated with both hydrophilic and hydrophobic brushes to obtain amphiphilicity,[73] which can therefore self-assemble into vesicular nanostructures with designed stimuli responsive property. (Figure 1.13)

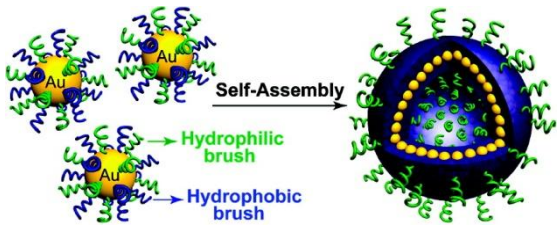

Figure 1.13 Schematic illustration of self-assembly of amphiphilic nanocrystals with mixed polymer brushes into vesicular structures.[73]

1.6 Application for drug delivery

In addition to providing a facile model system of the more complex cell membrane, vesicles, along with micelles[74] and dendrimers[75, 76] have been applied in encapsulation technology for drug delivery[77] and cosmetics, delivering vitamins and oils. The potential applications for polymers to aid in the delivery of drugs has gained more and more interest and polymers have been developed that have the ability to disrupt and penetrate the bilayer membrane[78, 79]. It has also been demonstrated that nano-aggregates, such as shell cross-linked micelles can deliver target molecules to a site and release the contents under the correct conditions[80-83] and that the delivery rates may be modified with small modifications to the makeup of the aggregate forming species[84]. Indeed, phospholipids have been formulated into "transferosomes", vesicles made from a mixture of phospholipids, with a highly flexible hydrophilic membrane such that they can aid in the transdermal transfer of an encapsulated drug[85].

It is possible to attach biologically actives or interesting molecules such as biotin to a polymer chain, which has a very strong specific interaction with avidin. [86, 87]These modified polymer chains can then be included into a vesicle or micelle with a view to a biological or bio-recognition application[88]. One obvious criterion for biomedical applications is that the delivery vehicle itself does no harm to the target organism in which it is used and to this end much recent research has focused on the synthesis of biocompatible[36, 89], biodegradable, [35, 90, 91]vesicles or "nanocapsules"[92]

1.7 Aims and scope of investigation

This thesis investigates the reinforcement of polymersomes with particles and their structural morphologies. The thesis is outlined as follow:

In Chapter 2, vesicles are formed from PBMA-PDMAEMA block copolymers. In an attempt to reinforce the vesicle bilayer by the assembly of colloidal nanoparticles, the polymersomes are treated with variety of particles and analysed by microscopy technique.

In Chapter 3, stimuli responsive polymersomes are fabricated via microfluidic approach and the embedded micron sized particles are the key to this bubble generating property. Both instant and slow release behaviours are studied via microscopic technique and ion selective electrode measurement.

In Chapter 4, the morphological transitions of the polymersomes when exposed to small hydrophobic molecules are studied. The influence of the small organic molecules can be unexpectedly harmful to the vesicle structure.

1. Vriezema, D.M., et al., *Self-Assembled Nanoreactors.* Chemical Reviews, 2005. **105**(4): p. 1445-1490.
2. Blanazs, A., S.P. Armes, and A.J. Ryan, *Self-Assembled Block Copolymer Aggregates: From Micelles to Vesicles and their Biological Applications.* Macromol Rapid Commun, 2009. **30**(4-5): p. 267-77.
3. Cameron, N.S., M.K. Corbierre, and A. Eisenberg, *1998 E.W.R. Steacie Award Lecture Asymmetric amphiphilic block copolymers in solution: a morphological wonderland.* Canadian Journal of Chemistry, 1999. **77**(8): p. 1311-1326.
4. Zhang, L. and A. Eisenberg, *Multiple Morphologies of "Crew-Cut" Aggregates of Polystyrene-b-poly(acrylic acid) Block Copolymers.* Science, 1995. **268**(5218): p. 1728-1731.
5. Mai, Y. and A. Eisenberg, *Self-assembly of block copolymers.* Chemical Society Reviews, 2012. **41**(18): p. 5969-5985.
6. Riess, G., *Micellization of block copolymers.* Progress in Polymer Science, 2003. **28**(7): p. 1107-1170.
7. Kabanov, A.V., E.V. Batrakova, and V.Y. Alakhov, *Pluronic block copolymers as novel polymer therapeutics for drug and gene delivery.* J Control Release, 2002. **82**(2-3): p. 189-212.
8. Maysinger, D., et al., *Fate of micelles and quantum dots in cells.* Eur J Pharm Biopharm, 2007. **65**(3): p. 270-81.
9. Bütün, V., et al., *A brief review of 'schizophrenic' block copolymers.* Reactive and Functional Polymers, 2006. **66**(1): p. 157-165.
10. Erhardt, R., et al., *Janus Micelles†.* Macromolecules, 2001. **34**(4): p. 1069-1075.
11. Erhardt, R., et al., *Amphiphilic Janus Micelles with Polystyrene and Poly(methacrylic acid) Hemispheres.* Journal of the American Chemical Society, 2003. **125**(11): p. 3260-3267.
12. Voets, I.K., et al., *Double-Faced Micelles from Water-Soluble Polymers.* Angewandte Chemie International Edition, 2006. **45**(40): p. 6673-6676.
13. Li, Z., M.A. Hillmyer, and T.P. Lodge, *Control of Structure in Multicompartment Micelles by Blending μ-ABC Star Terpolymers with AB Diblock Copolymers.* Macromolecules, 2005. **39**(2): p. 765-771.
14. Dan, N. and S.A. Safran, *Junctions and end-caps in self-assembled non-ionic cylindrical micelles.* Advances in Colloid and Interface Science, 2006. **123–126**(0): p. 323-331.
15. Won, Y.-Y., H.T. Davis, and F.S. Bates, *Giant Wormlike Rubber Micelles.* Science, 1999. **283**(5404): p. 960-963.
16. Won, Y.-Y., et al., *Cryogenic Transmission Electron Microscopy (Cryo-TEM) of Micelles and Vesicles Formed in Water by Poly(ethylene oxide)-Based Block Copolymers.* The Journal of Physical Chemistry B, 2002. **106**(13): p. 3354-3364.
17. Bang, J., et al., *Sphere, Cylinder, and Vesicle Nanoaggregates in Poly(styrene-b-isoprene) Diblock Copolymer Solutions.* Macromolecules,

2006. **39**(3): p. 1199-1208.
18. Jain, S. and F.S. Bates, *On the Origins of Morphological Complexity in Block Copolymer Surfactants.* Science, 2003. **300**(5618): p. 460-464.
19. Jain, S., et al., *Disordered Network State in Hydrated Block-Copolymer Surfactants.* Physical Review Letters, 2006. **96**(13): p. 138304.
20. Geng, Y. and D.E. Discher, *Hydrolytic Degradation of Poly(ethylene oxide)-block-Polycaprolactone Worm Micelles.* Journal of the American Chemical Society, 2005. **127**(37): p. 12780-12781.
21. Zhu, J. and W. Jiang, *Self-Assembly of ABC Triblock Copolymer into Giant Segmented Wormlike Micelles in Dilute Solution.* Macromolecules, 2005. **38**(22): p. 9315-9323.
22. Cui, H., et al., *Block Copolymer Assembly via Kinetic Control.* Science, 2007. **317**(5838): p. 647-650.
23. Pochan, D.J., et al., *Toroidal Triblock Copolymer Assemblies.* Science, 2004. **306**(5693): p. 94-97.
24. Zhong, S., et al., *Helix self-assembly through the coiling of cylindrical micelles.* Soft Matter, 2008. **4**(1): p. 90-93.
25. Zhang, L., K. Yu, and A. Eisenberg, *Ion-Induced Morphological Changes in "Crew-Cut" Aggregates of Amphiphilic Block Copolymers.* Science, 1996. **272**(5269): p. 1777-1779.
26. Discher, B.M., et al., *Polymersomes: Tough Vesicles Made from Diblock Copolymers.* Science, 1999. **284**(5417): p. 1143-1146.
27. Zhang, L. and A. Eisenberg, *Multiple Morphologies and Characteristics of "Crew-Cut" Micelle-like Aggregates of Polystyrene-b-poly(acrylic acid) Diblock Copolymers in Aqueous Solutions.* Journal of the American Chemical Society, 1996. **118**(13): p. 3168-3181.
28. Napoli, A., et al., *Oxidation-responsive polymeric vesicles.* Nat Mater, 2004. **3**(3): p. 183-9.
29. Nardin, C., et al., *Polymerized ABA Triblock Copolymer Vesicles.* Langmuir, 1999. **16**(3): p. 1035-1041.
30. Schillén, K., K. Bryskhe, and Y.S. Mel'nikova, *Vesicles Formed from a Poly(ethylene oxide)−Poly(propylene oxide)−Poly(ethylene oxide) Triblock Copolymer in Dilute Aqueous Solution.* Macromolecules, 1999. **32**(20): p. 6885-6888.
31. Sauer, M., et al., *Ion-carrier controlled precipitation of calcium phosphate in giant ABA triblock copolymer vesicles.* Chemical Communications, 2001(23): p. 2452-2453.
32. LoPresti, C., et al., *Polymersomes: nature inspired nanometer sized compartments.* Journal of Materials Chemistry, 2009. **19**(22): p. 3576-3590.
33. Liu, F. and A. Eisenberg, *Preparation and pH Triggered Inversion of Vesicles from Poly(acrylic Acid)-block-Polystyrene-block-Poly(4-vinyl Pyridine).* Journal of the American Chemical Society, 2003. **125**(49): p. 15059-15064.
34. Brannan, A.K. and F.S. Bates, *ABCA Tetrablock Copolymer Vesicles.* Macromolecules, 2004. **37**(24): p. 8816-8819.

35. Meng, F., et al., *Biodegradable Polymersomes.* Macromolecules, 2003. **36**(9): p. 3004-3006.
36. Ghoroghchian, P.P., et al., *Bioresorbable Vesicles Formed through Spontaneous Self-Assembly of Amphiphilic Poly(ethylene oxide)-block-polycaprolactone.* Macromolecules, 2006. **39**(5): p. 1673-1675.
37. Bangham, A.D. and R.W. Horne, *Negative staining of phospholipids and their structural modification by surface-active agents as observed in the electron microscope.* Journal of Molecular Biology, 1964. **8**(5): p. 660-IN10.
38. Kickelbick, G., et al., *Spontaneous Vesicle Formation of Short-Chain Amphiphilic Polysiloxane-b-Poly(ethylene oxide) Block Copolymers.* Langmuir, 2003. **19**(8): p. 3198-3201.
39. Howse, J.R., et al., *Templated formation of giant polymer vesicles with controlled size distributions.* Nat Mater, 2009. **8**(6): p. 507-511.
40. Angelova, M.I., et al., *Preparation of giant vesicles by external AC electric fields. Kinetics and applications,* in *Trends in Colloid and Interface Science VI*, C. Helm, M. Lösche, and H. Möhwald, Editors. 1992, Steinkopff. p. 127-131.
41. Taylor, P., et al., *A novel technique for preparation of monodisperse giant liposomes.* Chemical Communications, 2003(14): p. 1732-1733.
42. Bagatolli, L.A. and E. Gratton, *Two-photon fluorescence microscopy observation of shape changes at the phase transition in phospholipid giant unilamellar vesicles.* Biophys J, 1999. **77**(4): p. 2090-101.
43. Bucher, P., et al., *Giant Vesicles as Biochemical Compartments: The Use of Microinjection Techniques.* Langmuir, 1998. **14**(10): p. 2712-2721.
44. Mueller, P., T.F. Chien, and B. Rudy, *Formation and properties of cell-size lipid bilayer vesicles.* Biophys J, 1983. **44**(3): p. 375-81.
45. Menger, F.M. and M.I. Angelova, *Giant Vesicles: Imitating the Cytological Processes of Cell Membranes.* Accounts of Chemical Research, 1998. **31**(12): p. 789-797.
46. MacDonald, R.C., et al., *Small-volume extrusion apparatus for preparation of large, unilamellar vesicles.* Biochim Biophys Acta, 1991. **1061**(2): p. 297-303.
47. Subbarao, N.K., et al., *Characteristics of spectrin-induced leakage of extruded, phosphatidylserine vesicles.* Biochimica et Biophysica Acta (BBA) - Biomembranes, 1991. **1063**(1): p. 147-154.
48. Hunt, C.A. and G.E. McCasland, *Liposome technology, vol. 1: Preparation of liposomes; vol. 2: Incorporation of drugs, proteins, and genetic materials; vol. 3: Targeted drug delivery and biological interaction. Edited by Gregory Gregoriadis. CRC Press, Inc., 2000 Corporate Boulevard N.W., Boca Raton, FL 33431. 1984. Vol. 1: 268 pp. 18 × 26 cm. $83.00. Vol. 2: 231 pp. 18 × 26 cm. $83.00. Vol. 3: 292 pp. 18 × 26 cm. $83.00.* Journal of Pharmaceutical Sciences, 1985. **74**(7): p. 802-802.
49. Bailey, W.J. and L.L. Zhou, *Synthesis of polymerized vesicles with hydrolyzable linkages.* Macromolecules, 1992. **25**(1): p. 3-11.
50. Hauschild, S., et al., *Direct Preparation and Loading of Lipid and Polymer Vesicles Using Inkjets.* Small, 2005. **1**(12): p. 1177-1180.

51. de Gans, B.J., P.C. Duineveld, and U.S. Schubert, *Inkjet Printing of Polymers: State of the Art and Future Developments.* Advanced Materials, 2004. **16**(3): p. 203-213.
52. Stachowiak, J.C., et al., *Inkjet formation of unilamellar lipid vesicles for cell-like encapsulation.* Lab on a Chip, 2009. **9**(14): p. 2003-2009.
53. Hickey, R.J., et al., *Controlling the Self-Assembly Structure of Magnetic Nanoparticles and Amphiphilic Block-Copolymers: From Micelles to Vesicles.* Journal of the American Chemical Society, 2011. **133**(5): p. 1517-1525.
54. Moscho, A., et al., *Rapid preparation of giant unilamellar vesicles.* Proc Natl Acad Sci U S A, 1996. **93**(21): p. 11443-7.
55. Discher, D.E. and A. Eisenberg, *Polymer Vesicles.* Science, 2002. **297**(5583): p. 967-973.
56. Okushima, S., et al., *Controlled production of monodisperse double emulsions by two-step droplet breakup in microfluidic devices.* Langmuir, 2004. **20**(23): p. 9905-8.
57. Kim, S.-H., et al., *Multiple Polymersomes for Programmed Release of Multiple Components.* Journal of the American Chemical Society, 2011. **133**(38): p. 15165-15171.
58. Zhao, Y., et al., *Microfluidic Generation of Multifunctional Quantum Dot Barcode Particles.* Journal of the American Chemical Society, 2011. **133**(23): p. 8790-8793.
59. Abbaspourrad, A., et al., *Polymer Microcapsules with Programmable Active Release.* Journal of the American Chemical Society, 2013. **135**(20): p. 7744-7750.
60. Shum, H.C., J.-W. Kim, and D.A. Weitz, *Microfluidic Fabrication of Monodisperse Biocompatible and Biodegradable Polymersomes with Controlled Permeability.* Journal of the American Chemical Society, 2008. **130**(29): p. 9543-9549.
61. Shum, H.C., et al., *Dewetting-Induced Membrane Formation by Adhesion of Amphiphile-Laden Interfaces.* Journal of the American Chemical Society, 2011. **133**(12): p. 4420-4426.
62. Thurmond, K.B., T. Kowalewski, and K.L. Wooley, *Water-Soluble Knedel-like Structures: The Preparation of Shell-Cross-Linked Small Particles.* Journal of the American Chemical Society, 1996. **118**(30): p. 7239-7240.
63. Guo, A., G. Liu, and J. Tao, *Star Polymers and Nanospheres from Cross-Linkable Diblock Copolymers.* Macromolecules, 1996. **29**(7): p. 2487-2493.
64. Tao, J., et al., *Star and Cylindrical Micelles of Polystyrene-block-poly(2-cinnamoylethyl methacrylate) in Cyclopentane.* Macromolecules, 1997. **30**(9): p. 2738-2745.
65. Zhang, K., et al., *Cationic shell-crosslinked knedel-like nanoparticles for highly efficient gene and oligonucleotide transfection of mammalian cells.* Biomaterials, 2009. **30**(5): p. 968-977.
66. Zhang, K., et al., *Shape Effects of Nanoparticles Conjugated with*

Cell-Penetrating Peptides (HIV Tat PTD) on CHO Cell Uptake. Bioconjugate Chemistry, 2008. **19**(9): p. 1880-1887.
67. Zhang, K., et al., *Composite soft-matter nanoscale objects: Nanocylinder-templated assembly of nanospheres.* Soft Matter, 2009. **5**(19): p. 3585-3589.
68. Sanson, C., et al., *Doxorubicin Loaded Magnetic Polymersomes: Theranostic Nanocarriers for MR Imaging and Magneto-Chemotherapy.* ACS Nano, 2011. **5**(2): p. 1122-1140.
69. Lin, Y., et al., *Self-directed self-assembly of nanoparticle/copolymer mixtures.* Nature, 2005. **434**(7029): p. 55-59.
70. Haryono, A. and W.H. Binder, *Controlled arrangement of nanoparticle arrays in block-copolymer domains.* Small, 2006. **2**(5): p. 600-11.
71. Sanchez-Gaytan, B.L., et al., *Interfacial Assembly of Nanoparticles in Discrete Block-Copolymer Aggregates.* Angewandte Chemie, 2007. **119**(48): p. 9395-9398.
72. Mai, Y. and A. Eisenberg, *Controlled Incorporation of Particles into the Central Portion of Vesicle Walls.* Journal of the American Chemical Society, 2010. **132**(29): p. 10078-10084.
73. Song, J., et al., *Plasmonic Vesicles of Amphiphilic Gold Nanocrystals: Self-Assembly and External-Stimuli-Triggered Destruction.* Journal of the American Chemical Society, 2011. **133**(28): p. 10760-10763.
74. Gaucher, G., et al., *Block copolymer micelles: preparation, characterization and application in drug delivery.* Journal of Controlled Release, 2005. **109**(1–3): p. 169-188.
75. Pantos, A., et al., *Interaction of Functional Dendrimers with Multilamellar Liposomes: Design of a Model System for Studying Drug Delivery.* Langmuir, 2005. **21**(16): p. 7483-7490.
76. Morgan, M.T., et al., *Dendritic supramolecular assemblies for drug delivery.* Chemical Communications, 2005(34): p. 4309-4311.
77. Tanner, P., et al., *Polymeric Vesicles: From Drug Carriers to Nanoreactors and Artificial Organelles.* Accounts of Chemical Research, 2011. **44**(10): p. 1039-1049.
78. Thomas, J.L., S.W. Barton, and D.A. Tirrell, *Membrane solubilization by a hydrophobic polyelectrolyte: surface activity and membrane binding.* Biophys J, 1994. **67**(3): p. 1101-6.
79. Hoffman, A.S., et al., *Design of "Smart" polymers that can -direct intracellular drug delivery.* Polymers for Advanced Technologies, 2002. **13**(10-12): p. 992-999.
80. Stewart, S. and G. Liu, *Block Copolymer Nanotubes.* Angewandte Chemie, 2000. **112**(2): p. 348-352.
81. Kiser, P.F., G. Wilson, and D. Needham, *A synthetic mimic of the secretory granule for drug delivery.* Nature, 1998. **394**(6692): p. 459-462.
82. Burger, K.N.J., et al., *Nanocapsules: lipid-coated aggregates of cisplatin with high cytotoxicity.* Nat Med, 2002. **8**(1): p. 81-84.

83. Li, Y., et al., *Synthesis of Reversible Shell Cross-Linked Micelles for Controlled Release of Bioactive Agents†.* Macromolecules, 2006. **39**(8): p. 2726-2728.
84. Agrawal, S.K., et al., *Novel drug release profiles from micellar solutions of PLA–PEO–PLA triblock copolymers.* Journal of Controlled Release, 2006. **112**(1): p. 64-71.
85. Cevc, G., et al., *Overcoming Semipermeable Barriers, Such as the Skin, with Ultradeformable Mixed Lipid Vesicles, Transfersomes, Liposomes, or Mixed Lipid Micelles.* Langmuir, 2003. **19**(26): p. 10753-10763.
86. Drechsler, U., et al., *Highly Efficient Biocatalysts via Covalent Immobilization of Candida rugosa Lipase on Ethylene Glycol-Modified Gold–Silica Nanocomposites.* Advanced Materials, 2004. **16**(3): p. 271-274.
87. Salem, A.K., et al., *Porous Polymer and Cell Composites That Self-Assemble In Situ.* Advanced Materials, 2003. **15**(3): p. 210-213.
88. Joralemon, M.J., et al., *Synthesis, characterization, and bioavailability of mannosylated shell cross-linked nanoparticles.* Biomacromolecules, 2004. **5**(3): p. 903-13.
89. Photos, P.J., et al., *Polymer vesicles in vivo: correlations with PEG molecular weight.* J Control Release, 2003. **90**(3): p. 323-34.
90. Matsuda, T., I.K. Kwon, and S. Kidoaki, *Photocurable biodegradable liquid copolymers: synthesis of acrylate-end-capped trimethylene carbonate-based prepolymers, photocuring, and hydrolysis.* Biomacromolecules, 2004. **5**(2): p. 295-305.
91. Ahmed, F. and D.E. Discher, *Self-porating polymersomes of PEG–PLA and PEG–PCL: hydrolysis-triggered controlled release vesicles.* Journal of Controlled Release, 2004. **96**(1): p. 37-53.
92. Shenoy, D.B., et al., *Layer-by-Layer Engineering of Biocompatible, Decomposable Core−Shell Structures.* Biomacromolecules, 2003. **4**(2): p. 265-272.

Chapter 2 Polymer Vesicles with a Colloidal Armour of Nanoparticles

2.1 Introduction

The word “polymersome” has been coined in 1999[1] to describe a hollow bilayer-based suprastructure that consists of amphiphilic polymer molecules in liquid medium, while conventionally, researchers has been using “liposome” for such structure assembled from phospholipids molecules. The availability of a plethora of synthetic macromolecular amphiphiles through advances in living polymerisation methods has led to a surge in the preparation of vesicles made from polymer molecules.[1, 2] Polymer vesicles have interesting chemical and physical properties, which outperform synthetic liposomes made from phospholipids. One of the key features is that these polymer nanocontainers are more mechanically robust, as a result of their increased bilayer thickness, stronger chain interaction and polymer chain entanglement,[3] which makes these hollow structures interesting as potential drug delivery vehicles.[4] Tailored synthesis of the macromolecular building blocks provides added complexity and functionality to their design. Use of biodegradable,[5] oxidative responsive,[6] or pH/sugar responsive block copolymers[7] in the fabrication of polymer vesicles allows for triggered bilayer disintegration inducing permeability or vesicle rupture. Examples focusing on mechanical reinforcement include the ability to cross-link the bilayer of polymer vesicles made from poly(ethylene oxide)-*block*-polybutadiene,[8, 9] or provide a polymeric scaffold through intra-bilayer polymerisation.[10]

It is plausible to consider adding functionality and potentially enhanced mechanical strength to polymersomes by decorating their outer surface with an armour of colloidal matter. The inspiration was taken from Nature, how it safeguards mechanical strength in certain classes of cells and organisms. In addition to the mechanical strength provided by the cytoskeleton of the cell, plants, fungi, and certain bacteria have an additional cell wall as outermost boundary. Organisms that attracted

more interest were ones with a cell wall composed of an armour of colloidal objects, for example, bacteria coated with S-layer proteins,[11] and coccolithophorids which have a $CaCO_3$-based nanopatterned colloidal armour.[12]

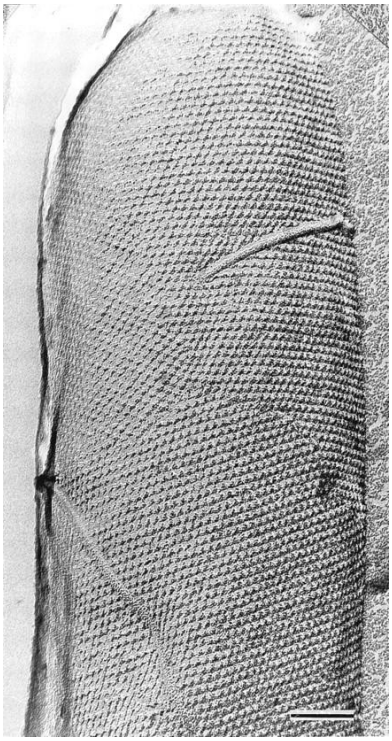

Figure 2.1 Electron micrograph of a freeze-etched preparation showing a whole cell with a hexagonally ordered S-layer lattice. Scale bar: 100 nm.[12]

Velev demonstrated that synthetic liposomes could be coated with a layer of ferritin.[13] Weitz and co-workers showed that crystalline rafts of microspheres could be formed on the outside of vesicles made from mixed low-molar-mass surfactants.[14, 15]

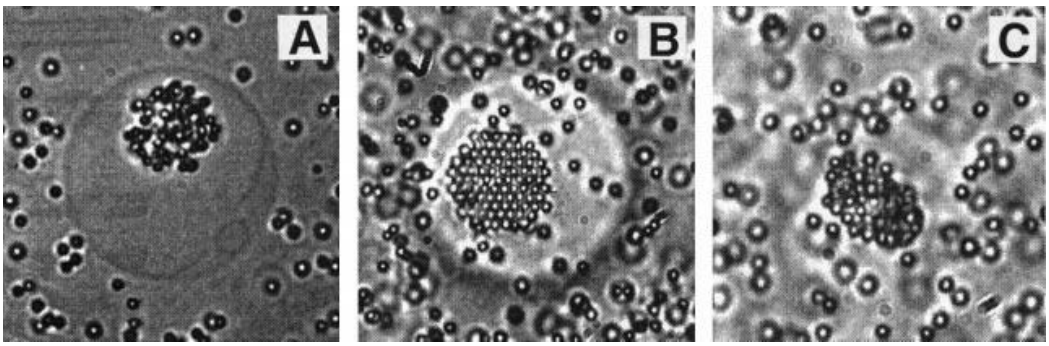

Figure 2.2 (**A**) Disordered and (**B**) more ordered rafts of particles adsorbed to the surface of a tense DDAB vesicle, seen as the outlines in the picture. The particles in

the rafts undergo Brownian motion, restricted by their neighbors. (**C**) Flaccid vesicle covered with particles.[15]

Noteworthy is the work by Lecommandoux and co-workers who prepared polymer vesicles which had magnetic maghemite nanoparticles incorporated into the hydrophobic region of the bilayer.[16] Electrostatic attraction was used in this work as drive for assembly on the outside of the bilayer. Caruso and others have shown by using a layer-by-layer approach that electrostatic attraction can be used successfully in the preparation of a great variety of nanoparticle hybrid capsules.[17] Wooley and co-workers decorated cylindrical micelles with shell-cross-linked knedel-like nanospheres.[18]

In this work it is shown not only that the polymer vesicles can be provided with a colloidal armour made from a variety of nanoparticles, but also that postmodification of the supracolloidal structure through film-formation and formation of a hydrogel can be made in certain condition. Furthermore, ordering and packing patterns, including patterns observed when polymersomes are exposed to a binary mixture of colloids of different size and assembly behaviour when insufficient particles are applied are addressed briefly.

2.2 Experimental

2.2.1 Synthesis of N-(n-propyl)-2-pyridyl methanimine (Propyl ligand)

2.2.1.1 Materials

n-Propylamine (98%), pyridine-2-carboxaldehyde (97%), diethyl ether (98%), magnesium sulphate (98%) All used as delivered.

2.2.1.2 Method

Propylamine (110 mL, 1.23 mol) was added dropwise to a stirred solution of pyridine-2-carboxaldhyde (40 mL) in diethylether (40 mL) at 0 ℃. $MgSO_4$ (12 g) was added afterwards and the solution was stirred at ambient temperature for 10 h. The solution was then filtered and the solvent was removed under reduced pressure. The remaining liquid was dark orange in colour. Purification of the product was proceeded by vacuum distillation in a rotary evaporator at 46 ° C under reduced pressure. The resulting product was a bright yellow liquid. As a final step, the product was kept under a nitrogen atomosphere at 4 ℃.[19]

^{1}H NMR ($CDCl_3$, δ, ppm): 8.53 (1H, m, Pyr-H), 8.30 (1H, s, Pyr-C<u>H</u>=N-), 7.90 (1H, m, Pyr-H), 7.62 (1H, m, Pyr-H), 7.20 (1H, m, Phr-H), 3.62 (2H, t, J=6.4Hz, -C=N-C<u>H</u>$_2$), 1.65 (2H, m, CH_2-C<u>H</u>$_2$-CH_3), 0.85 (3H, t, J=6.3Hz, CH_2-C<u>H</u>$_3$)

^{13}C NMR (CDCl3, δ, ppm): 161.45 (Pyr-C<u>H</u>=N-) 154.4, 149.2, 136.3, 124.3, 121.1 (Pyr) 63.1 (-C=N-C<u>H</u>$_2$-) 23.5 (CH_2-C<u>H</u>$_2$-CH_3), 11.6 (CH_2C<u>H</u>$_3$)

2.2.3 Synthesis of Poly(*n*-butyl methacrylate) -*block*-poly(2-(dimethylamino) ethyl methacrylate) (pBMA-*block*-pDMAEMA) (PBMA-PDMAEMA) by atom transfer radical polymerisation (ATRP)

2.2.3.1 Materials

All organic solvents were of analytical grade. Ethyl α-bromoisobutyrate (98%, Aldrich), 2-(dimethylamino) ethyl methacrylate (DMAEMA, 98%, Aldrich), CuBr was obtained from Sigma-Aldrich and purified before use according to the method of Keller and Wycoff (Keller, R. N.; Wycoff, H. D. *Inorg. Synth*. **1947**, *2*, 1). Prior to use *n*-butyl methacrylate (BMA, 99%, Sigma-Aldrich) were passed through a short column packed with Aluminium oxide (98%, basic, Sigma-Aldrich) in order to remove the radical polymerisation inhibitor.

2.2.3.2 Method

In a typical ATRP procedure, a Schlenk tube was charged with solvent, purified monomer, the initiator, and the Cu(I) catalyst. The mixture was de-aerated by three freeze-pump-thaw cycles, placed under a nitrogen gas atmosphere, and subsequently immersed into a preheated oil bath of 90 ℃. Next the ligand, PPMI was injected into the system by syringe to start the reaction. After the polymerisation, the tube was rapidly cooled and exposed to air. The polymer was purified by precipitation in methanol at -30 ℃ and further dried under vacuum. To synthesise pBMA, 10 g of toluene, BMA (10 g, 70 mmol), ethyl α-bromoisobutyrate (0.185 g, 0.95 mmol), CuBr (0.138 g, 0.96 mmol) were charged in the Schlenk tube. After the system reached 90 ℃, PPMI (0.3 mL, 1.94 mmol) was injected and the solution turned to dark brown. The reaction was performed for 4 hours before quenching with cold water. Molar mass distributions of the polymers were analysed by Gel Permeation Chromatography (GPC) spectra were on a Varian 390-LC equipped with autosampler, refractive index detector utilizing chloroform as mobile phase, and mixed D colums. Specific calibration was carried out using poly(methyl methacrylate) standards with molecular

weight range from 1000 to 1,000,000. M_n calc = 10000 Da. M_n (GPC-$CHCl_3$) = 11600 Da. PDI (GPC-$CHCl_3$) = 1.14. M_n (GPC-THF) = 12000 Da. PDI (GPC-THF) =1.13. To synthesise the block copolymer, the same protocol was applied except using the pBMA product as macroinitiator and DMAEMA as monomer. M_n calc = 15000 Da. Mn (GPC-$CHCl_3$) = 14700Da. PDI (GPC-$CHCl_3$) = 1.10. M_n (GPC-THF) = 15300Da. PDI (GPC-THF) = 1.10

The actual molecular weight was calculated by comparing the two peaks at 4.05ppm and 3.91 ppm in the ^{1}H NMR spectrum, which arise from PDMAEMA and PBMA block respectively.

2.2.4 Synthesis of polymer latex particles by soap-free emulsion polymerisation

2.2.4.1 Material

Divinyl benzene (80%, Fluka), potassium persulfate (KPS, 99%, Aldrich), 4-styrenesulfonic acid, sodium salt hydrate (99%, Aldrich), Ludox TM-40 sol (colloidal silica, 40 wt% in water) were used as received. Prior to use *n*-butyl methacrylate (BMA, 99%, Sigma-Aldrich), ethyl acrylate (EA, 99%, Fluka), methacrylic acid (MAA, 99%, Aldrich), styrene (99%, Aldrich), were passed through a short column packed with Aluminium oxide (98%, Sigma-Aldrich) in order to remove the radical polymerisation inhibitor.

2.2.4.2 Method

Polystyrene, poly(n-butyl methacrylate), and poly(ethyl acrylate-co- methacrylic acid) polymer latexes with monodisperse size distributions were prepared by soap-free emulsion polymerisations. Typically 10 g of monomer, 190 g of water were charged to a double walled glass reactor with an overhead stirrer. The mixture was purged and placed under a nitrogen gas atmosphere. Next the temperature was raised to 70 ℃, after which 0.1 g of potassium persulfate dissolved in 2 mL of water was added to start the polymerisation. Emulsion polymerisations were allowed to proceed for 6 h. The polymer latexes were cleaned by dialysis against deionised water for 7 days.

Particle size distributions of the polymer latexes were measured by dynamic light scattering (DLS) using a Malvern Zetasizer Nano. Data was acquired over three runs of each 12 scans and analysed using a Contin algorithm. Z_{ave} (PS) = 189 nm. PDI (PS) = 0.01. Z_{ave} (pBMA) = 167 nm. PDI (pBMA) = 0.03. Z_{ave} (pEA-MAA) = 137 nm. PDI (pEA-MAA) = 0.05.

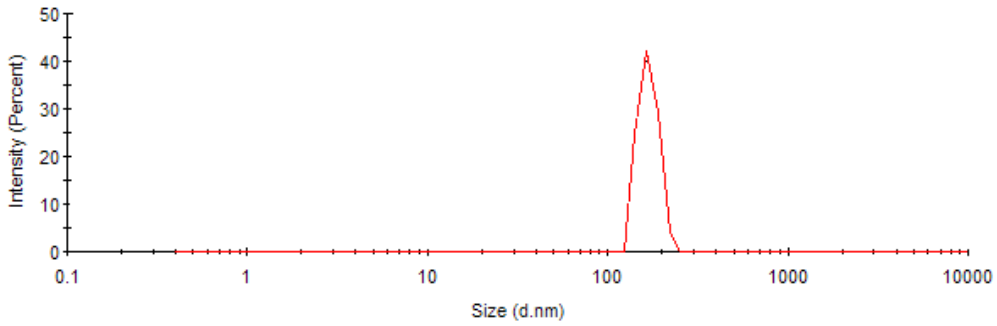

Figure 2.3 Dynamic light scattering result of the size distribution of polystyrene (PS) latex sample. Z_{ave}(d,nm) = 189 nm, polydispersity index = 0.01.

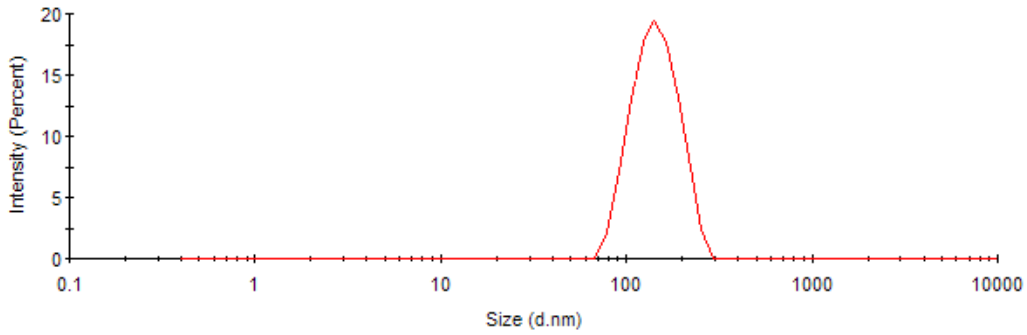

Figure 2.4 Dynamic light scattering result of the size distribution of poly(n-butyl methacrylate) (PBMA) latex sample. Z_{ave}(d,nm) = 167 nm, polydispersity index = 0.03.

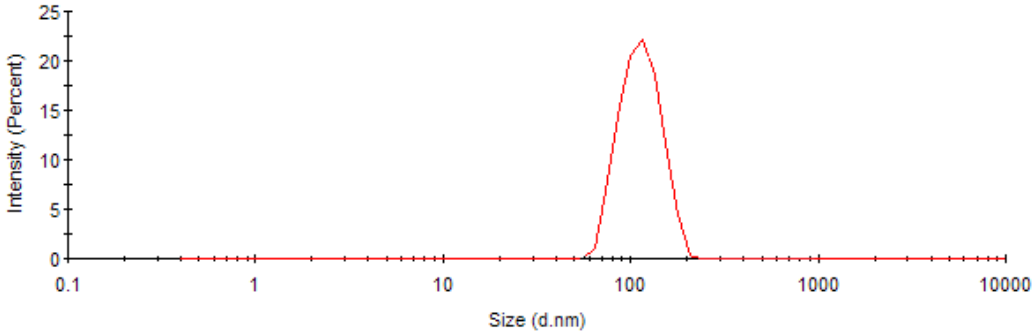

Figure 2.5 Dynamic light scattering result of the size distribution of poly(ethyl acrylate-co- methacrylic acid) (PEA-MAA) latex sample. Z_{ave}(d,nm) = 137 nm, polydispersity index = 0.05.

2.2.5 Preparation of polymersomes by the method of reverse solvent addition

0.01g of block copolymer was dissolved in 10 ml tetrahydrofuran (THF) in a round bottom flask. An aqueous acetic acid solution (pH = 5) was then added using a syringe pump at a rate of 1.5 mL/min whilst stirring was applied up to a total volume of the system of 100 ml. Next the THF was removed by dialysis against the aqueous acetic acid solution. The size distribution of polymersome samples was studied by the same technique for polymer latex particles as abovementioned.

2.2.6 NS-TEM preparation with trehalose presence

Lacey carbon coated copper grids (400 Mesh, Agar scientific) were glow discharged for 5 - 10 seconds at 20 μA using a Cressington 208 carbon coater, to encourage attraction between sample and grid. 8 μl of sample solution with 3% trehalose were placed onto the grid and washed with 100 μl of 1% Uranyl Acetate solution. The final droplet was allowed to remain on the grid for 60 seconds to ensure complete staining. All liquid was blotted off and samples were stored in a TEM grid box before

transferring to the microscope. TEM images were taken on a Jeol-2010 transmission electron microscope at an accelerating voltage of 200 kV. Images were recorded with a Gatan UltraScan™ 1000 camera.

2.2.7 Preparation of particle armoured vesicles

All the samples were prepared by using 2 mL of pBMA-DMAEMA vesicle dispersion that were prepared in 2.2.5 mixed with 2 drops (~0.1 g) of diluted polymer latexes at 1 wt%. The sample of vesicles with PS particles was prepared 24 hours before EM characterisation and kept at 40 ℃ to allow rearrangement of particles on the surface of polymersome. The samples of vesicles with pBMA particles and with silica particles were prepared and imaged after 10 minutes of annealing time. Vesicle samples with pEA-MAA latex particles was prepared as pBMA, and the pH was then adjusted to 8 by introducing pH = 8 sodium hydrogen carbonate buffer solution under the monitor of a pH-meter. The latter to disintegrate the poly(HASE) latex particles.

2.2.8 Cryo-TEM sample preparation

Cryogenic transmission electron microscopy was performed on Jeol 2010F TEM with 200kV Field Emission Gun and Gatan UltraScan^{TM} 4000 camera. All Cryo-TEM samples were prepared using Agar Sc. S166-3H Lacey Carbon Film, 300 Mesh Cu (25). Typically, 5 μL sample solution was pipette onto a grid loaded on the sample preparation device. The grid was then blotted and plunged into liquid ethane cooled by liquid nitrogen. The sample was transferred into the CryoTEM sample holder in the liquid nitrogen and then imaged directly in the EM.

2.2.9 Cryo-SEM sample preparation

Cryogenic scanning electron microscopy was performed on ZEISS SUPRA 55-VP

equipped with cold stage and sample preparation chamber. The accelerating voltage was set to 1-3kV to avoid burning sample and platinum target was used for sputter coating. For the Cryo-SEM sample preparation, typically, the specimen stub was tapped on the surface of the solution to take the sample by capillary action till fulfilled. The stub was then rapidly frozen in the solid nitrogen (<-210 ℃) which obtained by slash the liquid nitrogen (-196 ℃) under vacuum. The sample was stabilised on the pre-frozen stub adaptor and transferred under vacuum to a cold stage in the preparation chamber, which is mounted on the side of the SEM chamber. Both the anti-contamination plates in the chamber and microscope were cooled down to -186 ℃ while both the cold stages were set to -125 ℃. After fracturing the ice on the surface, the sample was then sublimated at -90 ℃ for 1 minute. Sputter coating was applied using platinum target after cooling the sample back down to -125 ℃. The stub adaptor was subsequently transferred under vacuum into the SEM chamber then was located on the cold stage specifically tailored to the SEM.

2.3 Results and discussion

2.3.1 Molecular weight of block copolymer poly(n-butyl methacrylate)-block-(2-(dimethylamino)ethyl methacrylate)

The synthesised PBMA was analysed by Gel Permeation Chromatography (GPC) against PMMA standards using two mixed D columns with THF as the mobile phase. A molecular weight of 12.1 kg mol^{-1} with a PDI of 1.13 was obtained. Although GPC calibrated against PMMA cannot give an absolute molecular weight for the first block the low polydispersity (1.13) does indicate that the length of the polymer chains in the product are of a similar length, as would be expected for this reaction. The block copolymer that was synthesised in the second step was also analysed by GPC, which gave a value of 15.3 kg mol^{-1} with a PDI of 1.10. The absolute molecular weight of PBMA (rather than the PMMA equivalent molecular weight) was determined from GPC data using Benoit's universal calibration equation combined with the Mark-Houwink-Kuhn-Sakurada empirical relation[20]:

$$[\eta]_{PMMA} \times M_{Rel} = [\eta]_{PBMA} \times M_{Abs}$$

$$[\eta] = K \times M^{\alpha}$$

Therefore,

$$M_{Abs} = \left(\frac{K_{PMMA}}{K_{PBMA}} {M_{Rel}}^{1+\alpha_{PMMA}}\right)^{\frac{1}{\alpha_{PBMA}+1}}$$

Where M_{Rel} is the equivalent molecular weight of PBMA relative to PMMA, M_{Abs} is the actual molecular weight of the PBMA and K and α are the Mark-Houwink parameters for PMMA and PBMA polymers in a given solvent. The Mark-Houwink parameters for these polymers in THF at 30 ℃ are given in table 3.1[20-22]:

Polymer	K(10^{-5} dL g^{-1})	α
PMMA	7.56	0.731
PBMA	14.8	0.664

Therefore the actual molecular weight of PBMA block can be derived, which gave a value of 11.8 kg mol^{-1}. After the subtraction of the initiator end group value, the number of BMA unit in the first block was (11800-195)/142.2≈80.

The molecular weight of the PBMA-PDMAEMA block co-polymer was calculated by designating areas of the NMR spectra and assigning these areas a relevant number of protons from the PBMA and PDMAEMA blocks. From the ^1H NMR spectrum, the $–OCH_2–$ hydrogen shows two broad peaks around 4 ppm for each block, which gave an integral ratio of 4.03 to 1.00. Therefore, it can be concluded that the DP of Poly(dimethylamino ethyl methacrylate) block is 20 approximately, which the molecular mass of this block is 157.2×20=3144 g mol^{-1}. This is in good agreement with the molecular weight difference measured by GPC (3.2 kg mol^{-1}).

2.3.2 Unmodified Polymersome formation and EM analysis

A sample of poly(n-butyl methacrylate)$_{80}$-block-(2-(dimethylamino)ethyl methacrylate)$_{20}$ was dissolved in THF at a concentration of 10 g L^{-1} and pH 5 acetic acid solution was added slowly to protonate DMAEMA group in the polymer chains and to induce aggregation and self-assembly of the block copolymer into vesicles. Theoretically, when the hydrophilic block length is around 20% DP, the block copolymer chain may self-assemble into vesicle formation according to the packing parameter theory. However, due to the less fluidity and extremely larger size of the hydrophobic part comparing with classic phospholipids molecule, the block copolymer amphiphiles can hardly be directly suspended in aqueous systems. Therefore, by reverse solvent addition approach, the block copolymer chains were first dissolved in a solvent, which is considered to be good for both blocks. The second step is to slowly add a second solvent, which is good solvent for one block but not the other. As the concentration of the second solvent (normally water) increases, the polymer chains arrange themselves to reduce the unfavourable interactions of hydrophobic block and the water. This process, however, can be “frozen” if the fluidity of the polymer bilayer decreases along with the dilution of the good solvent.

Van Hest and co-workers reported a reverse transformation, from swollen spherical polymersomes in water–dioxane–THF ternary mixtures into stomatocytes upon dialysis against pure water. In their study, due to the high glass transition temperature of the hydrophobic part (polystyrene block) of the vesicle, the shape of the vesicle was frozen at this non spherical shape before the full relaxation of the system. It takes longer for block copolymer chains to rearrange in aqueous media due to the lower mobility of the polymer chains. In extreme cases, when the THF solution of block copolymer was directly added into large amount of aqueous solution, the amphiphiles will mostly self-assemble into micelles rather than vesicles. (Figure 2.6)

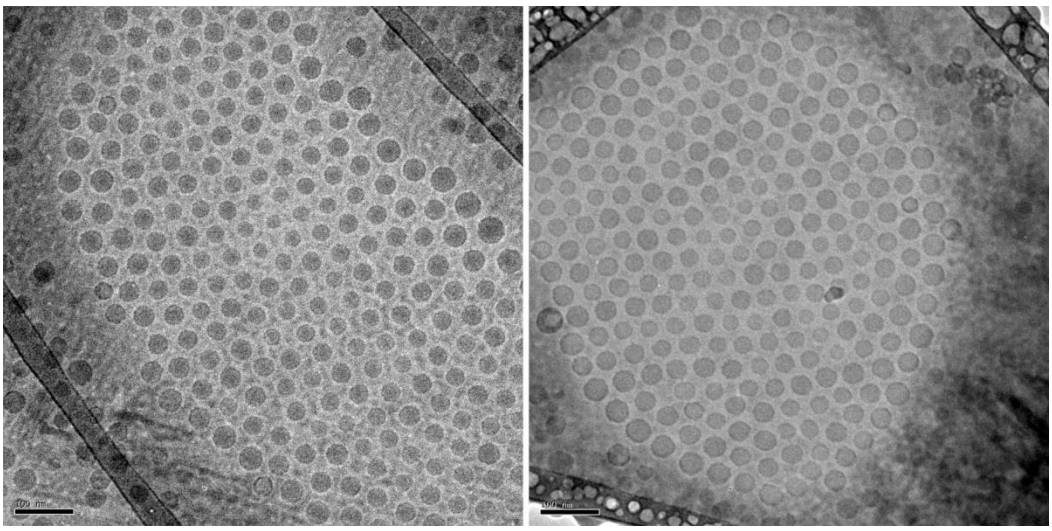

Figure 2.6 Cryo-TEM images of micelles formed from poly poly(n-butyl methacrylate)$_{80}$-block-(2-(dimethylamino)ethyl methacrylate)$_{20}$, the sample was prepared by adding polymer solution directly into aqueous media. Scale bar = 100 nm.

After polymersome formation by reverse solvent addition method, The THF was removed by dialysis against water of pH 5. This was to maintain protonation of the *tert*-amino groups (pK_a, 8.5). The unilamellar nature of the cationic polymersomes was confirmed by cryogenic transmission electron microscopy (cryo-TEM).(Figure 2.10) Dynamic light scattering measurements showed an average diameter of approximately 1.0 μm with a dispersity of 0.14 indicating a broad size distribution of vesicles. (Figure 2.7)

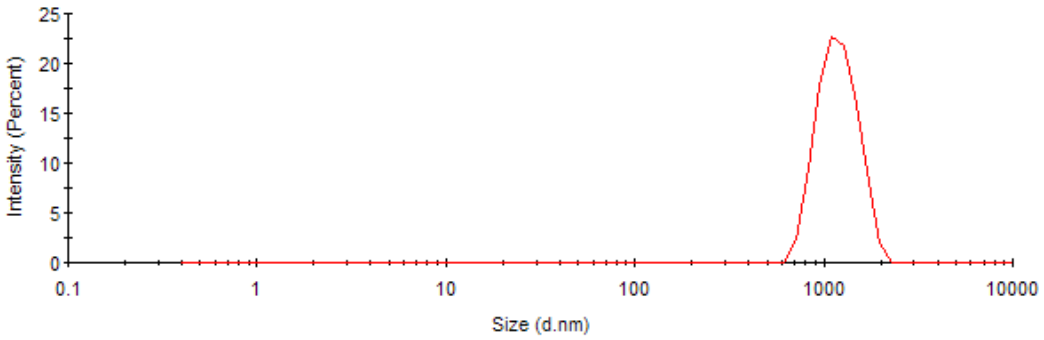

Figure 2.7 Dynamic light scattering result of the size distribution of polymersome sample prepared from PBMA-block-PDMAEMA. Z_{ave}(d,nm) = 1109 nm, polydispersity index = 0.14.

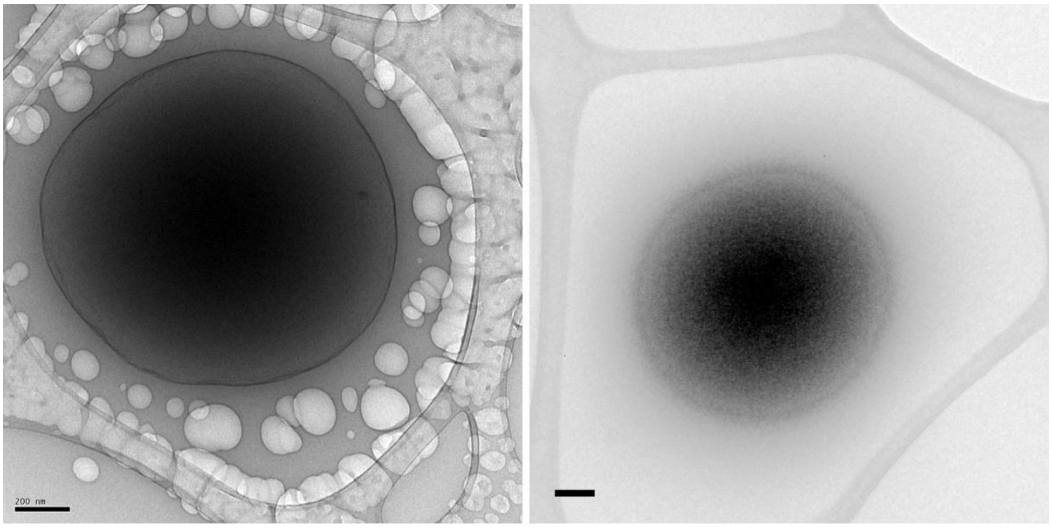

Figure 2.8 Ambient temperature negative stain TEM images of the polymersomes with 3% trehalose presence. Scale bar = 200nm.

Trehalose is believed to replace the hydrogen bonds between water and the hydrophilic group with hydrogen bonds between its own OH groups and the DMAEMA block, thus preventing bilayer disruption and maintaining polymer bilayer integrity in the absence of water.[23, 24] The shell of the vesicle, however, appears to be thinner than that of under Cryo-TEM due to the dehydration of the sample.

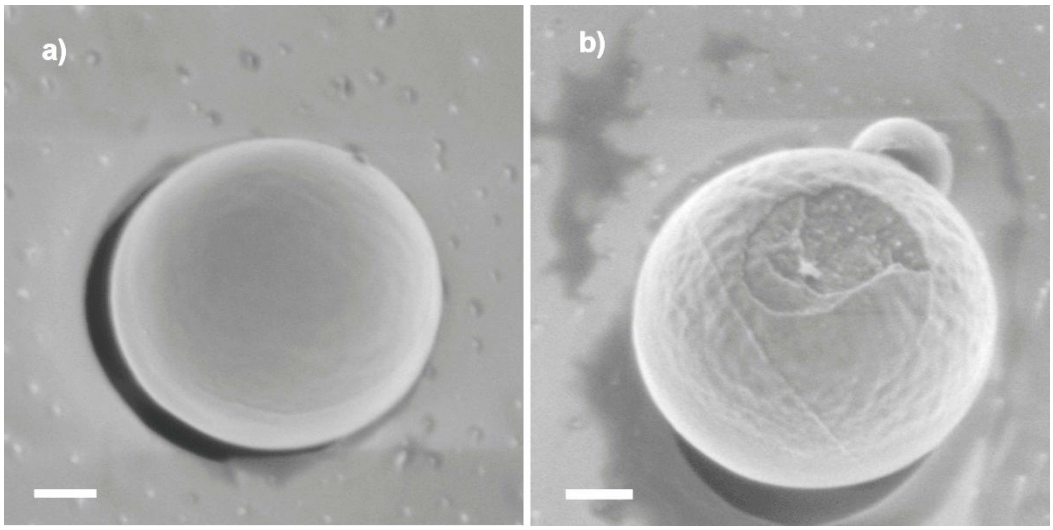

Figure 2.9 Cryo-SEM images of polymersomes formed from block copolymer. a) A polymersome with smooth surface. b) A polymersome after cold fracture shows the interface of the bilayer shell. Scale bar = 200nm

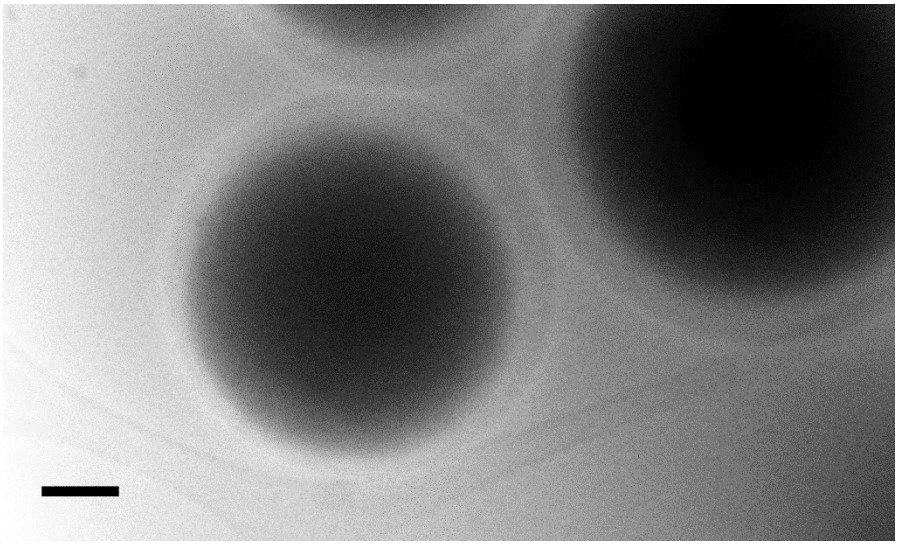

Figure 2.10 Cryo-TEM image of polymersomes formed from block copolymer. The dark core arises from thick ice, which the electron beam can hardly penetrate, however, at the edge of the polymersomes, the contrast shows a dark corona arises from the polymer bilayer. Scale bar = 200 nm

The polymersomes formed from poly(n-butyl methacrylate)$_{80}$-block-(2-(dimethylamino)ethyl methacrylate)$_{20}$ show that a smooth and spherical structure

was formed, which indicates that during the solvent addition process, the system was allowed relaxation (Figure 2.9 and 2.10). In Figure 2.9 (b), one single polymersome was broken at the top by cold fracture in the cryo-SEM sample preparation chamber. It clearly shows that a layer of polymer shell was formed and the inside content of the vesicle is the same as the background, which is believed to be ice. In summary it is concluded that $PBMA_{80}$-b-$PDMAEMA_{20}$ forms micelles when directly adding polymer solution into the aqueous environment regardless of the right HLB value for vesicle formation. However, when the addition process is reversed, polymersome solution was successfully produced and one effect of the solvent (THF) is to fluidise or plasticise the hydrophobic block, allowing it to flex and rearrange into vesicular and other structures, when the minimum energy conditions allow.

2.3.3 Polymersomes armoured with polystyrene latex particles

As the polymersomes formed from $PBMA_{80}$-b-$PDMAEMA_{20}$ show a positively charged behaviour in aqueous at pH 4-5, it was proposed to make use of electrostatic attraction of negatively charged colloids onto the positively charged polymer vesicles as adhesion force. Assembly took place through collision of the colloidal particles with the polymersome, hereby relying on Brownian motion. Typically, to a 2 mL polymersome dispersion in water at pH 5, 0.1 g of a 1 wt % aqueous dispersion of colloids was added. Figure 2.11 is a cryogenic scanning electron microscopic (cryo-SEM) image of a collection of polymersomes armoured with a layer of monodisperse polystyrene latex particles (average particle diameter ca. 190 nm). Images resemble the assembly of particles on emulsion droplets, thereby protecting the droplet from coalescence through Pickering stabilisation.[25-27]

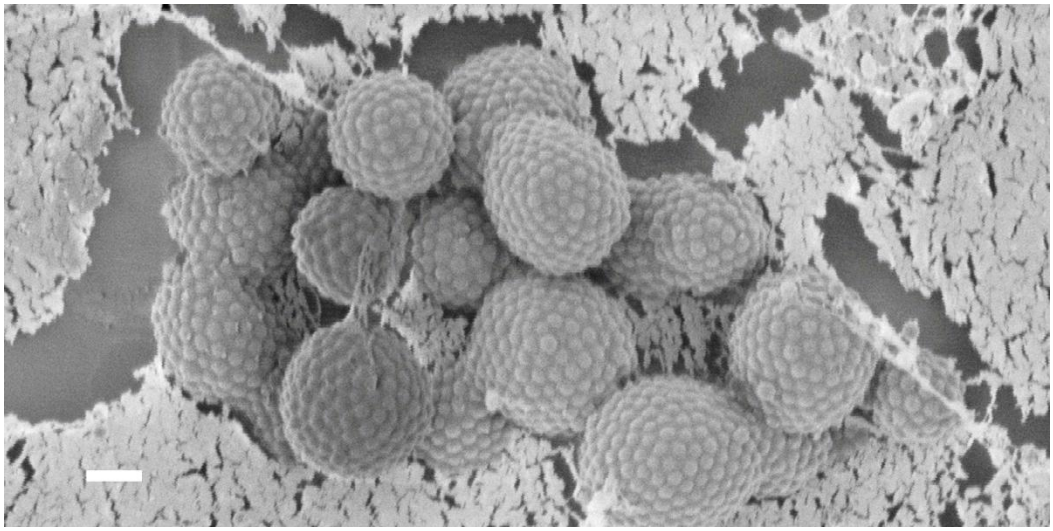

Figure 2.11 Cryo electron microscopy images of polymer vesicles armoured with polystyrene latex spheres. Scale bar = 500 nm.

Considering the size of the objects that were analysed under Cryo-SEM, longer sublimation time should be allowed in order to remove sufficient ice that covers the polymersomes. The average sublimation rate at -95 ℃ is 1 μm per minute from observation, however, this can vary slightly depending on the cold stage type as well as the temperature of anticontamination plate. Approximately 3 minutes sublimation was allowed for the sample in Figure 2.11, which allows the entire layer of the polymersomes exposed for observation. What is stricking in this image is the packing order of the polystyrene spheres onto the surface of the vesicle. Collisions as a result of Brownian motion are random, which implies that particles can rearrange themselves once adhered, and/or that adhesion is reversible. This ordering process occurs in order to achieve the optimal packing configuration through minimisation in free energy. The use of monodisperse particles plays a key role in achieving the high packing order and thus 2D crystallisation of the particles on the soft interface.[28, 29] Employment of particles with a broader size distribution would reduce order fading out grain boundary scars.[29] (See Figure 2.12)

The time scale to fully cover the polymersomes can be estimated by linking packing patterns to the Smoluchowski and Stokes−Einstein diffusion equations, with indicative values in the order of one minute.[27]

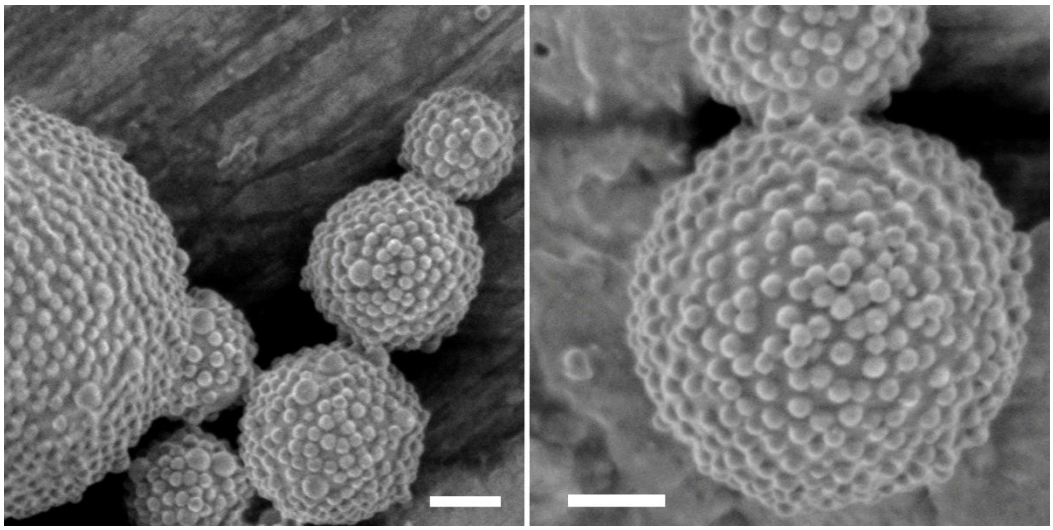

Figure 2.12 Cryo-SEM images of polymersomes armoured with PS particles with a broader size distribution. Scale bar = 500 nm.

In order to relax the system and obtain ordered packing patterns, an annealing time exceeding this time scale by several orders of magnitude needs to be allowed. Indeed a more random arrangement of polystyrene spheres onto the polymer vesicles would be observed if the samples were quenched and analysed by cryo-SEM after 10 min of incubation time. In our annealed systems, Fibonacci number patterns was observed, which suggest that the armoured polymersomes can relax to adopt a stress-free packing geometry.[30] (See Figure 2.13)

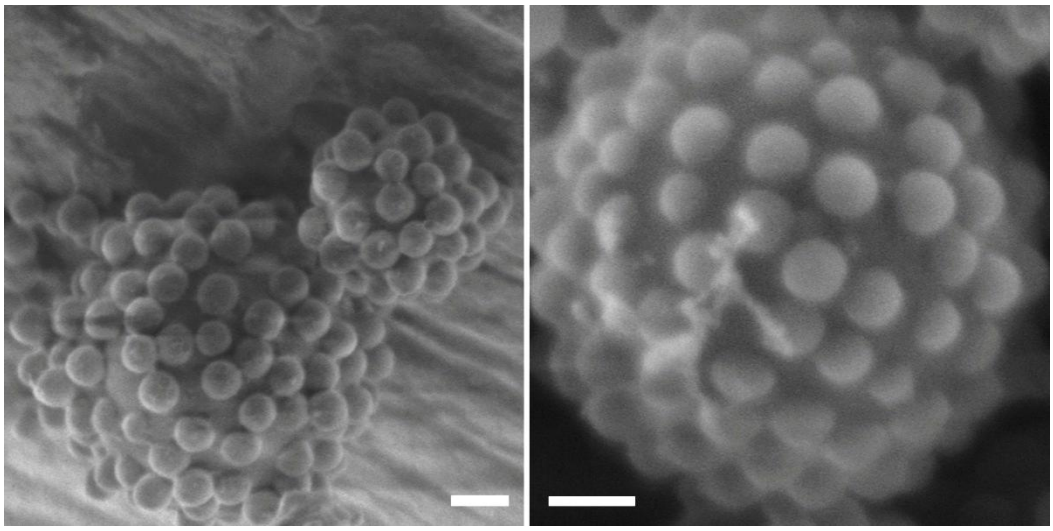

Figure 2.13 Cryo-SEM images of polymersomes covered with PS particles prepared about 10 minutes after mixing. Scale bar = 200 nm.

Cryo-TEM analysis was also performed in this case. The diameter of most polymersomes is approximately 1 μm and an object with this range of size tends to then attract more water around during sample preparation and forms thicker ice layer, which will prevent electron beam from penetrating the sample. Therefore, in some of the cases, the polymersomes with larger size absorb more energy from electron beam and result in polymersomes with "cooked" inside content when exposed under the beam for too long. Nevertheless, this phenomenon in the other hand shows more clearly the hollow structure of the polymersomes and gives better idea of the morphology. (See Figure 2.14)

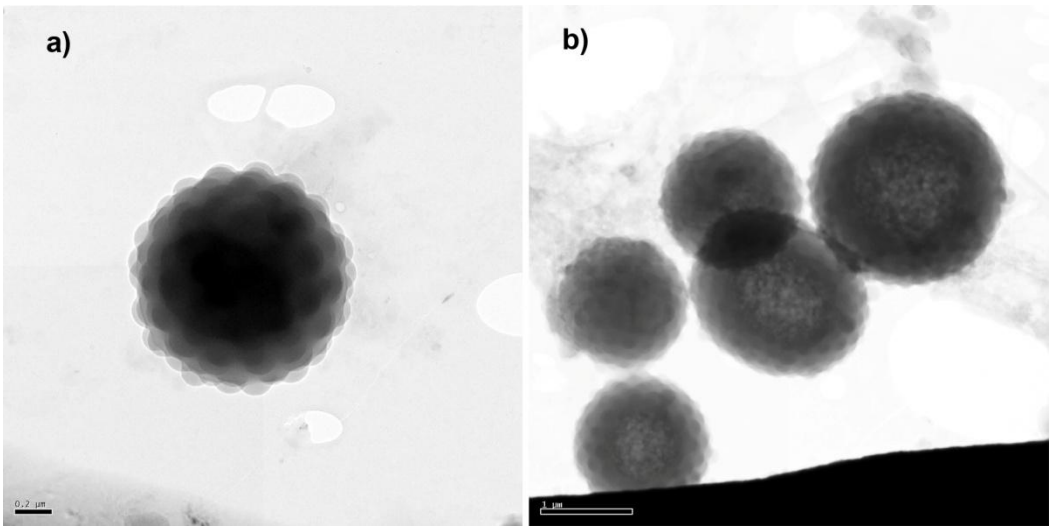

Figure 2.14 Cryo-TEM images of polymersomes armoured with PS particles exposure time a) 2 seconds b) 10 seconds. Scale bar = (a) 200 nm and (b) 1μm.

Again, the cryo-TEM analysis shows a well packed surface morphology, which is in agreement with the observation under cryo-SEM in Figure 2.9. More images taken by cryo-EM were shown in Figure 2.15.

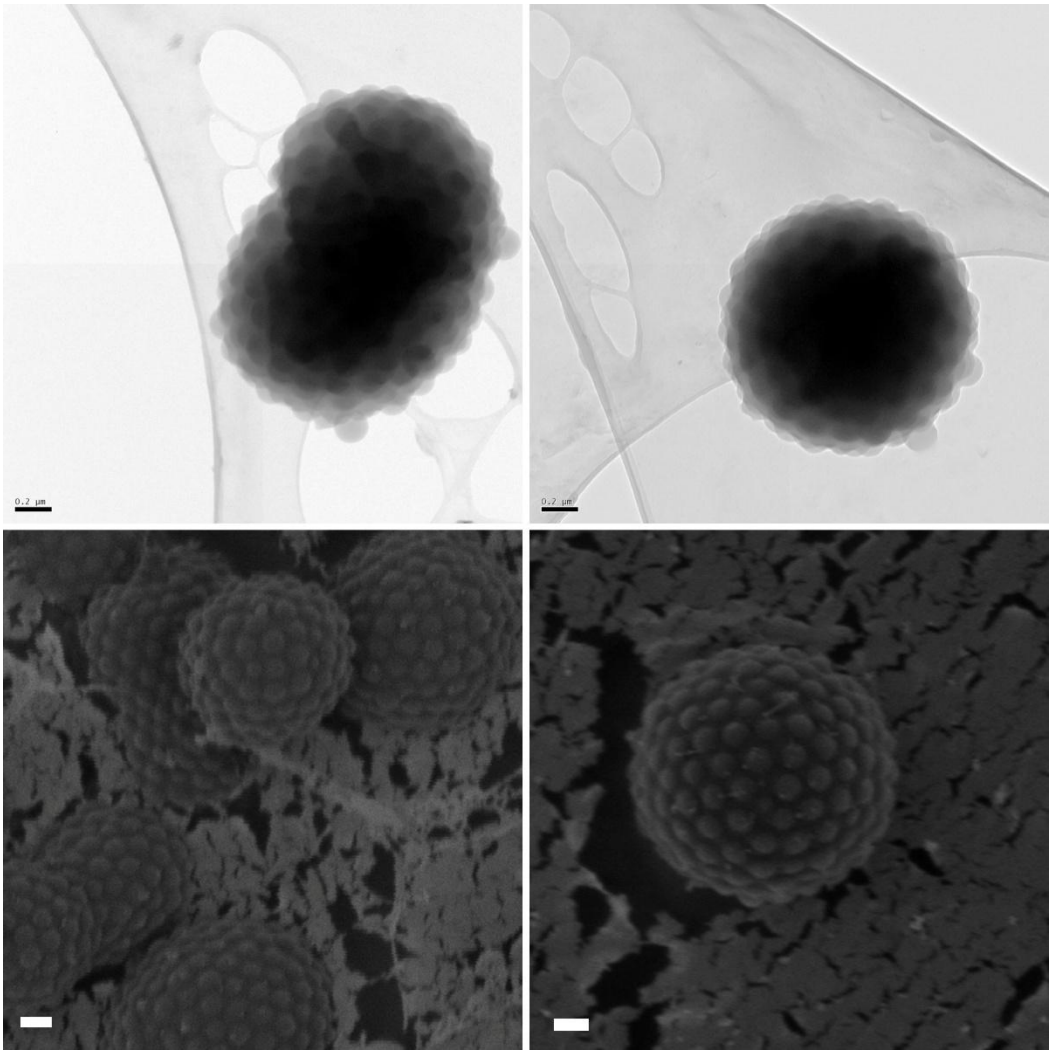

Figure 2.15 Cryo-TEM (top two) and Cryo-SEM (bottom two) images of polymersomes covered with PS particles. Scale bar = 200 nm

2.3.4 Polymersomes armoured with inorganic particles

By exploring the versatility of the method, it was therefore investigated to not only make use of polystyrene latex particles as colloidal building blocks for the supracolloidal armour, but also to use inorganic nanoparticles. First, TiO_2 particles was tried, which has an average size of 400 nm with broad size distribution. Within the sample preparation process, the polymersome solution showed more and more transparent after mixing with TiO_2 particle suspension in water. The reason of which is of the high density of titanium oxide particles (4.23 g cm^{-3}), which causes the sedimentation of the vesicles. Furthermore, due to the size and shape of these particles, it is even harder for the polymersomes to be fully covered by the particles. Figure 2.16 shows that polymersomes were rarely covered by any TiO_2 particles and large particles even causes coagulation of some polymersomes.

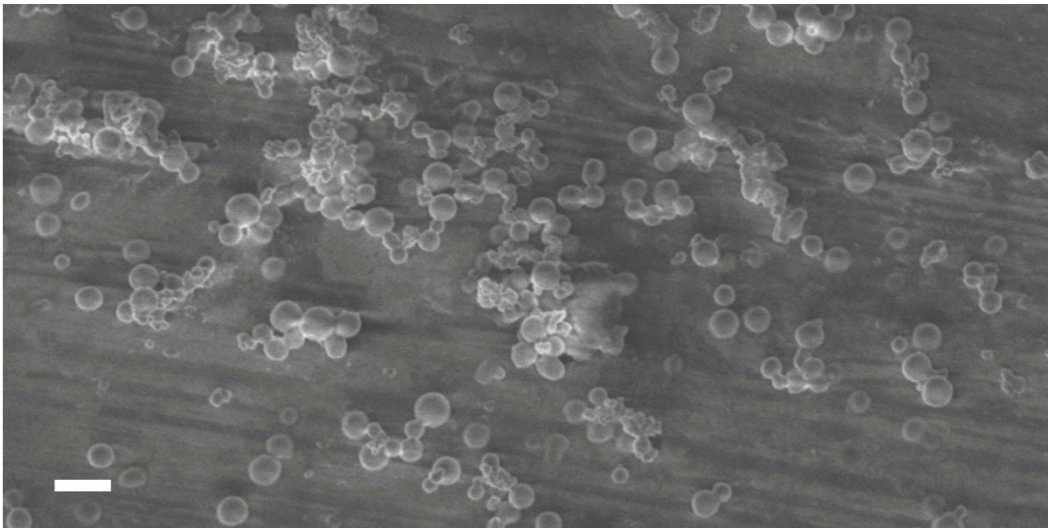

Figure 2.16 Cryo-SEM image of polymersomes mixed with TiO_2 particles. Scale bar = 1 μm

It is therefore, more worthwhile to try a regularly shaped and smaller sized colloidal object. Cryo-TEM images in Figure 2.17 and 2.18 show indeed the cationic polymersomes can be armoured with a layer of silica nanoparticles of average diameter of approximately 24 nm (Ludox-TM40), resulting in a hybrid organic−inorganic vesicular structure. It is evident from this image that the hollow

bilayer-based structure of the vesicle is preserved and that the particles are adhered to the outer surface. Packing patterns of the silica nanoparticles are less ordered as a result of their more polydisperse nature. (Figure 2.19)

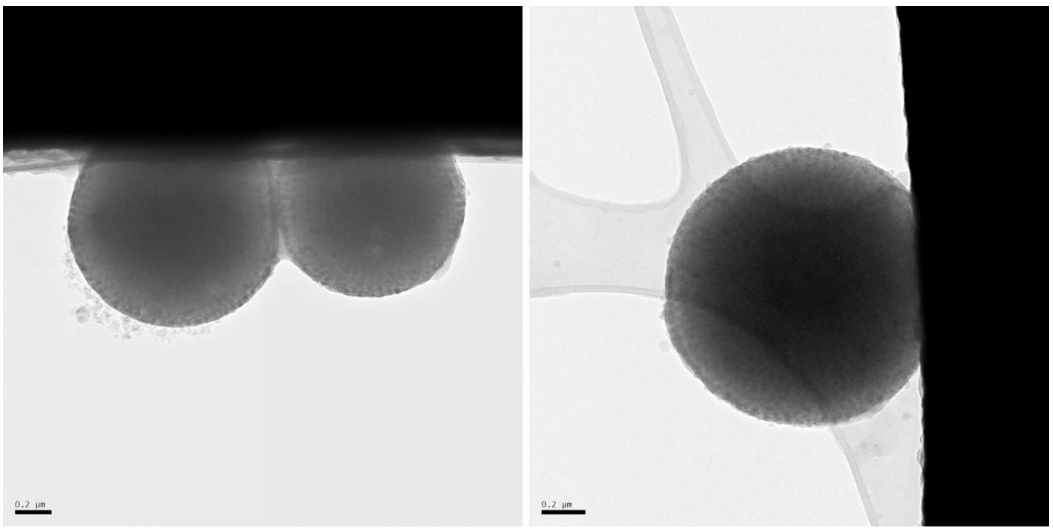

Figure 2.17 Cryo-TEM images of polymersomes armoured with silica particles. Focus is on the equatorial plane which shows clearly only the outside of the polymersomes are covered with particles. Scale bar = 200 nm.

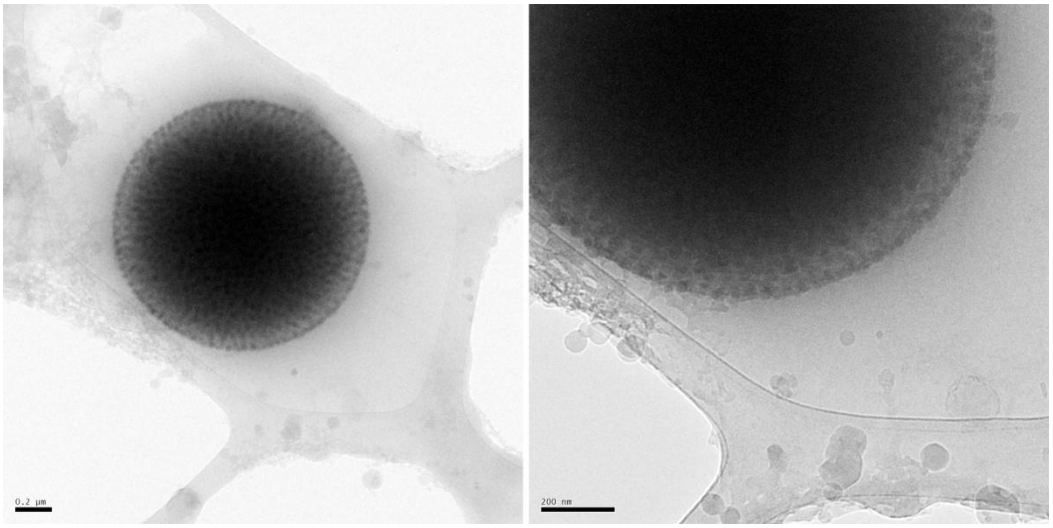

Figure 2.18 Cryo-TEM images of polymersomes armoured with silica particles. A close-up look of the object shows a dark corona formed from silica, which suggests that the surface was fully covered with these inorganic objects. Scale bar = 200 nm.

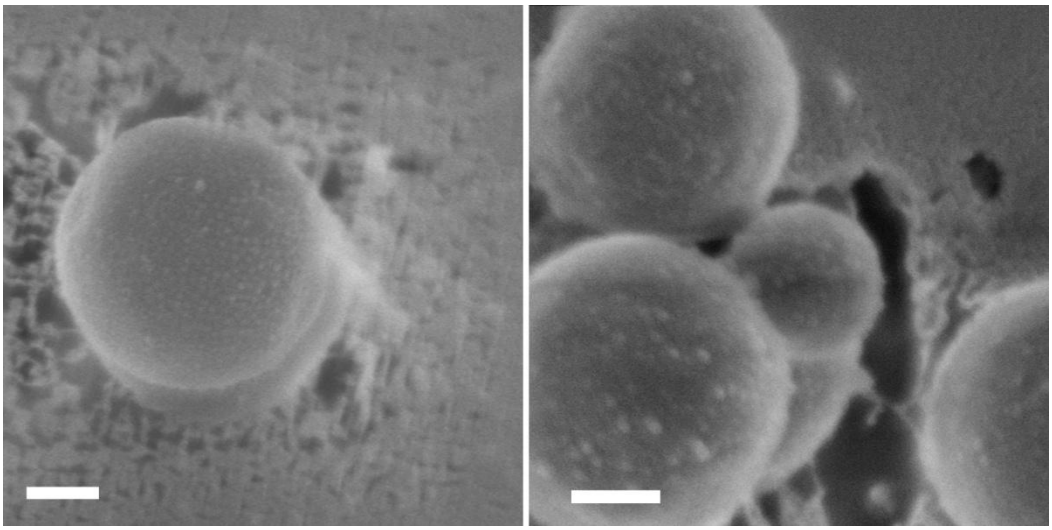

Figure 2.19 Cryo-SEM images of polymersomes armoured with silica particles show less ordered packing patterns compared with the ones with PS particle armour. Scale bar = 200 nm

Unlike TiO_2 particles, these anionic silica particles provide not only full coverage armour to the cationic polymersomes but also maintain the stability of the system. The sample remained translucent without any precipitation in the sample vial and the polymersomes that were observed under cryo-SEM were mostly found in the ice rather than on the sample stub. One of the possible reasons is that the silica particles have a higher charge density than the bilayer surface, which not only neutralised the positive charge of the vesicle but also provided extra negative charge on the outside. The overall charge of the polymersomes was then reversed and therefore maintains the colloidal stability. On the other hand, differ from TiO_2 particles, these silica particles have much less density as well as the average size, which leads to a less chance of precipitation.

2.3.5 Polymersomes armoured with film forming nanoparticles.

The polymersomes can be provided with autohesion and thus film-formation of an armour of "soft" polymer latex spheres, effectively wrapping the polymer vesicle in a plastic bag. Therefore the use of negatively charged poly(butyl methacrylate) latex particles as colloidal building blocks was made. From the cryo-SEM analysis (Figure 2.20), it can indeed be observed that the armour no longer is composed of a collection of discrete assembled polymer latex spheres, but that the particles have undergone partial film formation.

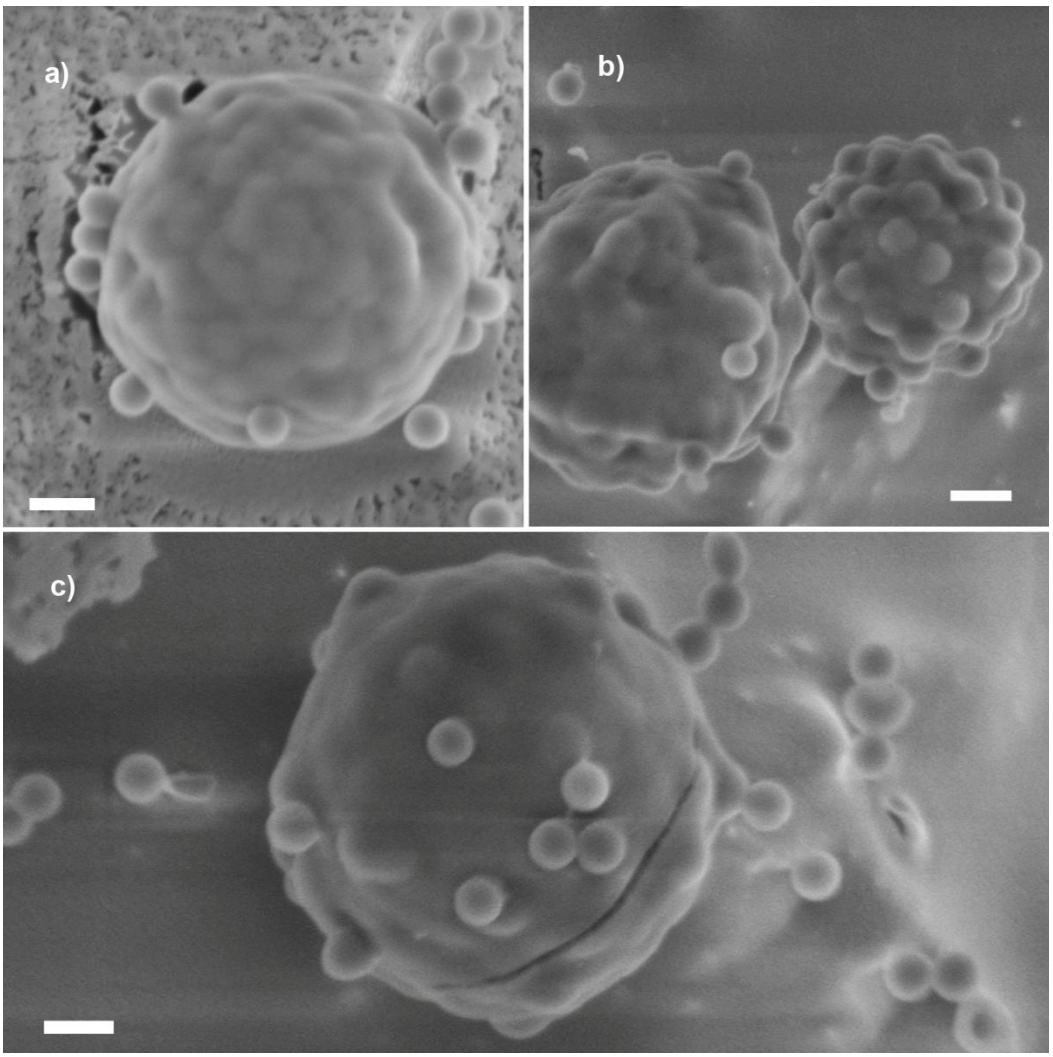

Figure 2.20 Cryo-SEM images of polymersomes armoured with PBMA nanoparticles. The crevasse shown in (c) suggests a structure of integrated colloidal armour instead of individual particles. Scale bar = 200 nm

Poly(n-butyl methacrylate) has a glass transition temperature around 15 ℃, which is not "soft" enough to film form at ambient temperature. However, in this case, film formation of PBMA nano spheres was observed on the surface of the polymersomes. The sample was prepared in the same way as the one with PS particle armour without taking any annealing procedure. One possible explanation is that the electrostatic stabilisation was weakened by the neutralisation of the two opposite charges. Therefore the PBMA particles can no longer repulse each other after adsorption. From Figure 2.20 (b) and (c) it can be clearly seen that some part of the polymersomes have more than one layer of PBMA particles, caused by net positive charge after one layer coverage, which suggests a higher charge density on the polymersome surface than on the PBMA particles.

Furthermore, a sample of polymersomes mixed with latex spheres made of butyl acrylate and methyl methacrylate in presence of approximately 1.5 mol% of 2-ureido-4-pyrimidinone methacrylate monomer (UPy monomer). The method has been reported by Yunhua and co-workers [31]. This UPy containing soft particles has a T_g of -4 ℃ which not only can be film formed at ambient temperature but also provides stronger mechanical properties due to the multiple hydrogen bonding interaction between UPy groups. A sample of the mixture was analyzed by SEM at ambient temperature instead of cryogenic mode. Figure 2.21 shows that the polymersomes survived under vacuum at ambient temperature and maintained the spherical shape by the protection of the film formed from latex spheres. Differ from PBMA film, particle packing patterns can hardly be seen on the UPy containing PMMA-PBA film. The adhesion between armoured polymersomes and sample stub surface is very common, which can be attributed to the low glass transition temperature and the strong interaction between UPy groups. It has been observed that the polymersome solution shows significant white mini meter sized precipitation approximately 30 minutes after the sample preparation, which is considered to be the aggregation of these UPy containing polymer film covered vesicles.

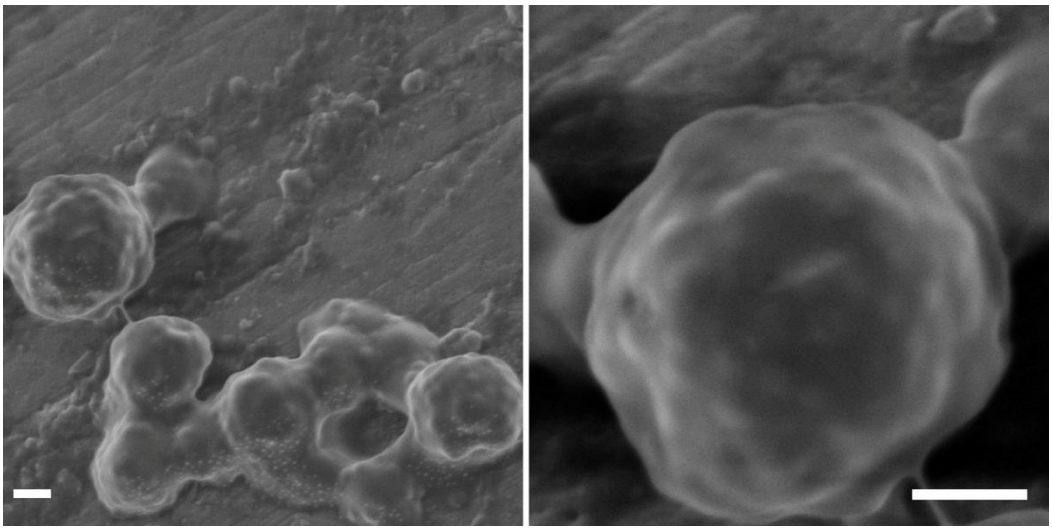

Figure 2.21 SEM images of polymersomes armoured with UPy containing soft particles taken at ambient temperature. Scale bar = 500 nm.

In summary, polymersomes formed from poly(n-butyl methacrylate)$_{80}$-block-(2-(dimethylamino)ethyl methacrylate)$_{20}$ can be coated with a layer of film formed from soft nanoparticles. The temperature is not necessarily to be adjust to the ideal film formation temperature as the heterocoagulation process enables the soft particles to film form at the surface by neutralising their surface charge thus removing the repulsion between each other. It is plausible to think that not only the thickness of the wall was increased, but also an extra layer of protection composed of stronger substances was provided. Considering the fact that vesicles were more and more studied for nanocontainer use, particularly in the area of drug delivery system and nano-reactors, this process can not only be of great value to control the overall rigidity of the reinforced polymersomes, but also can be an effective tool to alter its permeability and thus control for the release or uptake of desired substances.

2.3.6 Polymersomes armoured with gel formation latex spheres.

Based on the observation result of film forming latex particles armoured polymersomes, another type of supracolloidal armour of latex spheres which had the ability to dissolve partially and form an aqueous based gel-phase was provided to the polymersomes. It is hereby plausible to make use of waterborne polyHASE, which consists of polymer latex spheres made from a mixture of ethyl acrylate (60 wt %) and methacrylic acid (40 wt %). Emulsion polymerisation at low pH yields latex spheres which upon pH increase to approximately 7.0 unwrap their polymer chains and expand into a gel. Figure 2.22 shows that at lower pH, the polymersomes were covered with a thin layer of PEA-MAA film, the slightly uneven surface that arises from particle packing pattern is in a good agreement of the low T_g of the polymer particles.

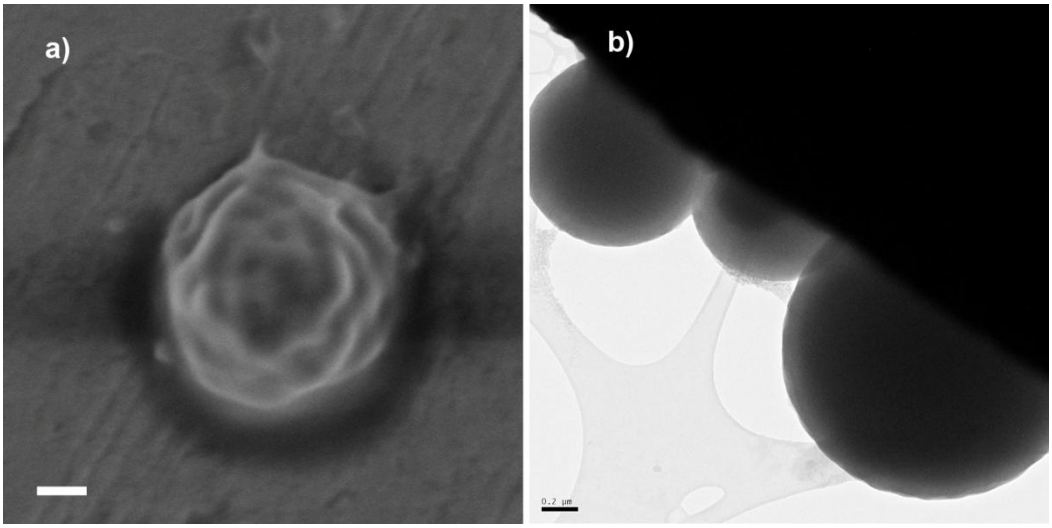

Figure 2.22 (a) Cryo-SEM and (b) Cryo-TEM images of polymersomes armoured with PEA-MAA film formed from latex spheres at pH 4. Scale bar = 200 nm.

After adjusting the pH by adding sodium hydrogen carbonate buffer solution into the system, the carboxylic group in the film was then partially deprotonated and hereby dissolves in the aqueous. A gel phase consists of over 90% of water was formed and wrapped around the polymersomes. (See Figure 2.23)

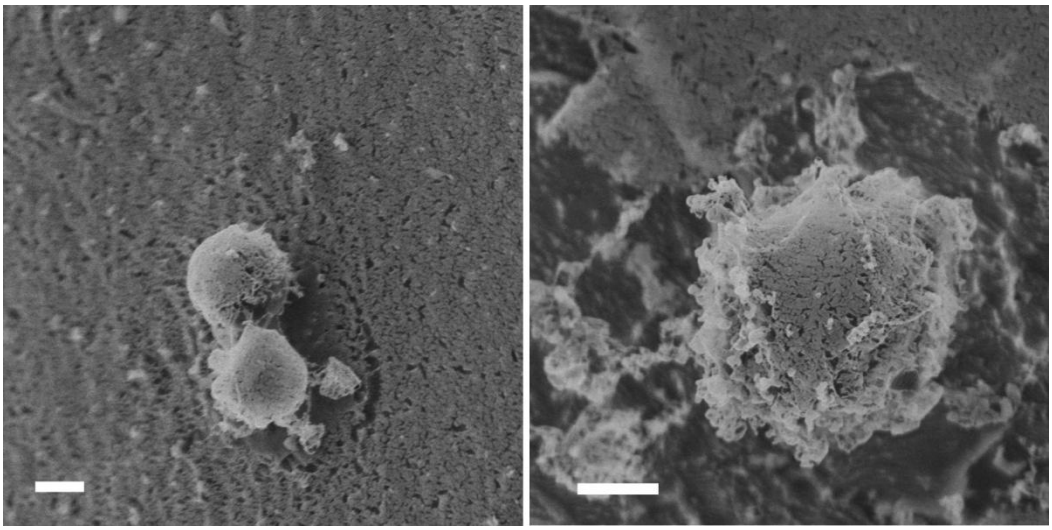

Figure 2.23 Cryo-SEM images of polymersomes covered with a layer of polyHASE gel. Scale bar: 1 μm.

Before cryo-SEM imaging, the sample was heated up from -125 ℃ to -90 ℃ in the preparation chamber in order to sublimate most of the water that covered the objects. After 5 minutes sublimation, approximately 5 μm thick ice was removed from the surface and thus the remaining porous network that wrapped around the polymersomes was mostly polymer chains.(white fabric like structure in Figure 2.23) The polymer gel provided not only a thicker layer of armour but also provided steric stabilisation to the polymersomes. (Figure 2.23) Moreover, cryo-TEM images in Figure 2.24 show that at some points of the armoured polymersomes, the outline of the armour surface and the surrounding water phase faded out due to the hydration of the armoured layer, which weakened its contrast in cryo-TEM imaging. This could result in a polymersome with potential stealth surface property when applying in *vivo* as the major part of this gel armour consists of water, which potentially can be considered safe by the immunity system.

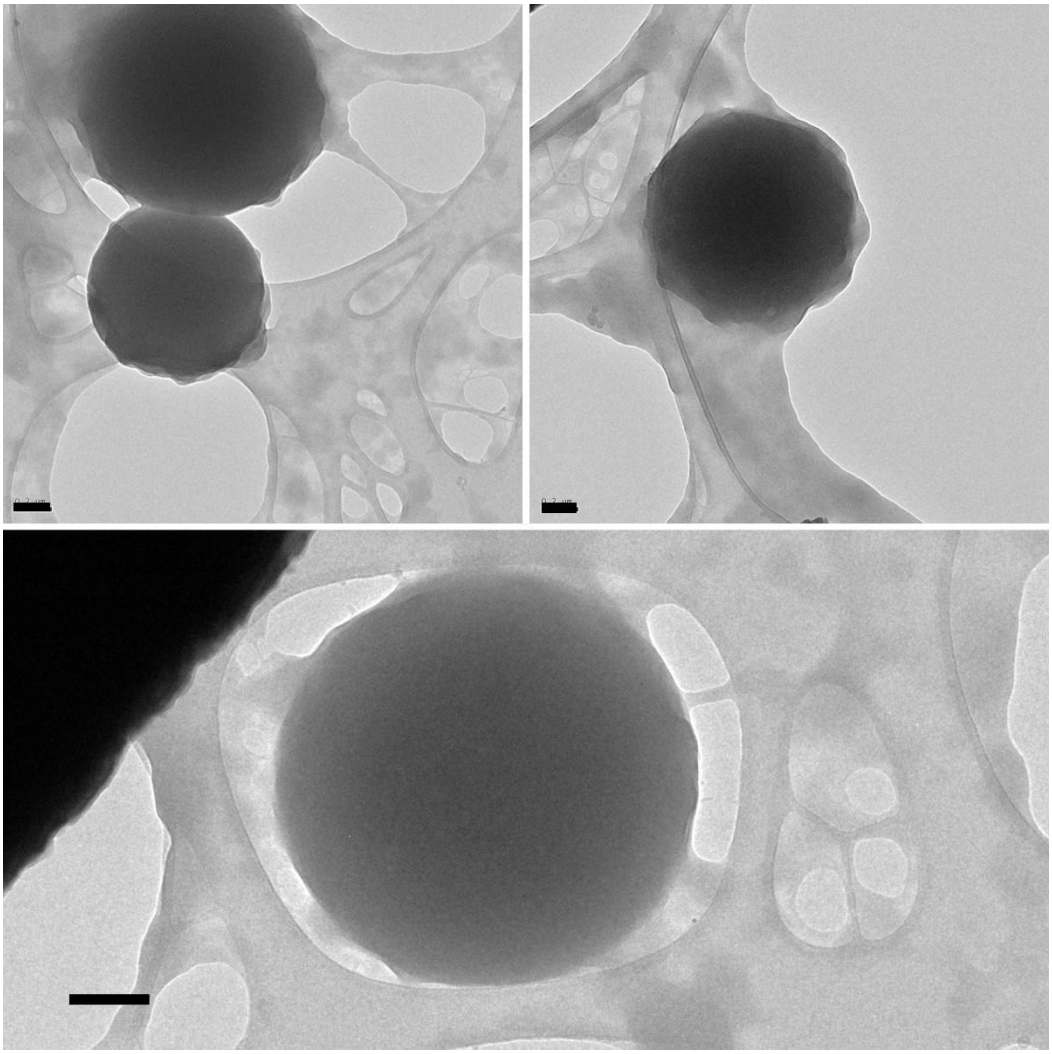

Figure 2.24 Cryo-TEM images of PEA-MAA latex particle armoured vesicles after pH = 8 buffer solution treatment. The particle armour was film formed in the acidic environment. After adjusting the pH to 8, the PEA-MAA armour formed a layer of gel. Scale bar = 200 nm.

2.3.7 Asymmetric assembly of nano particles on polymersomes

As described in 2.3.3, in order to obtain ordered packing patterns on the polymersome surface, both monodisperse particles with sufficient annealing time are required. The use of monodisperse particles plays a key role in achieving the high packing order and thus 2D crystallisation of the particles on the soft interface. More importantly, the annealing time with indicative value in the order of hours or even days needs to be allowed due to the less fluidity of the polymer bilayer compared with lipids system. Figure 2.25 shows a significant change when the system was allowed to relax over time. Image (a) was taken immediately after quenching PS latex particles into the vesicle solution. It is observed that the surface of the polymersomes has yet been fully covered due to the short time that allowed for heterocoagulation of the particles, while the polymersome in (b) starts to show ordered packing patterns. After 24 hours annealing, a beautiful hexagonal packing pattern was observed on the polymersome surface. It is worth noting that the particles seem to sink into the bilayer over time, as shown in (c), only halves of the particles can be seen. However, it is unclear whether these particles only cause deformation of the bilayer or have already been embedded in the bilayer.

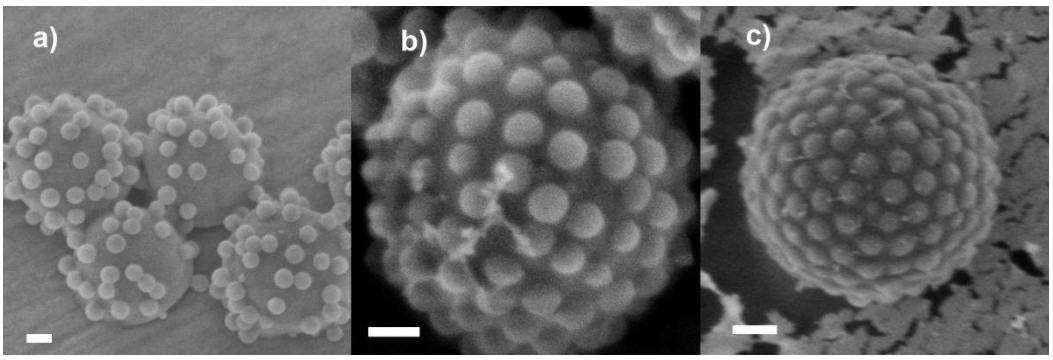

Figure 2.25 Cryo-SEM images of polymersomes armoured with the same PS particles. Samples were analyzed (a) 1 minute (b) 4 hours (c) 24 hours after mixing. Scale bar = 200 nm.

Nevertheless, it is clear that the fluidity of the bilayer plays the key role of rearrangement of adsorbed particles. Therefore, one question should be asked: Will

packing geometries of supracolloidal armour form if polymer vesicles are exposed to a binary mixture of negatively charged polystyrene latex spheres of different sizes?

To study the annealing process of two different sized particles on the polymersomes, polystyrene latex spheres of 200 nm and 120 nm in diameter were applied to the system. Annealing time of 14 hours was allowed before Cryo-SEM analysis.

The mass ratio of the large and small particles in the two samples was 3:1 and 1:1 respectively, thus the theoretical occupied area percentage of small particles can be calculated as follow:

$$P = \frac{\frac{1}{V_{120}} A_{120}}{\frac{B}{V_{200}} A_{200} + \frac{1}{V_{120}} A_{120}}$$

V is the volume of each particle, A is the area that each particle occupied on the surface and B is the mass ratio between large and small particles.

Therefore,

$$P = \frac{1}{\frac{V_{120} A_{200}}{V_{200} A_{120}} B + 1} = \frac{1}{\frac{D_{120}}{D_{200}} B + 1} = \frac{1}{\frac{3}{5} B + 1}$$

D is the diameter of the particle.

For the two samples that have been studied, the area percentage that occupied by small particles are 36% and 63%.

Cryo-SEM images in Figure 2.26 shows a good agreement to the area occupation percentage that was calculated for the small particles. The surface of the polymersomes was mostly covered by large particles, which show only random packing patterns even after a relative long time annealing process. However, the small particles, which have a diameter of 120 nm, shows more ordered packing geometries. (Green area) Ideally, on a sheet of unilamellar bilayer with infinite area, particles can freely move and rearrange into more ordered packing patterns in order to achieve the optimal packing configuration through minimisation in free energy. However, in actual observation, the surface area of each polymersome is limited. Once it is almost fully covered as shown in Figure 2.26, the space that allow particles' rearrangement is

very little, thus restricts the particle immigration rate in a similar way of a traffic jam.

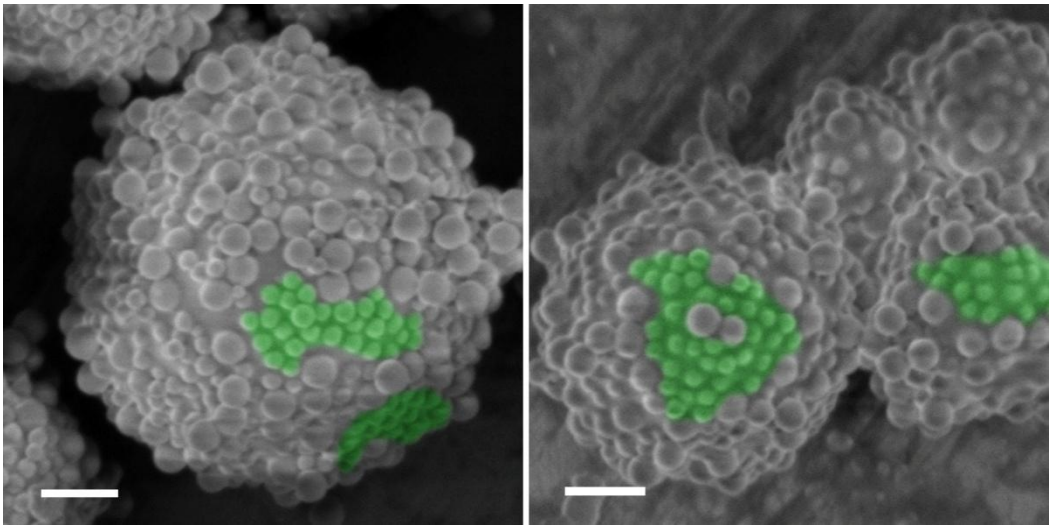

Figure 2.26 Cryo-SEM images of polymersomes armoured with a mixture of two different sized polystyrene latex spheres. The total mass ratio between large and small particles was 3:1. Green area shows the partly ordered packing behaviour of the small particles. Scale bar = 500 nm.

In the sample with a large to small particle mass ratio of 1:1, the actual area percentage that occupied by small particles seems to be significant higher (82%) than calculated value (63%). (See Figure 2.27) It is believed that with the same interaction depth between the particles and the bilayer, smaller spheres have relatively larger adsorbed surface area to exposed surface area ratio, which indicates a stronger adhesion than larger particles. Moreover, after first few minutes' assembly of the particles, the space in between particles on the bilayer has decreased, which produces numerous small gaps before particles close packing. This results in a less probability for the large particles to be adsorbed on the surface especially when the area of the gap is much smaller than of which the particle occupies.

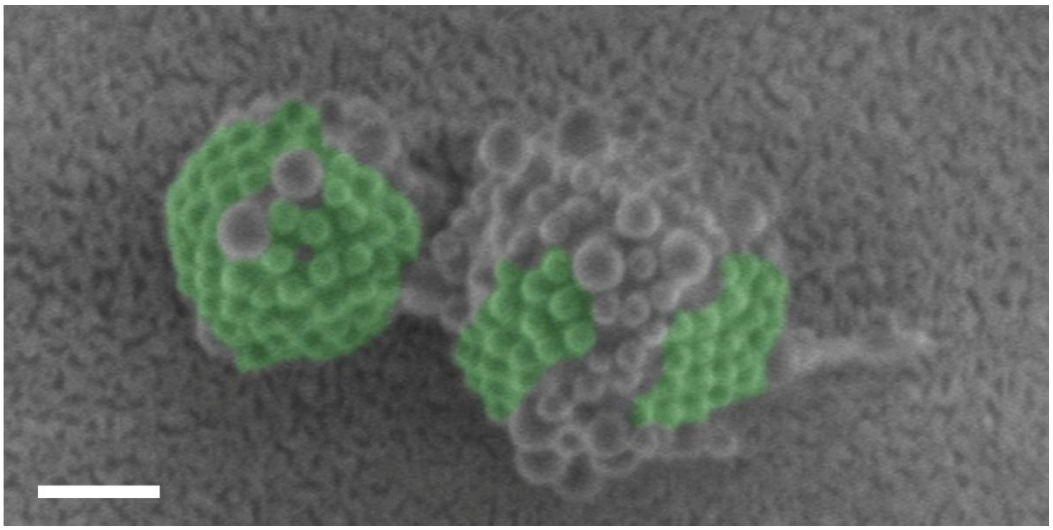

Figure 2.27 Cryo-SEM images of polymersomes covered with a mixture of two different sized PS spheres. The total mass ratio between the two is 1:1. Scale bar = 500 nm.

The packing patterns of the small particles shows more ordered geometry in this sample as expected. Therefore, it is concluded that polymersomes exposed to a binary mixture of two different sized latex spheres can form ordered packing geometries on the surface. However, an extremely long annealing time is needed to completely separate the particles.

Discher and co-workers showed that divalent cation can induce phase separation to a two component polymersome system with different hydrophilic part[32] over time. Therefore, it is plausible to consider applying anionic particles to a two components vesicle system to induce phase separation. The polymersome solution was prepared from the mixture of PBMA-b-PDMAEMA and PBMA-b-PHEMA block copolymer. The sample was then treated with anionic polystyrene particles with a diameter around 166 nm.

It is shown in Figure 2.29 that the polymersomes has a relatively smaller size around 600 nm. This is attributed to the better solubility of polyHEMA block in aqueous, which results in a larger volume fraction in water for each PBMA-b-PHEMA block copolymer chain, and therefore a higher curvature structure (smaller curvature radius).

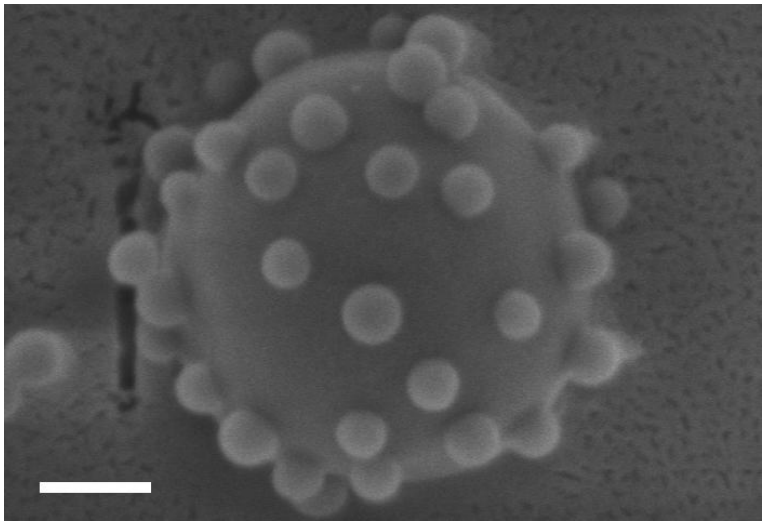

Figure 2.28 Cryo-SEM images of PBMA-b-PDMAEMA and PBMA-b-PHEMA mixed polymersomes exposed to the anionic polystyrene nano spheres taken immediately after mixing. Scale bar = 200 nm

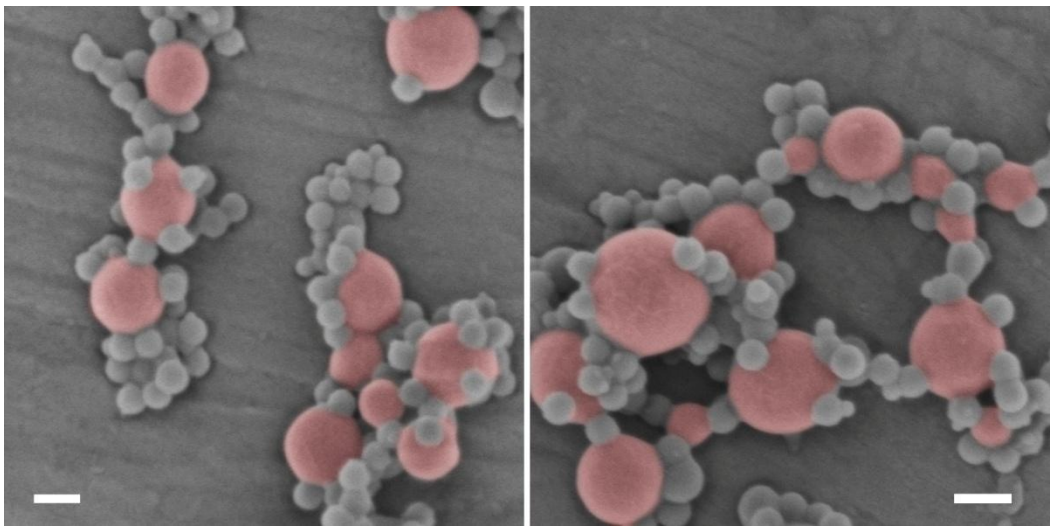

Figure 2.29 Cryo-SEM images of PBMA-b-PDMAEMA and PBMA-b-PHEMA mixed polymersomes exposed to the anionic polystyrene nano spheres taken after 48 hours according to Discher's study. Red spheres indicate the polymersomes. Scale bar = 200 nm.

Unlike pure PBMA-b-PDMAEMA polymersomes, these vesicles were only partially charged on the surface due to the zero charge contribution from PHEMA groups, which in principle cannot be fully covered by anionic latex particles. As it is shown in

Figure 2.29, these hybrid polymersomes along with polystyrene particles form a cross-linked network by electrostatic attraction between each other. In Discher's research, divalent cations only provide local crossbridging and causes segregation into stable gel domains to the vesicles, while in this case however, anionic nanoparticles provided long distance crossbridging between vesicles, therefore, connected polymersomes between each other.

Particles that assemble on the vesicles have gone through a heterocoagulation process, thus a random distribution of these spheres was supposed to be observed. However, due to the lower energy state of packed particles as well as the fluidity of the bilayer, these adsorbed spheres can rearrange along with the movement of the bilayer ending in an asymmetrical packing pattern, in which the particles assemble into groups on the surface of the polymersomes. (See Figure 2.30) This process can take days according to Discher's research when using calcium cation as the inducer. In this study, samples were analysed before and after 48 hours relaxation time. (Figure 2.28 and Figure 2.30) This observation again suggests a fluidic nature of the polymeric bilayer formed from PBMA based block copolymer.

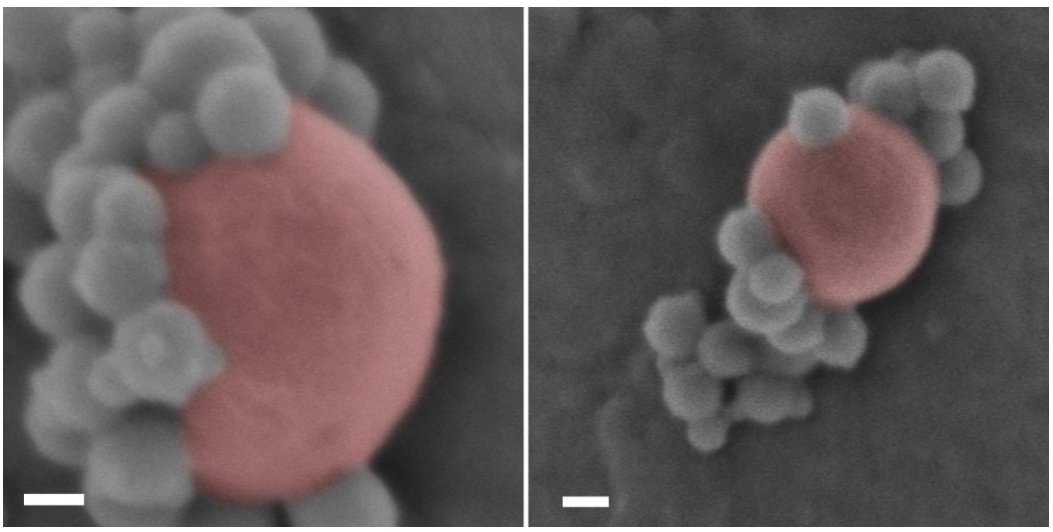

Figure 2.30 Cryo-SEM image of hybrid polymersomes exposed to anionic polystyrene nano spheres taken 48 hours after mixing. Scale bar = 100 nm

2.4 Conclusions

In summary, poly(n-butyl methacrylate)-block-(2-(dimethylamino)ethyl methacrylate) block co-polymer was synthesised with a DP ratio of 80:20, which according to the packing parameter theory is considered to form vesicle structure in aqueous media. However, when the same block co-polymer was dissolved in THF and then added into water, it only formed micelles instead of vesicles due to the poor migrant rate of the polymer in water and metastable state in the form of micelle. Therefore, reverse solvent addition method was applied, which allows the system to relax by providing extra fluidity to the polymer in the presence of THF. Electron microscopes were utilised in both normal mode and cryogenic mode in order to study the structure of polymersomes that were made. Cryo-TEM images shows the core-shell structure with a relatively dark ring on the outside although the core of the vesicles remains black due to the thick ice, through which the electron beam can hardly penetrate. Observation under cryo-SEM was consist with cryo-TEM results, which suggests a smooth surface spherical objects with a thin polymer layer as the shell were obtained. The fabrication of polymer vesicles with a colloidal armour made from a variety of nanoparticles is then demonstrated. Polystyrene nanoparticles were extensively studied for model system, which in this case became the first choice for the armoured system. KPS initiator was utilised for polymer lattices synthesis in order to provide negative charge on the surface of the particles, while the PDMAEMA groups provide positive charge for the polymersomes when protonated by trace acetic acid in the solution. Electrostatic attraction was the dominant interaction between nanoparticles and polymersomes, which were both colloidally stable afore mixing. In order to maintain the stability of the colloidal system, either a steric stabiliser was introduced or extra charge was provide during the neutralisation process. In this study, polystyrene nanoparticles and inorganic silica particles both successfully maintain the stability while providing an armour to the polymersomes. In addition, it is shown that the armoured supracolloidal structure can be postmodified through film-formation of soft polymer latex particles on the surface of the polymersome, hereby effectively

wrapping the polymersome in a plastic bag, as well as through formation of a hydrogel by disintegrating an assembled polymer latex made from poly(ethyl acrylate-co-methacrylic acid) upon increasing the pH, which in addition, sterically stabilised the system. Furthermore, asymmetrical assembly of nanoparticles on the polymersome surface was studied. Both binary mixture of different sized polystyrene nano spheres application and nanoparticle induce phase separation shows the fluidic nature of the polymeric bilayer. It is worth noting that, due to the lower fluidity of the polymer bilayer compared with liposomes, the relaxation time in the order of hours, even days needs to be allowed.

By providing an armour to the polymer vesicles, the mechanical properties may potentially be enhanced as the overall thickness was significantly increased. The functionality of the vesicles can also be changed in order to fit the application through this approach, however, more characterisations are needed to provide information in details of the changes. At least, it is believed that this bilayer decorating approach opens interesting pathways in the already versatile application areas of polymersomes.

1. Discher, B.M., et al., *Polymersomes: Tough Vesicles Made from Diblock Copolymers.* Science, 1999. **284**(5417): p. 1143-1146.
2. Discher, D.E. and A. Eisenberg, *Polymer Vesicles.* Science, 2002. **297**(5583): p. 967-973.
3. Bermudez, H., et al., *Molecular Weight Dependence of Polymersome Membrane Structure, Elasticity, and Stability.* Macromolecules, 2002. **35**(21): p. 8203-8208.
4. van Dongen, S.F.M., et al., *Biohybrid Polymer Capsules.* Chemical Reviews, 2009. **109**(11): p. 6212-6274.
5. Meng, F., et al., *Biodegradable Polymersomes.* Macromolecules, 2003. **36**(9): p. 3004-3006.
6. Napoli, A., et al., *Oxidation-responsive polymeric vesicles.* Nat Mater, 2004. **3**(3): p. 183-189.
7. Kim, K.T., et al., *A Polymersome Nanoreactor with Controllable Permeability Induced by Stimuli-Responsive Block Copolymers.* Advanced Materials, 2009. **21**(27): p. 2787-2791.
8. Discher, B.M., et al., *Cross-linked Polymersome Membranes: Vesicles with Broadly Adjustable Properties.* The Journal of Physical Chemistry B, 2002. **106**(11): p. 2848-2854.
9. Ahmed, F., et al., *Block Copolymer Assemblies with Cross-Link Stabilization: From Single-Component Monolayers to Bilayer Blends with PEO−PLA†.* Langmuir, 2003. **19**(16): p. 6505-6511.
10. Li, F., et al., *Stabilization of Polymersome Vesicles by an Interpenetrating Polymer Network.* Macromolecules, 2006. **40**(2): p. 329-333.
11. Sára, M. and U.B. Sleytr, *S-Layer Proteins.* Journal of Bacteriology, 2000. **182**(4): p. 859-868.
12. Young, J.R., et al., *Coccolith Ultrastructure and Biomineralisation.* Journal of Structural Biology, 1999. **126**(3): p. 195-215.
13. Velev, O.D., *Assembly of protein structures on liposomes by non-specific and specific interactions.* Advances in Biophysics, 1997. **34**(0): p. 139-157.
14. Aranda-Espinoza, H., et al., *Electrostatic Repulsion of Positively Charged Vesicles and Negatively Charged Objects.* Science, 1999. **285**(5426): p. 394-397.
15. Ramos, L., et al., *Surfactant-Mediated Two-Dimensional Crystallization of Colloidal Crystals.* Science, 1999. **286**(5448): p. 2325-2328.
16. Lecommandoux, S., et al., *Magnetic Nanocomposite Micelles and Vesicles.* Advanced Materials, 2005. **17**(6): p. 712-718.
17. Wang, Y., A.S. Angelatos, and F. Caruso, *Template Synthesis of Nanostructured Materials via Layer-by-Layer Assembly†.* Chemistry of Materials, 2007. **20**(3): p. 848-858.
18. Zhang, K., et al., *Composite soft-matter nanoscale objects: Nanocylinder-templated assembly of nanospheres.* Soft Matter, 2009. **5**(19): p. 3585-3589.
19. Haddleton, D.M., et al., *Atom Transfer Polymerization of Methyl Methacrylate*

Mediated by Alkylpyridylmethanimine Type Ligands, Copper(I) Bromide, and Alkyl Halides in Hydrocarbon Solution. Macromolecules, 1999. **32**(7): p. 2110-2119.

20. Gaborieau, M., R. Graf, and H.W. Spiess, *Investigation of Chain Dynamics in Poly(n-alkyl methacrylate)s by Solid-State NMR: Comparison with Poly(n-alkyl acrylate)s.* Macromolecular Chemistry and Physics, 2008. **209**(20): p. 2078-2086.
21. Chen, Y.-J., et al., *Mark-Houwink-Sakurada coefficients for conventional poly(methyl methacrylate) in tetrahydrofuran.* Polymer Bulletin, 1993. **30**(5): p. 575-578.
22. Hutchinson, R.A., et al., *Determination of Free-Radical Propagation Rate Coefficients for Alkyl Methacrylates by Pulsed-Laser Polymerization.* Macromolecules, 1997. **30**(12): p. 3490-3493.
23. Crowe, J.H., J.F. Carpenter, and L.M. Crowe, *THE ROLE OF VITRIFICATION IN ANHYDROBIOSIS.* Annual Review of Physiology, 1998. **60**(1): p. 73-103.
24. Tang, M., A.J. Waring, and M. Hong, *Trehalose-protected lipid membranes for determining membrane protein structure and insertion.* Journal of Magnetic Resonance, 2007. **184**(2): p. 222-227.
25. Aveyard, R., B.P. Binks, and J.H. Clint, *Emulsions stabilised solely by colloidal particles.* Advances in Colloid and Interface Science, 2003. **100–102**(0): p. 503-546.
26. Lin, Y., et al., *Nanoparticle Assembly and Transport at Liquid-Liquid Interfaces.* Science, 2003. **299**(5604): p. 226-229.
27. Colver, P.J., C.A.L. Colard, and S.A.F. Bon, *Multilayered Nanocomposite Polymer Colloids Using Emulsion Polymerization Stabilized by Solid Particles.* Journal of the American Chemical Society, 2008. **130**(50): p. 16850-16851.
28. Lipowsky, P., et al., *Direct visualization of dislocation dynamics in grain-boundary scars.* Nat Mater, 2005. **4**(5): p. 407-411.
29. Fortuna, S., et al., *Packing Patterns of Silica Nanoparticles on Surfaces of Armoured Polystyrene Latex Particles.* Langmuir, 2009. **25**(21): p. 12399-12403.
30. Li, C., X. Zhang, and Z. Cao, *Triangular and Fibonacci Number Patterns Driven by Stress on Core/Shell Microstructures.* Science, 2005. **309**(5736): p. 909-911.
31. Chen, Y., et al., *Multiple Hydrogen-Bond Array Reinforced Cellular Polymer Films from Colloidal Crystalline Assemblies of Soft Latex Particles.* ACS Macro Letters, 2012. **1**(5): p. 603-608.
32. Christian, D.A., et al., *Spotted vesicles, striped micelles and Janus assemblies induced by ligand binding.* Nat Mater, 2009. **8**(10): p. 843-849.
33. Sciortino, F., et al., *Equilibrium cluster phases and low-density arrested disordered states: The role of short-range attraction and long-range repulsion.* Physical Review Letters, 2004. **93**(5): p. -.

Chapter 3 Triggered Release of Polymersome by Bubble Generation via Bilayer Embedded Particles

3.1 Introduction

To overcome the limitations of self-assembly of amphiphiles into vesicles, the controlled flow of microfluidics has been used for their fabrication in recent years.[1] One strategy to fabricate these vesicles is to induce nucleation of polymersomes by mixing a polymer-containing organic solvent stream with a aqueous based liquid in a microfluidic device using a flow-focusing geometry.[1-3] During the solvent evaporation, the assembly of the dissolved diblock copolymers is directed into vesicle structures. The superior stability of polymersomes, the control of their size, structure, and encapsulation efficiency achieved with this technique enable polymersomes to be competitive alternatives to liposomes as delivery vehicles of all kinds of materials.[4-7] Nevertheless, many applications of polymersomes require triggered release of encapsulants.[8, 9] Within the last decade, researchers have designed delivery vehicles that respond to changes of pH, temperature, salt concentration, enzymes or oxidants.[4-6, 10-12] One strategy to trigger release without modifying conditions of the entire system is to incorporate functionalised particles into the vesicle membrane.[13-15] For example, vesicles containing magnetic iron oxide nanoparticles in their hydrophobic layer of the membranes can release encapsulants when an alternation magnetic field is applied, which causes localised heating of the magnetic nanoparticles, thus increase the permeability of the bilayer.[14, 15] One recent work that achieved by Sung *et al.* shows that at an elevated temperature (42 ℃), vesicles with ammonium bicarbonate (ABC) encapsulated can rapidly release doxorubicin drug by generating CO_2 bubbles from the inside due to the decomposition of ABC, which create permeable defects in the bilayer shell. (Figure 3.1)[16]

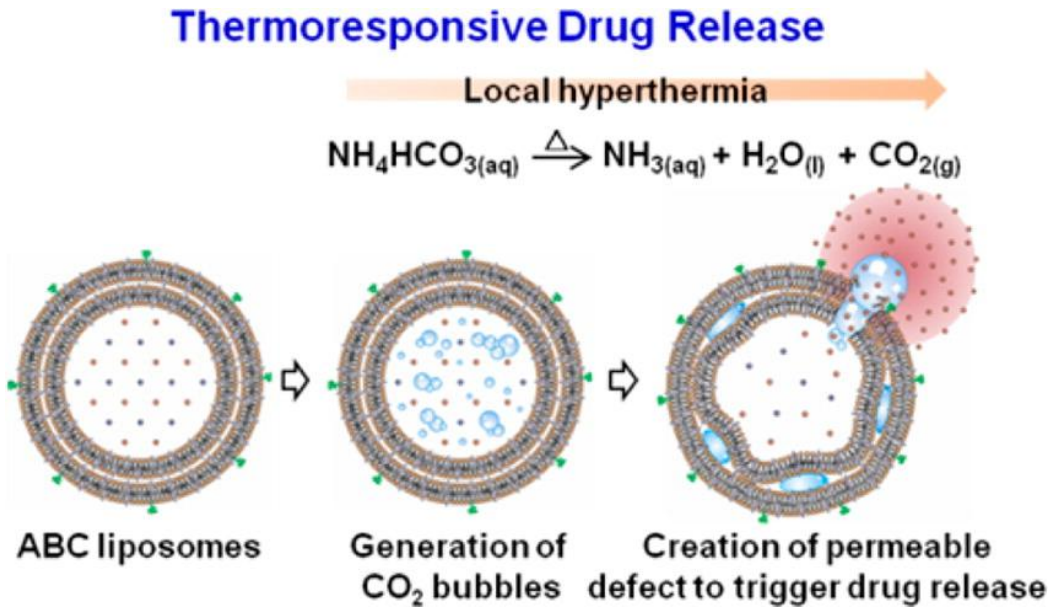

Figure 3.1 Schematic illustrations showing the structure and functions of the thermoresponsive, bubble-generationg liposomes.[16]

Utti *et al.* showed that photothermal effects can also be utilised to fabricate light responsive vesicles by incorporating metallic nanoparticles into thermo responsive membranes.[17] Weitz *et al.* have demonstrated a strategy to produce thermo- and photo-responsive polymersomes by using microfluidics. Gold nanoparticles were used along with polyNIPAM containing diblock copolymers to form a blend polymeric membrane. By varying the composition of the membrane, these polymersomes show different self-healing abilities once defects were created in the bilayer.[10]

In this work, the fabrication of polymersomes with manganese dioxide particle embedded is demonstrated. Hydrogen peroxide solution is used as stimulus to trigger the release of polymersomes. Different release behaviours are studied when applying hydrogen oxide solution with different concentrations. Both microscopy and ion selective electrode techniques were used to characterise the oxidation-responsive bubble generating system.

3.2 Experimental

3.2.1 W/O/W Double emulsion microfluidic device fabrication

3.2.1.1 Materials

Standard wall borosilicate glass capillaries (GC100-10, OD 1.0 mm, ID 0.58 mm), (GC200-7.5, OD 2.0 mm, ID 1.16 mm) were purchased from Harvard Apparatus. Clear C-FLEX® flexible PVC tubing (1/32″ID × 3/32″OD) was purchased from Cole-Parmer. Evo-Stik Two Part epoxy resin was applied to seal the capillaries where necessary. Harvard PHD 2000 infusion syringe pumps are used at pump mode. Leica DM 2500M optical microscope was used for observation of the produced objects and the alignment check of the device.

3.2.1.2 Method

The microfluidic device used for monodisperse W/O/W double emulsions preparation was made based on a glass capillary-needle approach, as shown schematically in Figure 3.2. The round capillaries with inner and outer diameters of 0.58 mm and 1.0 mm, respectively, were tapered to a smaller inner diameter with a laser puller in order to create a flow focusing effect to the middle phase. Two tapered capillaries were carefully aligned inside another round capillary with an inner diameter of 1.16 mm and outer diameter of 2.0 mm. A third capillary was then attached at the side of the outer tube to form a T-junction. PVC tubing was connected between syringes and each exit of the glass capillary. A 30 gauge needle was then bent at a 90 ° angle to perforate into the tubing and to reach the tip of the inside capillary. The glass part of the device was then left in the oven at 80 ℃ for 10 minutes in order to anneal the epoxy resin.

Differ from the classic double-emulsion device, the tapered end of the aligned inner capillaries enables the outer phase to be focused at the joint point, which squeeze the middle oil phase and significantly reduces the size of the double emulsion droplets that formed in the collection tube. The left side tapered capillary was treated with n-octadecyltrimethoxyl silane to render it hydrophobic.

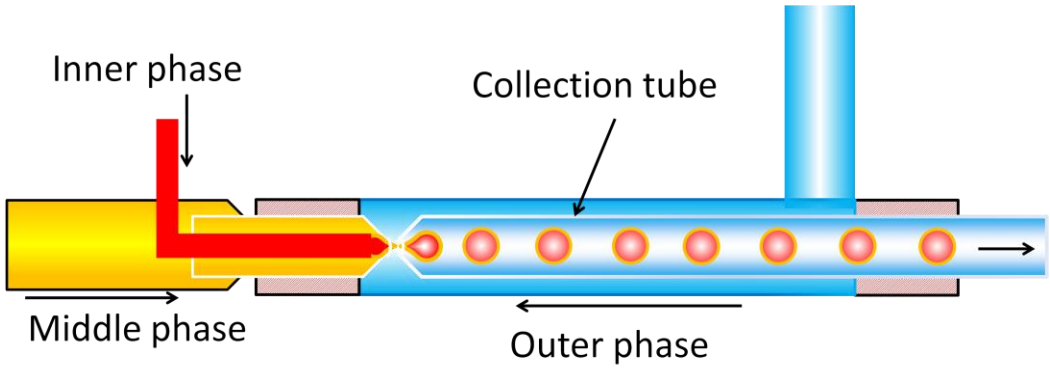

Figure 3.2. Schematic of the glass capillary microfluidic device for generating double-emulsion droplets. The device requires the middle phase (yellow) is immiscible with both the outer phase (blue) and inner phase (red). However, the outer phase can be miscible with the inner phase. Both inner capillaries are tapered at one end and in this case, the inner diameters after tapering are around 110 μm for the injection capillary and 120 μm for the collection capillary.

Typically, the microfluidic device is driven by three syringe pumps along with disposable plastic syringes. The outer phase pump is turned on first so that the outer capillary and collection capillary are fully filled with PVA solution. After wetting the walls of the tubes, the pump of the middle phase is switched on to generate single emulsion droplets at a certain rate. Next, the inner phase pump is turned on and double-emulsion droplets are generated. When shut down the system for the purpose of purging or solution replacement, the opposite sequence is applied, which inner phase pump is paused first then middle and outer phase pumps.

3.2.2 Preparation of monodisperse polymersomes formed from Poly(*n*-butyl methacrylate) -*block*-poly(2-(dimethylamino) ethyl methacrylate) (pBMA-*b*-pDMAEMA) by microfluidic double-emulsion device.

3.2.2.1 Materials

All organic solvents were of analytical grade. Poly(*n*-butyl methacrylate) -*block*-poly(2-(dimethylamino) ethyl methacrylate) (M_n = 15kDa., PDI = 1.10)was obtained by ATRP as described in Chapter 2. Poly(vinyl alcohol) (87%–89%) hydrolyzed (PVA, M_w = 31 kDa.) were purchased from Aldrich. Sodium fluoride (99.99% Aldrich), Hydrogen peroxide (30%), Manganese (IV) oxide particles (99% Aldrich), barium chloride dehydrate (99%, Aldrich) and sodium sulphate (99%, Aldrich) are used as received.

3.2.2.2 Method

5% PVA solution was used as outer phase to downsize and stabilise the oil droplets that formed in the collection capillary. The inner phase consisted of 0.2M NaF solution or 0.1M Na_2SO_4 solution. The middle hydrophobic phase consisted of 5 mg/mL diblock polymer in chloroform, in this case, $PBMA_{80}$-block-$PDMAEMA_{20}$. For particle embedded polymersomes preparation, manganese dioxide powder was added in the polymer solution (6 mg/mL) and ultrasonication was applied to homogenise the sample before loaded in the syringe. Typically, the flow rate was set to 0.15 mL/min for the outer-most phase, 0.005 mL/min for the middle phase and 0.005 mL/min for the inner phase. However, the flow rate can be optimised to obtain stable droplets generation at a rate of 306 per minute.

3.2.3 Characterisations of the double-emulsion droplets and the polymersomes formed

The double-emulsion droplets formed from microfluidics were obtained in the PVC

vial for further observation and study. A small sample was transferred in a glass well and then was observed under optical microscope (Leica DM 2500M) using both bright field and dark field. Photos and video clips were taken by Nikon D5100 DSLR that installed on the microscope and analysed by ImageJ and Photoshop.

Cryogenic scanning electron microscopy was performed on ZEISS SUPRA 55-VP equipped with cold stage and sample preparation chamber. Accelerating voltage was set to 2 kV to avoid burning sample and platinum target was used for sputter coating. For the Cryo-SEM sample preparation, the specimen stub was tapped on the surface of the aqueous to take polymersomes that formed from double-emulsion templates. The stub was then rapidly frozen in the solid nitrogen (<-210 ℃) which obtained by slash the liquid nitrogen (-196 ℃) under vacuum. The sample was stabilised on the pre-frozen stub adaptor and transferred under vacuum to the cold stage of the preparation chamber, which is mounted on the SEM chamber. Both the anti-contaminate plates in the preparation chamber and microscope were cooled down to -186 ℃ while both the cold stages were set to -120 ℃. After fracturing the ice on the surface, unlike nano scaled samples, this sample was then sublimated at -90 ℃ for 5 minutes. Sputter coating was applied at 10 mA for 60 seconds using platinum target after cooling the sample back down to -120 ℃. The stub adaptor was subsequently transferred under vacuum into the SEM chamber. The images taken from Cryo-SEM were then analysed by ImageJ.

3.2.4 Stimuli responsive study of particle embedded polymersomes prepared from microfluidics.

The polymersomes that collected from microfluidic device were stored in the PVC vial to allow for chloroform evaporation. For each experiment, 1 mL solution was collected in the glass well directly from microfluidics. After 20 minutes, under optical microscope, the polymersome samples were treated first with 0.2M barium chloride solution and then hydrogen peroxide solution using a micro pipette. The first sample consisted of polymersomes with only diblock polymer as middle phase solute and

0.2M sodium sulphate solution as inner phase. The second sample was prepared under the same conditions but with manganese dioxide particles in the middle phase. A concentration of 30 % H_2O_2 solution was applied to make up to a 10 % concentration in the sample. And then, the same experiment was performed with diluted H_2O_2, to make up to 0.1 % total concentration in the sample.

3.2.5 Ion Selective electrode measurement for polymersome release profile study.

In order to observe the release process, previous research has shown great interest in using the combination of fluorescent dyes and confocal laser scanning microscope. However, due to the contrast and threshold settings, small quantity release of fluorescent dyes may not be observed via this method. Therefore a fluorine selective electrode was introduced to quantitatively measure the ion concentration in real-time. These samples were prepared with 0.2M sodium fluoride solution as inner phase. For each sample, 3 mL polymersome solution was collected from the device in a PVC vial with 3 mL pre-added 5 % PVA solution. Fluorine selective electrode and reference electrode were connected to a voltmeter and were plugged into the solution to complete the circuit. (Figure 3.3) The readings were recorded for 12 hours and each measurement was repeated three times. The ISE was calibrated by using 4 standard solutions with fluorine ion concentration of 1000 ppm, 100 ppm, 10 ppm and 1 ppm respectively. The electrodes were washed with distilled water three times and dried between each measurement for calibration. A working curve was then plotted and the voltage readings were then converted to fluorine concentration. All samples were measured immediately after 20 minutes collection and the hydrogen peroxide solution was applied to the samples after around 70 minutes of the measurements start.

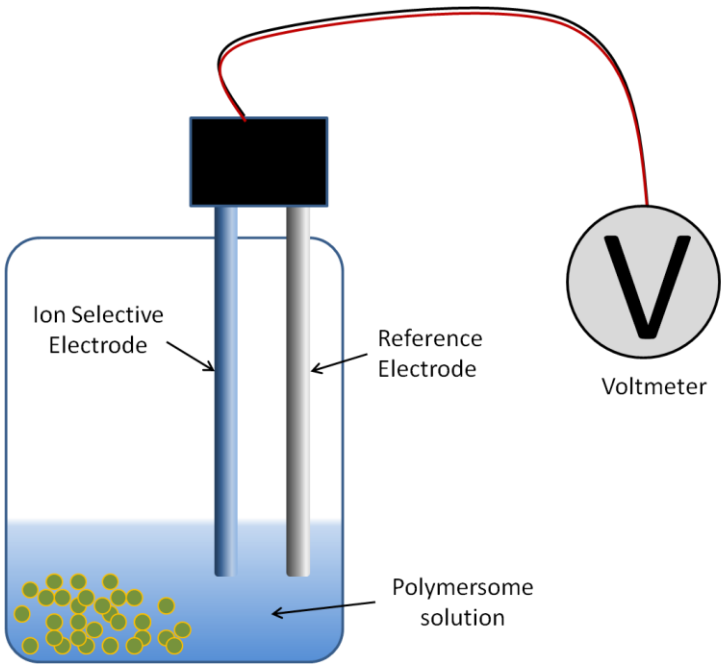

Figure 3.3 Schematic of ion selective electrode measurement. The polymersomes are collected at one side of the vial while the electrodes measure at the other side to minimise the artificial disturbance.

3.3 Results and discussion

3.3.1 Polymersomes formation from double-emulsion droplets as templates, observation and characterisation.

Water in oil in water (W/O/W) double-emulsion droplets with a diblock copolymer shell consists of $PBMA_{80}$-$PDMAEMA_{20}$ were generated as templates for the polymersomes using the microfluidic device. The amphiphilic diblock copolymers stabilised the inner drops against coalescence with the outermost aqueous phase, in this case, the 5 % PVA solution, while the PVA prevented coalescence of the oil droplets. Before the chloroform evaporation, the diblock copolymer adsorb at of inner/middle and the middle/outer interfaces, with the hydrophobic PBMA in the organic phase and the hydrophilic blocks of PDMAEMA in the inner and outer aqueous phases. Due to the relative high density of the chloroform (1.48 g/mL) compared with aqueous continuous phase, these double-emulsion droplets sink to the bottom of the sample vial. When using glass vials to collect and store the sample, the chloroform layer in the droplets often wet the container and destabilises the emulsions after an overnight storage. Toluene or hexane has a lower density than the continuous phase, but the evaporation rates of them are much lower than chloroform, which significantly delay the formation of polymersomes. When a mixture solvent of hexane and chloroform is used, since the solubility of chloroform in water (~8 g/L at 20 ℃) is much higher than that of hexane (~0.013 g/L at 20 ℃), chloroform in the oil shell diffuses into the continuous phase significantly faster than hexane, and then is evaporated at a much higher rate. The fraction of hexane therefore increases and turns the oil phase into a poor solvent for the diblock copolymers. The reduction in solvent quality of the oil phase results in attraction between the hydrophobic PBMA blocks, which causes a de-wetting transition. For the study of ion release from these polymersomes, de-wetting process make it almost impossible to calculate the effective interfacial area of the polymersomes. Therefore, chloroform is solely used in

the oil phase and PVC vials or Eppendorf tubes were used for the sample collection and storage.

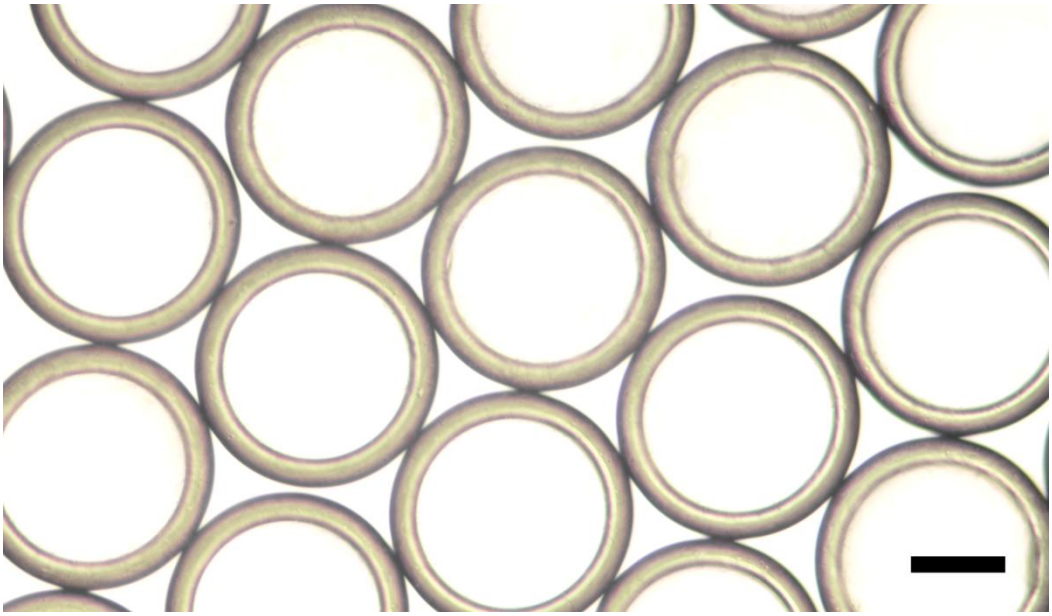

Figure 3.4 Monodisperse double-emulsion droplets generated from glass capillary microfluidic device. Flow rate: 0.20 mL/min (outer phase), 0.01 mL/min (middle phase) and 0.005 mL/min (inner phase). Scale bar: 100 μm

One of the advantages of a microfluidic technique is of the monodispersity of the particles or capsules that formed from droplets. Bright-field and dark-field images were obtained with 10 × objective lens and a 2 × eyepiece in front of the digital camera (Nikon D5100 DSLR). Figure 3.4 shows the double-emulsion droplets that generated using diblock copolymer only in the middle phase solution and PVA solution as inner drops under optical microscope. Ring-like structure can be observed, which confirms the core-shell structure of the double-emulsions. The outer radius R_o, of the double emulsions varied depending on the flow rate, inner diameter of both tapered injection and collection capillary. According to the research by Studart *et al,* droplet break-off during flow-induced dripping can be generally correlated to the moment when the shear force caused by outer fluid overcomes the pinning force arising from the surface tension.[18] This indicates that in dripping mode, droplet rupture occurs when the Capillary number C_a, which is described as the ratio between shear and interfacial forces F_{shear}/F_{γ}, reaches a critical value on the order of 1. Moreover, by considering

the forces that comprise the Capillary number, during growth, the droplet will remain attached to the capillary tip because of the interfacial tension force:

$$F_\gamma = \pi D_d \gamma_{1,2} \qquad (1)$$

Where, γ is the interfacial tension between the two fluids and D_d is the inner diameter of the injection capillary tip. The flow-focusing geometry applies a shear force that actively pushes the droplet off the tip, and it is described by equation (2):

$$F_{shear} = 3\pi\mu(d - D_d)(v_o - v_i) \qquad (2)$$

Where, μ is the viscosity of the outer phase, d is the diameter of the droplet, and v_o and v_i are the average velocities of the two fluids. Therefore, in order to generate smaller sized droplets in dripping mode by this flow-focusing microfluidic device, either increasing the viscosity of the outer fluid or increasing the injection rate difference between the two fluids, in this case, outer and middle phases, can be applied. Experimentally, when a higher concentration of PVA solution is used as outer phase, which results in a higher viscosity of the outer fluid, the protruding droplet size decreases significantly, and the possibility of the middle oil phase wetting the collection capillary is reduced as well. From equation (2), theoretically, when the ratio between the outer and middle infusion rates is changed from 15 to 20, in this case, the infuse rate of the outer phase pump was set to 0.2 mL/min instead of 0.15 mL/min; the size of the droplets can be approximately predicted by equation:

$$(d_0 - 110\ \mu m)(15 - 1) = (d_1 - 110\ \mu m)(20 - 1)$$

Where, d_0 and d_1 are the droplet diameters before and after increasing the flow rates ratio respectively. Since the pixel size of the CMOS of the camera is 4.78 μm and the total magnification rate is 20, the double-emulsion droplet size that measured from the images that taken from the sample with a flow rate of 0.15 mL/min, d_0, is approximately 340 μm. (Figure 3.5) Thus, d_1 can be estimated by the equation, which gives a value of 280 μm. Figure 3.4 shows the droplets that produced at infuse rate of a 0.20 mL/min and the size that measured from this sample is around 260 μm which is slightly smaller than the theoretical value. One of the possible reasons is that the presence of manganese dioxide particles reduces the surface tension between the outer and middle phase fluids.

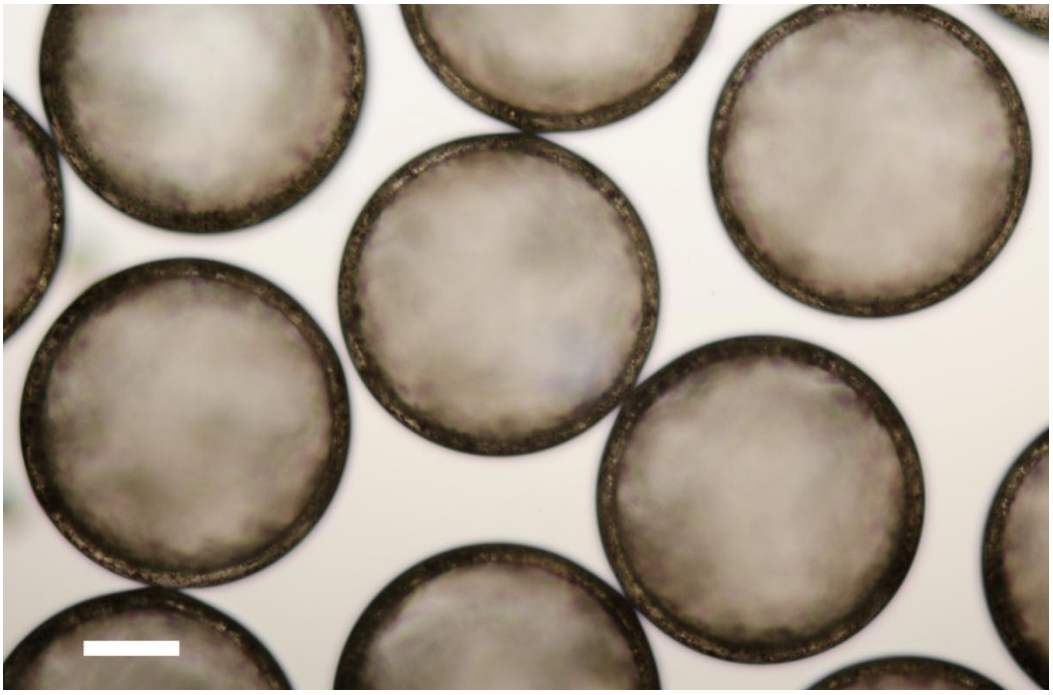

Figure 3.5 Double-emulsion droplets generated with an outer phase flow rate 0.15 mL/min, middle phase flow rate 0.005 mL/min and inner phase 0.005 mL/min. The image was taken by optical microscope 20 minutes after collection in a glass well. The average size of the droplets is 340 μm and the average diameter of the inner droplets is 317μm. Scale bar: 100 μm

According to the Kelvin equation:

$$ln\frac{p}{p_0} = \frac{2\gamma V_m}{rRT}$$

Where p is the actual vapor pressure, p_0 is the saturated vapour pressure, γ is the surface tension, V_m is the molar volume of the liquid, R is the universal gas constant, r is the radius of the droplet and T is the temperature. Because of the surface tension, the vapor pressure for small droplets of the liquid in suspension in greater than the standard vapor pressure of that same liquid when the interface is flat. Therefore, after approximately 80 minutes, the chloroform in the oil shell of the droplets was then mostly evaporated and polymersomes formed. When an inorganic salt is used as solute in the inner phase, the presence of chloroform layer prevents the ions from diffusing across the oil layer. However, along with the chloroform evaporation, the diffusion rate of the encapsulated solutes increases gradually. Theoretically, in a close

system, the release rate is a function of the effective area of the bilayer membrane and the concentration difference between the inside and outside solution. Therefore, the polymersomes with manganese dioxide particles in the bilayer, on one hand, should have a smaller effective interfacial area as the membrane is partially blocked by these solid beads of manganese dioxide.

To demonstrate the shell like nature of the polymersome membrane, suspensions of polymersomes were frozen in solid nitrogen and imaged by cryo-SEM. Cold fracture allows the section of the polymersomes to be seen under microscope. In Figure 3.6a, it shows that a thin and homogeneous wall was formed after chloroform evaporation. The polymer bilayer wall separates the inside structure that is typical of dried salt solution from the outside foam like dried PVA solution, which shows good encapsulation ability of the polymersomes. It is worth noting that in Figure 3.6b, there are a number of micron sized spherical objects in the surface of the polymer bilayer wall, which is believed to be manganese dioxide particles. Similar structure is shown in Figure 6c a single particle was captured in the middle of the wall and fractured during the sample preparation. However, it has yet been proved whether the particles were fully surrounded by the polymer chains or were only fitted in the wall as stoppers.

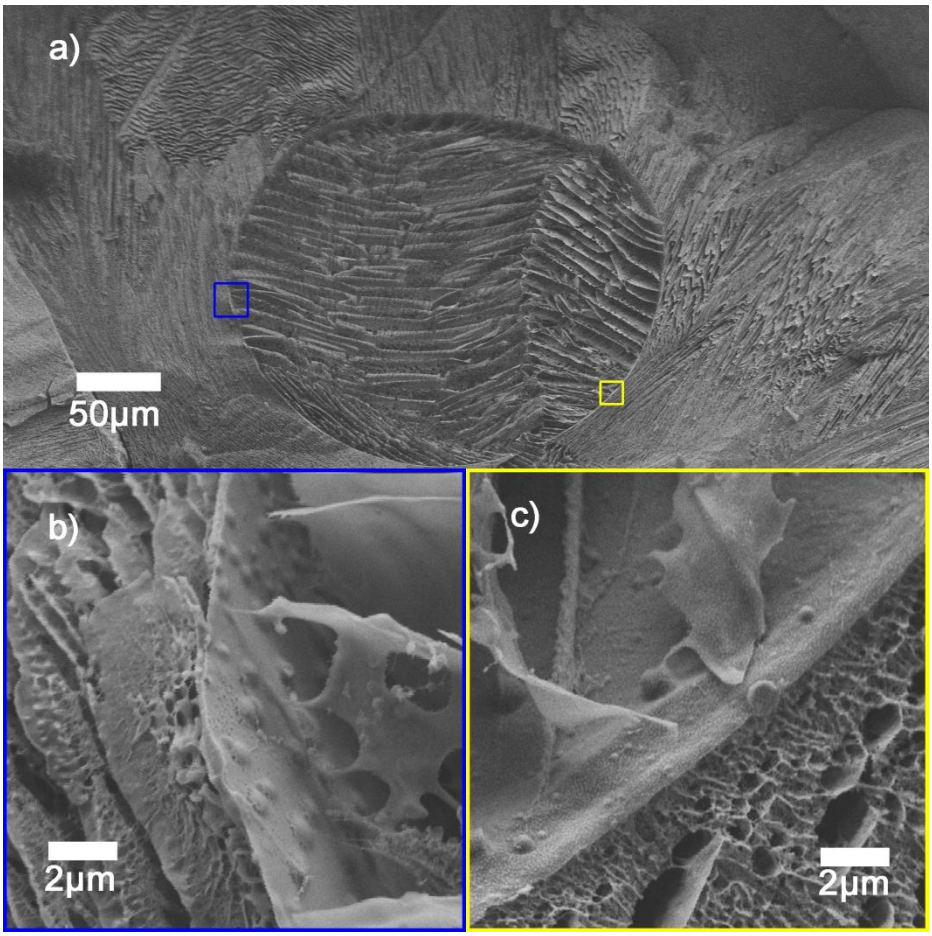

Figure 3.6 Cryogenic SEM images of polymersomes, (a) overview of the polymersome, (b) magnified view of the region in blue in panel (a), (c)magnified view of the region in yellow in panel (a).

From the observation under cryo-SEM, approximately 10-20% of the interfacial area of the polymersome membrane is occupied by the manganese dioxide particles. The initial concentration of the manganese dioxide particles in the oil phase is about 6 mg/mL, while the diblock copolymer concentration is 5 mg/mL. Due to the high density of the particles (5.03 g/cm^3), then the volume fraction of the manganese dioxide particles in the dried bilayer can be roughly calculated, which gives a value of approximately 20%. Since the particles that suspended in the oil phase gradually settled over time in the syringe during the microfluidic experiments, the actual amount of manganese dioxide particles that were transported into the droplets is lower than the original value, which consists with the observation.

3.3.2 Triggered release behaviour of the polymersomes by hydrogen peroxide stimulus

The release of the inner content was triggered by introducing hydrogen peroxide solution. In order to observe the release process, previous research has shown great interests in the combination of fluorescent dyes and confocal laser scanning microscope. However, due to the contrast and threshold settings, small quantity release of fluorescent dyes may not be observed via this method. Sodium sulphate solution was used as inner phase liquid for the microfluidics to generate polymersomes that to be observed under optical microscope. Ba^{2+} ions is considered to be very sensitive to SO_4^{2-} ions in aqueous, which produces Barium sulphate precipitation when react with each other. The low solubility of $BaSO_4$ (less than 0.3 mg/100 mL) enables trace SO_4^{2-} ion release to be observed under microscope in dark field with Ba^{2+} ion presence in the continuous phase.

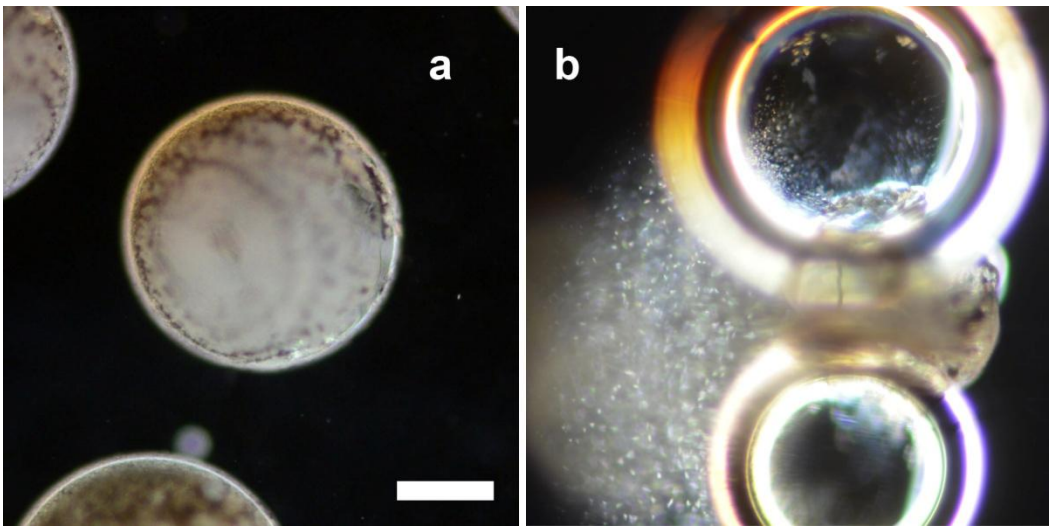

Figure 3.7 Images of polymersomes (a) before and (b) after the treatment of high concentration H_2O_2 taken in dark field. The small white dots are the barium sulphate solid particles that formed after the inner content being released. Scale bar: 150 μm

To demonstrate the concept, typically, a sample of 1 ml sodium sulphate encapsulated polymersomes was transferred in a reservoir under microscope, two or three drops of 0.1 M barium chloride was added to the sample and a 30% hydrogen peroxide

solution was applied immediately after. As soon as the hydrogen peroxide reached the surface of the polymersome via diffusion process, the decomposition was then catalyzed by the embedded manganese dioxide particles to generate O_2 bubbles. These gas bubbles grew rapidly, and ultimately open a wound on the bilayer surface to release SO_4^{2-} from the inside, which instantly reacted with Ba^{2+} in the continuous phase to form micron sized white crystal precipitation. (Figure 3.7)

In contrast to the bright field images, manganese dioxide particles that embedded in the bilayer give a bright white colour, while in bright field it is often shown as black dots. A video clip was taken to demonstrate the process of one single polymersome releasing the inner content after being triggered by a high concentration H_2O_2. A series of images was captured every second from the video clip and revealed the entire process of the release. Interestingly, in all cases, oxygen bubbles were generated at only a few locations on the surface of polymersomes when contact with hydrogen peroxide. Theoretically, any manganese dioxide particles that reach the hydrogen peroxide can be the centre of bubble generation. However, only a few bubbles were observed for each one of the polymersomes, and the reaction of H_2O_2 and manganese dioxide particle suspension was, in contrast, much more violent. One of the reasons is that as a catalyst in the reaction, these manganese particles can only participate when directly contact with H_2O_2; but within the polymersome bilayer, most of the particles were embedded and wrapped by polymer chains, which significantly reduces the surface area of the catalyst, therefore moderated the decomposition of H_2O_2. Furthermore, oxygen gas bubble tends to fuse and to grow into large ones instead of multiple smaller ones. Therefore, in all cases, under microscope, only one or two holes that opened by bubble generation were observed for each polymersome to release the inner content.

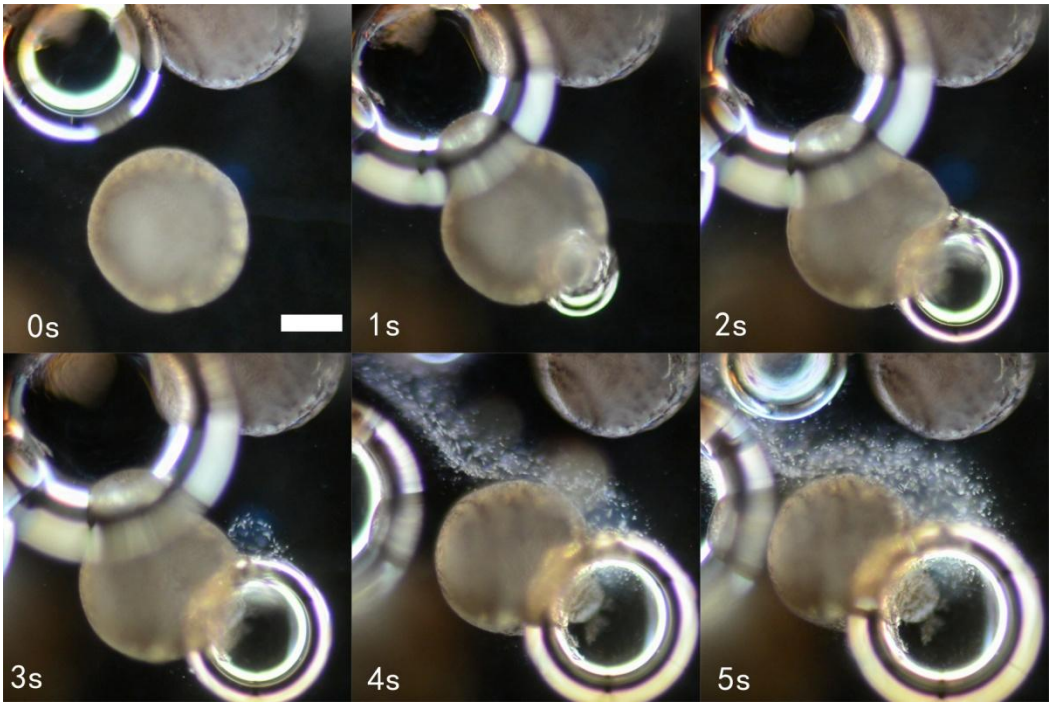

Figure 3.8 Series of dark field images captured from the video clip showing the process of the triggered release. It can be seen that along with the oxygen bubble growth (right bottom), white solid of barium sulphate starts to show where the inner content flows. Scale bar: 150 μm.

3.3.3 Polymersomes release behaviour when applied a low concentration of hydrogen peroxide stimulus

The mechanism encapsulated solutes are released strongly depends on the stimulus applied to trigger release from polymersomes. The hydrogen peroxide responsive polymersomes exhibit slow and sustained release of the inner content if a much lower concentration H_2O_2 solution is applied. To demonstrate the concept of this steady release, the same sample was taken and treated with first barium chloride and then hydrogen peroxide, however, this time, a final concentration of approximately 0.1 % was achieved in the sample suspension.

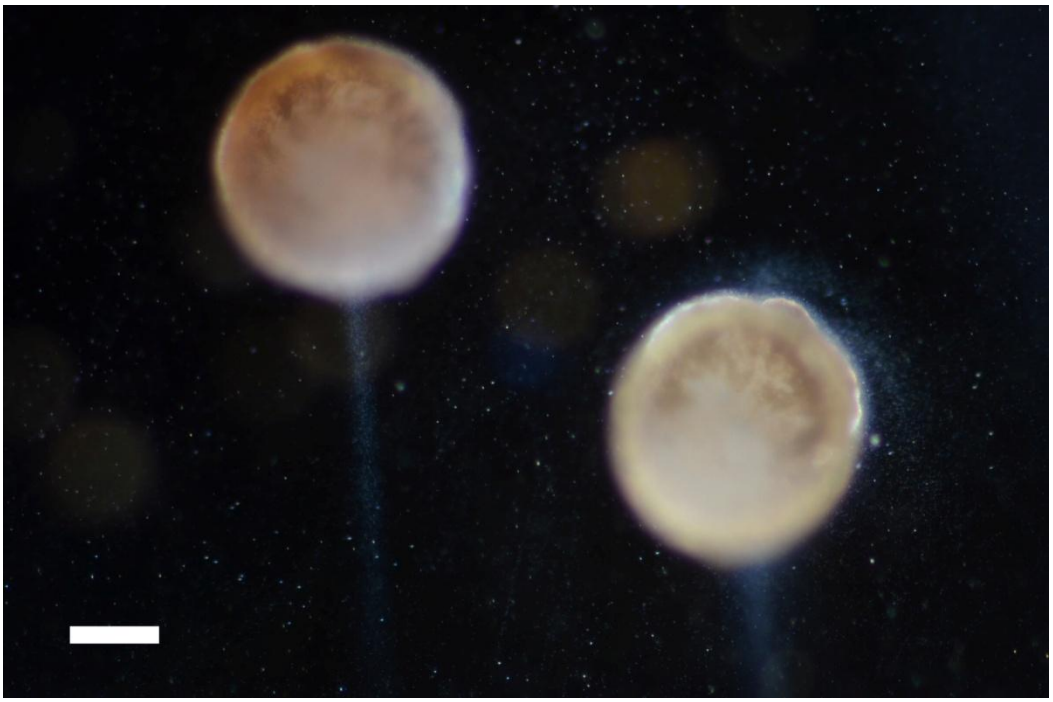

Figure 3.9 Dark field image of polymersomes release at low concentration H_2O_2 environment. The bright halo around and the white tails arise from $BaSO_4$ crystals. Scale bar: 100 μm

In this experiment, after the addition of stimulus to the system, these polymersomes became less spherical and went through a faster release stage, while maintaining their membrane integrity, as shown in Figure 3.9. Oxygen bubbles were rarely observed, however, barium sulphate that generated due to the release was still observable under

optical microscope. The surface of the polymersomes was no longer smooth and the bright tails of these polymersomes indicate the direction of the local aqueous flow possibly caused by faster water evaporation rate at the edge of the sample reservoir. Differ from large molecules, ion formed solutes can however diffuse through polymer membrane over time. It is worth noting that, when compare with polymersomes before H_2O_2 treatment (Figure 3.10a), the polymersomes show an ordinary spherical morphology and $BaSO_4$ precipitation can hardly be observed in the earlier stage of its natural release process.

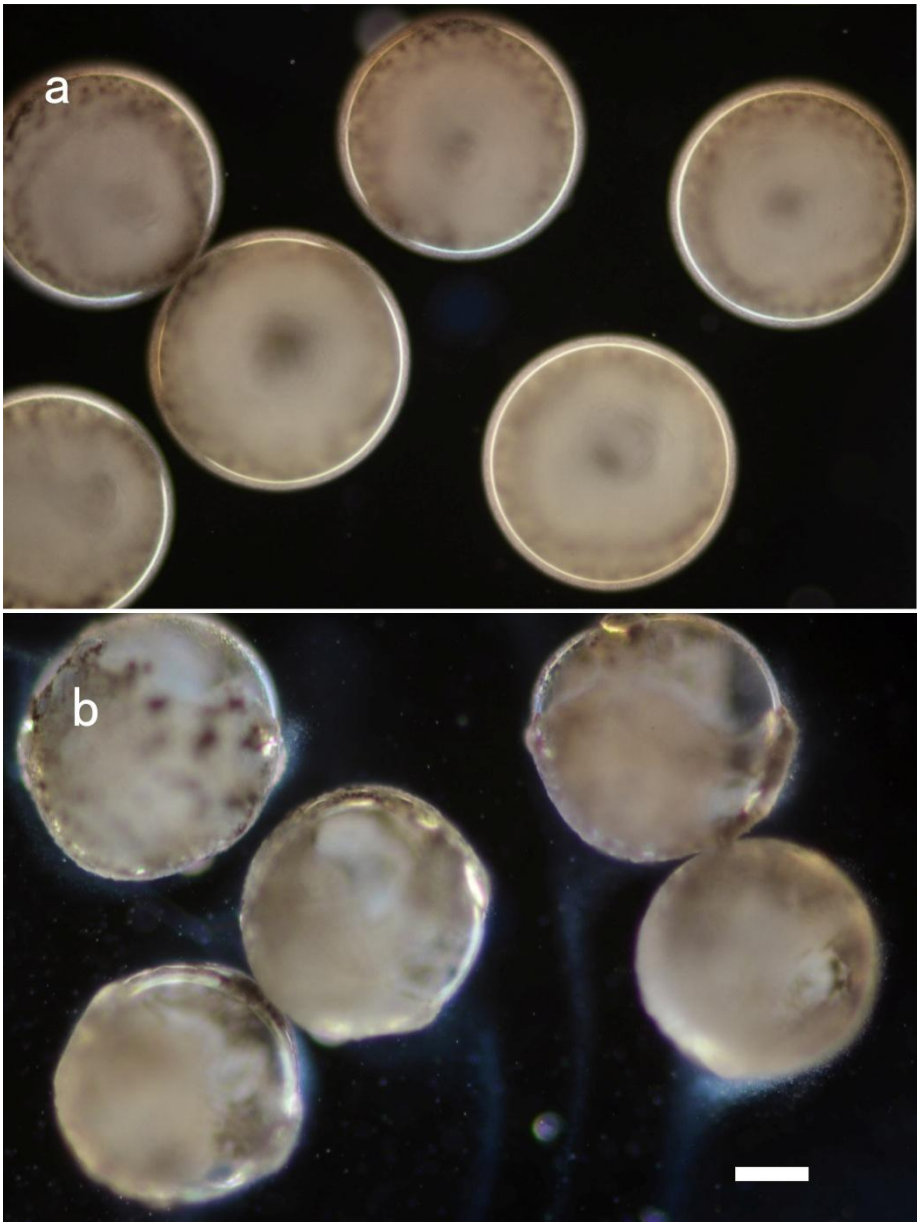

Figure 3.10. Dark field images of polymersomes (a) before (b) after low concentration H_2O_2 treatment. Scale bar: 100 μm.

3.3.4 Fluoride Ion Selective Electrode (ISE) measurements for polymersome releasing behaviour study.

Considering the high diffusion coefficient of ions, it is assumed that the ion, in this experiment, F^-, was instantly dispersed in the sample after being released by polymersomes. In the actual measurement, a relatively stable reading of the voltmeter can be obtained in a few seconds after adding a certain amount of F^- standard solution to a PVA solution as blank control. The voltmeter measures the potential difference between the two electrodes. According to the Nernst equation:

$$E = E^0 - \frac{RT}{F} \ln a_{F^-}$$

Where, E is the measured cell potential, E^0 is the standard cell potential, R is the ideal gas constant, T is the temperature, F is the Faraday constant and a_{F^-} is the activity of the fluoride ion, and the measured potential is proportional to the logarithm of the fluoride ion activity. By measuring a series of standard fluoride ion solutions with concentrations of 1 ppm, 10 ppm, 100 ppm and 1000 ppm, a working curve of a straight line can be plotted.

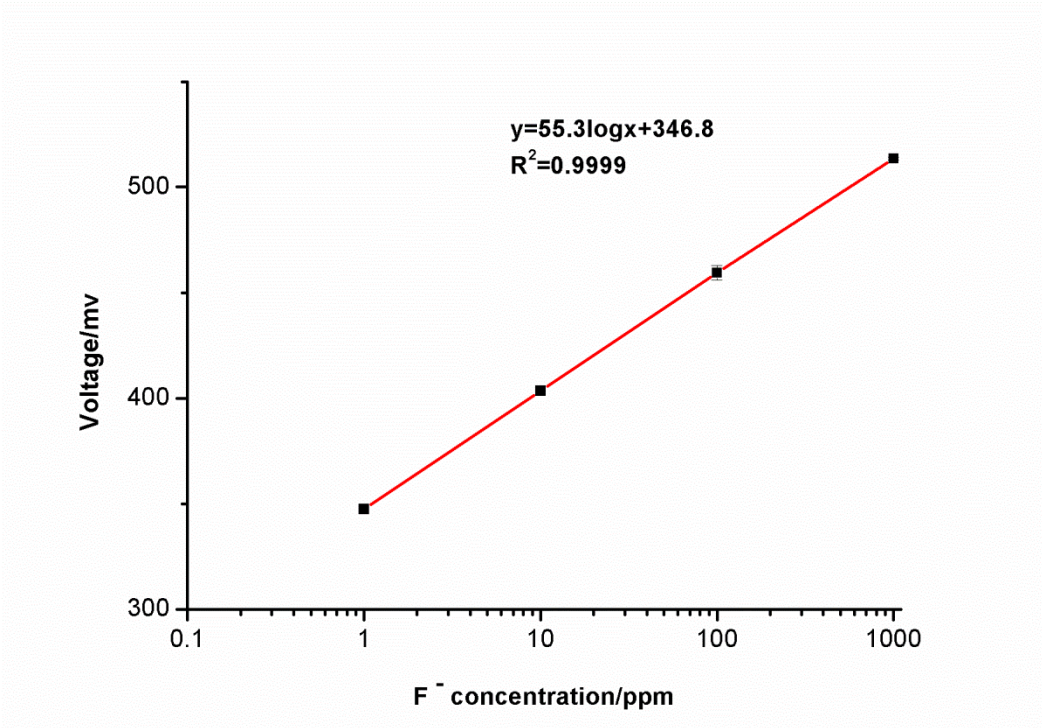

Figure 3.11. Working curve of fluoride selective electrode. The y axis is the opposite

number of the actual reading on the voltmeter and x axis is the fluoride ion concentration in ppm.

All samples were treated with ultrasonic bath to homogenise the system in order to determine the final concentration of fluoride ions. Thereafter, the voltage readings of each sample are converted to fluoride concentrations via the trend line equation of the working curve. Next, the concentration of fluoride ion was plotted versus time to demonstrate the release profile of each sample. Figure 3.22 shows the comparison of the release behaviour of the polymersomes prepared with and without manganese dioxide particles embedded.

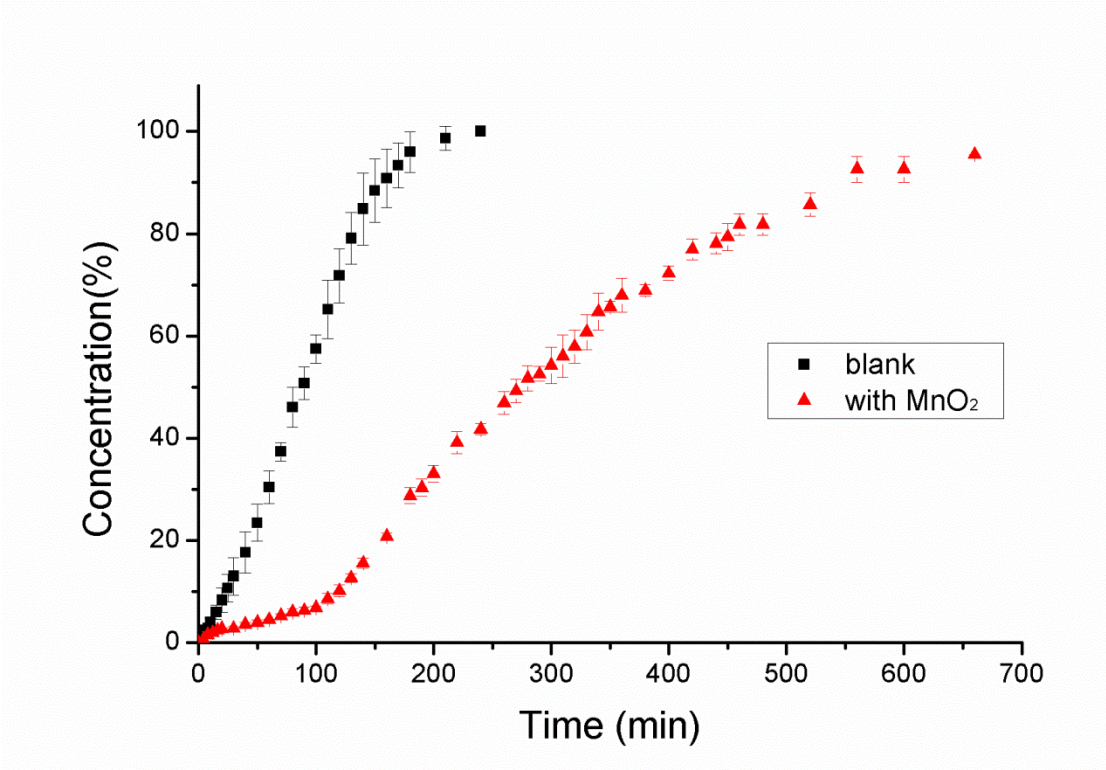

Figure 3.12 Fluoride ion concentration percentage of polymersomes with (red) and without (black) manganese dioxide particles embedded.

As it is shown in the graph, the polymersomes with manganese particles embedded have a significant lower release rate than the ones without. The fluoride concentration reaches about 100% in less than 4 hours time, while the particle embedded polymersomes only have less than 50% of fluoride ion released. It is worth noting that,

during the first 20-30 minutes of the measurement, the ion release was accelerating due to the chloroform evaporation. Its presence led to retardation, as thicker hydrophobic barrier has to be overcome by the ions. Once the organic phase was dried completely, the release rate reached the maximum rate and started to decelerate as the concentration difference between the inside and outside of the polymersomes decreased. However, this chloroform evaporation process, took much longer for the polymersomes with manganese dioxide particles than that of the blank. One potential explanation is that the occupation of the particles in the bilayer (ca. 20 vol% of the membranes) reduces the effective interfacial area of chloroform and continuous phase, thus slow down the evaporation rate of the organic solvent. Approximately 100 minutes were needed for the chloroform to be removed at ambient temperature for polymersomes with particles embedded.

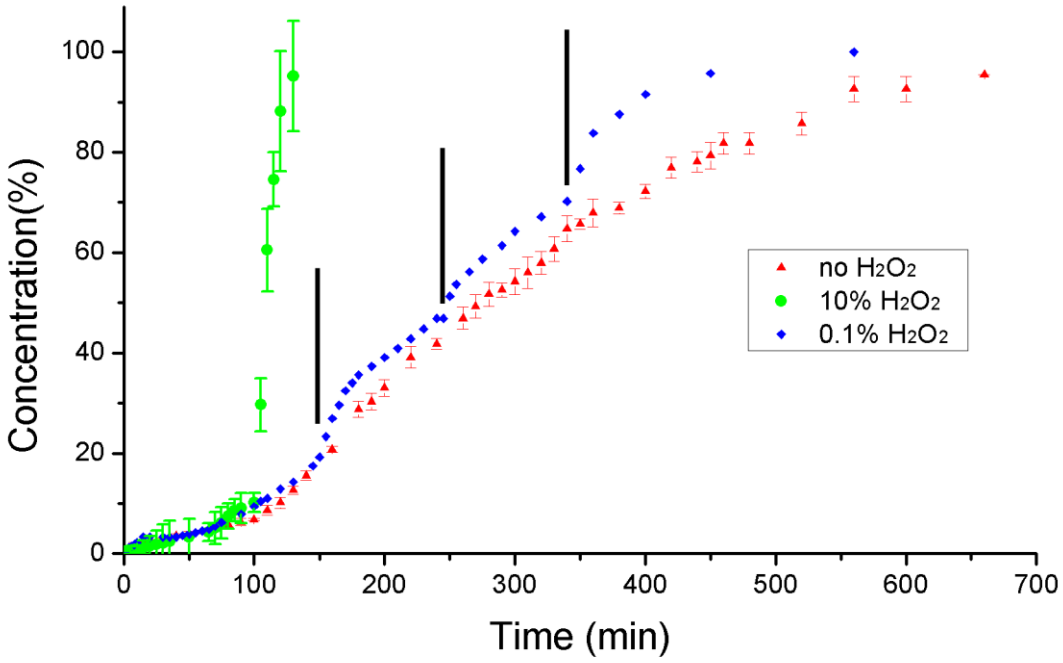

Figure 3.13 Fluoride concentrations of particle embedded polymersomes with 10% H_2O_2 (green), 0.1% H_2O_2 (blue) and no H_2O_2 (red) stimuli. Hydrogen peroxide solutions were added at 100 minutes for green and 150, 250, 340 minutes for blue (Black vertical lines).

The release behaviour of polymersomes exposed to different hydrogen peroxide solutions was studied by ISE method as well. In Figure 3.13, the red triangle plot shows the fluoride ion concentration change of polymersomes fabricated with manganese dioxide particles in the bilayer. When a diluted hydrogen peroxide solution was applied, the release rate increased significantly because of the agitation of the embedded particles when reacted with trace H_2O_2. (Blue diamond) Approximately 20-30 minutes after the stimulus, the release rate dropped to a similar level to that of the sample without H_2O_2 (in the region between 200 minutes and 250 minutes), which indicates that the hydrogen peroxide in the sample has been mostly consumed. The same treatment was applied at both 250 minutes and 340 minutes in order to confirm what was observed earlier. It is worth noting that during the third treatment, some bubbles were observable on the sample surface, which indicates that the system was saturated with oxygen. Unlike the sample without manganese dioxide particles, it took over 12 hours for the fluoride ion concentrations in these two samples to reach 100%. The exact mechanism of this temporary increased permeability is not fully understood. One potential explanation is that the catalytic breakdown of hydrogen peroxide to dioxygen and water at the site of the particles induces the formation of transient openings at the interface between the particles and the membrane, thus temporarily increasing membrane permeability. Blank experiment was carried out, in which deionised water was added instead of hydrogen peroxide solution. In theory, the driving force of release behaviour depends on the concentration difference between the two sides of the membrane. Therefore, as predicted, a small enhancement of release rate was observed in line with the artificial concentration change. However, this effect was negligible in comparison with the hydrogen peroxide catalytic trigger. Another question could be raised that whether this enhanced release behaviour is potentially caused by the self-destruction of a small number of vesicles upon addition of the hydrogen peroxide stimulus. It is therefore plausible to carry out live experiments with 50-60 vesicles counted before and after the release experiments under the observation of microscope. The light intensity of the microscope was adjusted to the minimum of requirement in order to minimise the

evaporation of water for these small scale samples. Additionally, glass slides were used to cover the sample well to prevent dehydration of the polymersomes. Less than 1 vesicle were found to be broken in each sample, which suggests that the bilayer permeability increase was caused by the manganese oxide particle catalytic reaction.

The green plot in the graph is the sample treated with high concentration of hydrogen peroxide as described before. The fluoride concentration in the continuous phase increased massively after stimulus addition as most polymersomes in the sample were nuked by vigorous bubble generation on the bilayer surface. The reading of the voltmeter increased rapidly and reached final concentration within a few minutes time, which consists with what was observed under microscope.

3.4 Conclusions.

In summary, the formation of polymersomes with micron sized particles embedded in the bilayer from double-emulsion templates can be achieved by using a glass capillary based microfluidic device. By adding manganese dioxide particles in the organic phase, the diblock copolymer shell is then partially filled with solid beads, which is in agreement with the Cryo-SEM observation. However, whether these particles were fully wrapped around by polymer chains remains unknown due to the difficulties of measuring chemical composition of the embedded area. One advantage of the microfluidic approach of polymersome fabrication is that 100% encapsulation can be achieved, which is considered to be essential for contents loading in some circumstances, whilst conventional vesicle formation and encapsulation methods leave significant percentage of the substances outside the vesicles. Although purification is no longer needed for these vesicles, the organic solvent that was involved in this approach, however, can cause other issues as the polymersomes that were prepared in this study require a drying process in order to remove the organic solvent. Up to approximately 100 minutes should be allowed before any release behaviour measurement in this study.

The embedded manganese oxide particles enable the polymersomes to respond to

hydrogen peroxide stimulation. By varying the concentration of the H_2O_2 solution, the release behaviour of the polymersomes is also varied. The results suggest that polymersomes with manganese particles at high H_2O_2 concentration have shown the ability to generate oxygen bubbles on the surface wherever the particles are exposed, which consequently tear the shell apart to release the encapsulated substances, whilst using low concentration of H_2O_2, the same polymersomes retain their membrane integrity with slightly higher release rate. The use of ion selective electrode enables real-time monitor of the release process which provides a better idea of how functionalised polymer bilayer affects the permeability to ions. Blank control experiments that were taken proved that the enhanced membrane permeability for low concentration treatment was indeed achieved by the local catalytic activity of the manganese oxide particles instead of vesicle destruction. It is worth noting that, by using ion selective electrode for the fluoride ion measurement, an electric field was applied to the solution, which may cause so called electroporation to the vesicles. Battaglia *et al* reported that biological macromolecules can be encapsulated into preformed polymersomes by controlled destabilisation of the vesicle membrane using this method. The visicles size and morphology remained unchanged after electroporation. Therefore, the release behaviour of polymersomes without stimulation in this study may arise from the same process, which explains how fluoride ion can travel across the polymeric membrane. However, the differences in the release behaviour of sample with different treatment suggest that the permeability of vesicular structures containing active colloidal particles as part of their membrane can be regulated by use of a chemical trigger. The ability to modify the polymer bilayer with functionalised particles creates new opportunities to facilitate the fabrication of complex vesicle structures with controlled permeability, which may be of interest to a range of scientific fields.

1. Shum, H.C., J.-W. Kim, and D.A. Weitz, *Microfluidic Fabrication of Monodisperse Biocompatible and Biodegradable Polymersomes with Controlled Permeability.* Journal of the American Chemical Society, 2008. **130**(29): p. 9543-9549.
2. Martino, C., et al., *Protein Expression, Aggregation, and Triggered Release from Polymersomes as Artificial Cell-like Structures.* Angewandte Chemie International Edition, 2012. **51**(26): p. 6416-6420.
3. Shum, H.C., et al., *Dewetting-Induced Membrane Formation by Adhesion of Amphiphile-Laden Interfaces.* Journal of the American Chemical Society, 2011. **133**(12): p. 4420-4426.
4. Onaca, O., et al., *Stimuli-Responsive Polymersomes as Nanocarriers for Drug and Gene Delivery.* Macromolecular Bioscience, 2009. **9**(2): p. 129-139.
5. Li, M.-H. and P. Keller, *Stimuli-responsive polymer vesicles.* Soft Matter, 2009. **5**(5): p. 927-937.
6. Meng, F., et al., *Biodegradable Polymersomes.* Macromolecules, 2003. **36**(9): p. 3004-3006.
7. Discher, D.E., et al., *Emerging applications of polymersomes in delivery: From molecular dynamics to shrinkage of tumors.* Progress in Polymer Science, 2007. **32**(8–9): p. 838-857.
8. Lomas, H., et al., *Polymersome-Loaded Capsules for Controlled Release of DNA.* Small, 2011. **7**(14): p. 2109-2119.
9. Discher, D.E. and F. Ahmed, *Polymersomes.* Annu Rev Biomed Eng, 2006. **8**: p. 323-41.
10. Amstad, E., S.-H. Kim, and D.A. Weitz, *Photo- and Thermoresponsive Polymersomes for Triggered Release.* Angewandte Chemie International Edition, 2012. **51**(50): p. 12499-12503.
11. Napoli, A., et al., *Oxidation-responsive polymeric vesicles.* Nat Mater, 2004. **3**(3): p. 183-189.
12. Kim, K.T., et al., *A Polymersome Nanoreactor with Controllable Permeability Induced by Stimuli-Responsive Block Copolymers.* Advanced Materials, 2009. **21**(27): p. 2787-2791.
13. Amstad, E., et al., *Triggered Release from Liposomes through Magnetic Actuation of Iron Oxide Nanoparticle Containing Membranes.* Nano Letters, 2011. **11**(4): p. 1664-1670.
14. Chen, Y., A. Bose, and G.D. Bothun, *Controlled Release from Bilayer-Decorated Magnetoliposomes via Electromagnetic Heating.* ACS Nano, 2010. **4**(6): p. 3215-3221.
15. Sanson, C., et al., *Doxorubicin Loaded Magnetic Polymersomes: Theranostic Nanocarriers for MR Imaging and Magneto-Chemotherapy.* ACS Nano, 2011. **5**(2): p. 1122-1140.
16. Chen, K.-J., et al., *A Thermoresponsive Bubble-Generating Liposomal System for Triggering Localized Extracellular Drug Delivery.* ACS Nano, 2012. **7**(1): p. 438-446.
17. Paasonen, L., et al., *Gold nanoparticles enable selective light-induced contents*

release from liposomes. J Control Release, 2007. **122**(1): p. 86-93.
18. Erb, R.M., et al., *Predicting sizes of droplets made by microfluidic flow-induced dripping.* Soft Matter, 2011. **7**(19): p. 8757-8761.

Chapter 4 Morphological transitions in polymer vesicles upon bilayer swelling with small hydrophobic molecules in water

4.1 Introduction

Amphiphilic molecules can self-assemble into a variety of complex supramolecular structures, including hollow structures such as unilamellar bilayer-based vesicles.[1-5] These fluid filled molecular sacs, from a simplistic view, can be seen as synthetic model analogues of primitive cell membranes and can contain a plethora of molecular and/or colloidal encapsulates. The majority of studies on vesicles is focused on waterborne systems and draws great interest from scientific communities dealing with miniaturisation and confinement of fluidic reactions,[6] human health, with vesicles serving as capsular drug carriers, and to those exploring the origin of life, in the form of synthetic cell membranes.[7] Linking chemical composition with the physical properties of the vesicular bilayer is important to understand and optimise vesicle design, with mechanical robustness of the vesicles and permeability of the bilayer for transport or containment of active ingredients being two key characteristics. A common class of unilamellar vesicles is fabricated from naturally occurring phospholipids, such as dimyristoylphosphatidylcholine (DMPC), dipalmitoylphosphatidylcholine (DPPC), or sphingomyelin. Because of their biological context such supramolecular hollow structures are also referred to as liposomes. These bilayer-based assemblies of amphiphilic molecules of low molar mass, also including the more synthetic analogue vesicles made from *e.g.* didodecyldimethylammonium bromide (DODAB), show only limited mechanical stability. This weakness can directly be correlated with the size of the molecular building blocks used and can predominantly be attributed to the limited thickness of the bilayer. A logical solution to this shortcoming is to use larger amphiphilic molecules in order to tailor membrane robustness and control the vesicular bilayer thickness, as well as influence its glass transition temperature and/or

melting point. The preparation of vesicular structures from amphiphilic block copolymers was pioneered by Eisenberg and Discher, coining these as "polymersomes".[8, 9] Advances in polymer synthesis of amphiphilic macromolecules have led to considerable interest in these polymeric vesicles, with fabricated polymersomes showing sophisticated features, such as triggered bilayer rupture or decomposition,[10] biodegradability,[11] and multi-component bilayers often showing phase-separated regions,[12] which can be referred to as "rafts" (Figure 4.1). A current trend is the interaction of polymer vesicles with nanoparticles, reporting incorporation of hydrophobic magnetic nanoparticles into the bilayer,[13] induced shape transformation through pearling of the bilayer membranes upon nanoparticle exposure,[14] or formation of polymer vesicles armoured with a layer of colloidal nanoparticles.[15]

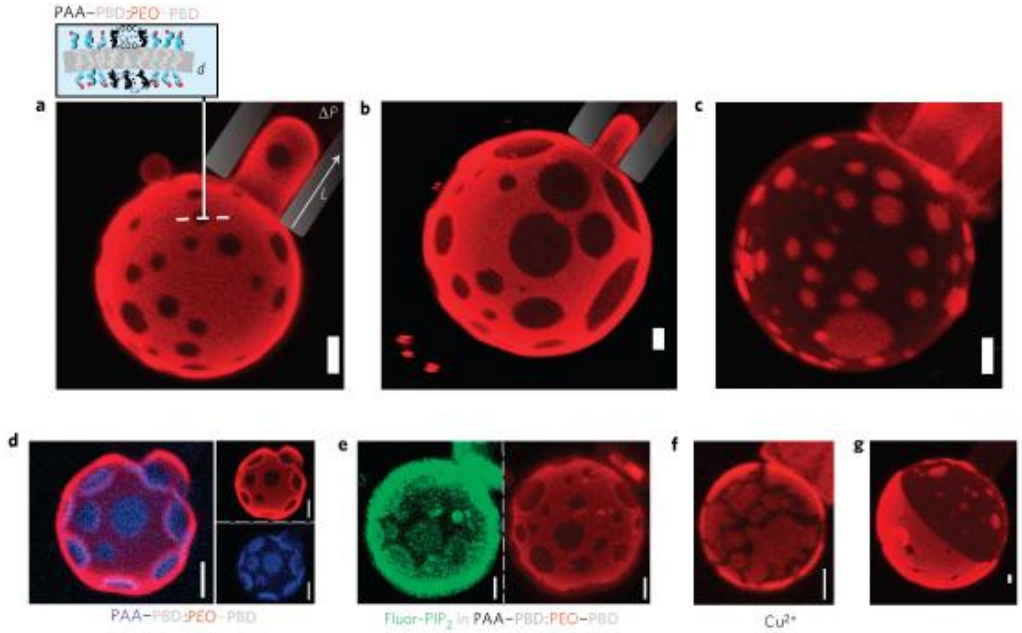

Figure 4.1 Cation induced, phase separation of charged poly(acrylic acid)-poly(butadiene) and neutral fluorencently labeled poly(ethylene oxide)-poly(butadiene) at different mixing ratio as described by Discher. [12]

One area that deserves further exploration, however, is how bilayer based vesicles behave when they are exposed to small liquid hydrophobic molecules, a situation of importance for example when vesicles are employed *in vivo* for medical applications.

It is plausible that swelling of the hydrophobic domains of the bilayer occurs by uptake of hydrophobic molecules. This phenomenon has for example been exploited advantageously as a method to reinforce the robustness of vesicles by swelling them with a hydrophobic monomer that subsequently is polymerised in order to thicken and thus strengthen the bilayer. Successful intrabilayer swelling of vesicles with hydrophobic monomers and subsequent radical polymerisation have been reported.[16-20] Intriguingly, in several cases after polymerisation a non-homogeneous distribution of a polymer throughout the bilayer was observed, commonly in the form of a polymer bead attached to the bilayer structure.[21-23] The principle cause of this beading has been postulated to be phase separation between the growing polymer and the vesicle bilayer.[22, 23] This is plausible when the polymer formed is incompatible with the amphiphilic molecules that form the bilayer, or could be possible if the free radius of gyration of the polymer molecules formed exceeds the thickness of the bilayer membrane. However, what is overlooked here is that the onset of phase separation can already be induced in the swelling stage. If true, this can have significant consequences in the physical properties and behaviour of vesicles upon their use as containers and delivery vehicles of drugs.

Brückner and Rehage observed that giant vesicles made from DMPC and DPPC underwent shape fluctuations when exposed to toluene, with occasional lens-shaped inclusions of solvent within the membrane.[24] Jung *et al.*[25] studied the interaction of DODAB vesicles and styrene indicating enhanced bilayer fluidity upon swelling and a drastic depression of the phase transition temperature. Moreover dynamic scanning calorimetric and fluorescent probe measurements suggested a non-homogeneous distribution and partial demixing of the solute and bilayer at ambient temperatures. These studies indicate that rearrangement of the amphiphilic molecules is possible and brought on by phase separation upon swelling which leads us to believe that more drastic morphological transformations of (polymer) vesicles can be induced.

Eisenberg *et al.* showed that polymer vesicles of poly(styrene)$_{410}$-*b*-poly(acrylic acid)$_{13}$ could undergo a drastic morphological transition into mesoscale aggregates

with an internal structure of hexagonally packed hollow hoops in a polystyrene matrix upon addition of salt in a *N*,*N*-dimethylformamide–water mixture.[26] Van Hest and coworkers reported a reverse transformation, from swollen spherical polymersomes in water–dioxane–THF ternary mixtures into stomatocytes upon dialysis against pure water (Figure 4.2)[27]

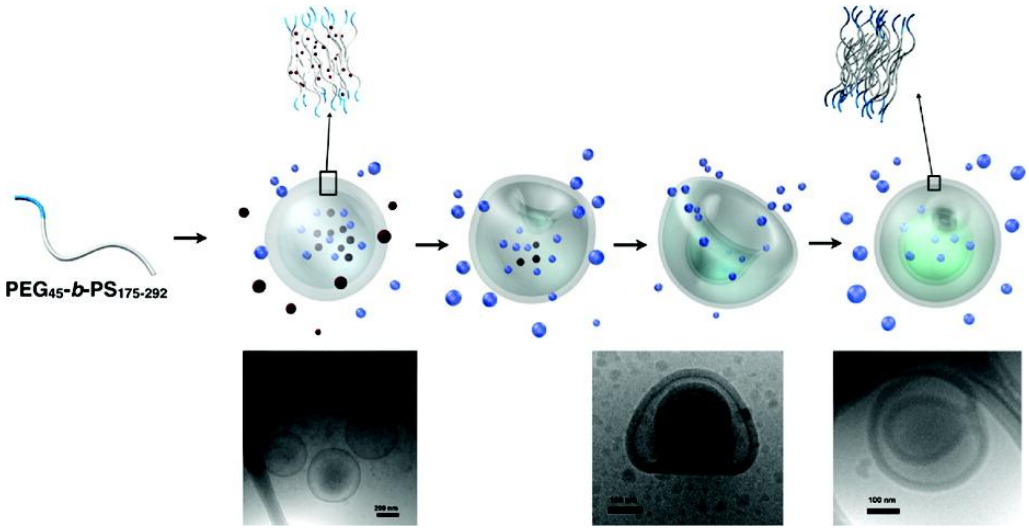

Figure 4.2 Shape transformation of polymersomes during dialysis of organic solvents (dark red spheres) against water (blue spheres) through a solvent-swollen bilayer membrane and cryo-TEM images of stomatocytes after shape transformation of polymersomes of PEG_{45}-*b*-PS_{230}[27]

Therefore, the preparation of polymer vesicles (polymersomes) from poly ((ethylene oxide)$_{45}$-block-(methyl methacrylate)$_{170}$) (PEG_{45}-$PMMA_{170}$) and poly(n-butyl methacrylate)$_{80}$-block-(2-(dimethylamino)ethyl methacrylate)$_{20}$ (PBMA-PDMAEMA) and the investigation of their morphological behaviour when dispersed in water saturated with the monomer methyl methacrylate (MMA) or n-butyl methacrylate (BMA) were proposed. Morphological changes upon swelling with the monomer of the exposed polymersomes were studied using cryogenic electron microscopy (both cryo-TEM and cryo-SEM). MMA and BMA were chosen as small hydrophobic molecules, as they are good solvents for the PMMA and PBMA parts of the block copolymer, which should in principle allow for randomised and thus homogeneous bilayer swelling.

4.2 Experimental

4.2.1 Materials

α-Hydroxy-Poly(ethylene glycol) (PEG)(ave mol. weight 2×10^3 g mol^{-1}, Aldrich), triethylamine (TEA)(BDH, 98%), Ethyl α-bromoisobutyrate (98%, Aldrich), poly(n-butyl methacrylate)$_{80}$-block-(2-(dimethylamino)ethyl methacrylate)$_{20}$ (PBMA-PDMAEMA, M_n=14.7k g mol^{-1}, PDI=1.10), n-butyl methacrylate (BMA, 99%, Sigma-Aldrich), Methyl methacrylate (Aldrich, 99%), tetrahydrofuran (THF) (Romil, "Hidry", 15 ppm water), 2-bromoisobutyryl bromide (Aldrich, 98%), dichloromethane (DCM)(BDH, 99%), Toluene (Fisher, 99%), diethylether (Fisher, 98%.), Copper (I) bromide (Aldrich, 98%) was purified according to the method of Keller and Wycoff (Veatch, S. L., Keller, S.L. Biophysical Journal 2003, 85, 3074), N-(n-propyl)-2-pyridylmethanimine (PPMI, 95%) was prepared using the procedure reported by Haddleton and co-workers (Haddleton, D. M.; Crossman, M. C.; Dana, B. H.; Duncalf, D. J.; Heming, A. M.; Kukulj, D.; Shooter, A. J. Macromolecules 1999, 32, 2110.), sodium hydrogen carbonate (BDH, 99%), and magnesium carbonate (BDH, 99%) were used as delivered.

4.2.2 Macroinitiator synthesis

The poly(ethylene glycol) macroinitiator was synthesised by reaction of the hydroxyl group of the PEG with an acid bromide. Dried (dessicator, overnight) PEG (0.01 mol) was dissolved in anhydrous THF with triethylamine (dried over molecular sieves) (0.149 mol) also bromoisobutyryl bromide (0.01 mol) added drop-wise from a syringe under nitrogen and the reaction was left to stir for 48 hrs at 25 ℃. Next, before being taken up into dichloromethane, (100 ml per 100 ml THF) the solution was washed (x3) with saturated sodium hydrogen carbonate (100 ml per 100 ml organic phase). The organic phase was dried over anhydrous magnesium sulphate and filtered. The solvent was removed under reduced pressure and the resulting liquid precipitated in cold

diethyl ether. The crude product was filtered and dried at reduced pressure to give a waxy solid. NMR spectra were recorded on a Brucker DPX 300 MHz spectrometer at 298K. ^{1}H NMR (D_2O, δ, ppm): 4.79 (2H, t, J=6.4Hz –CH_2OCO), 3.64 (2H, t, J=6.3Hz, -CH_2CH_2OCO), 3.51 (176H, m, (CH_2CH_2O)45), 3.36 (3H, s, -OCH_3), 1.89 (6H, s, -CH_3)

^{13}C NMR (DMSO, δ, ppm): 170.13, 77.09, 67.37, 64.00, 54.78, 29.68

4.2.3 PEG_{45}-$PMMA_{170}$ block copolymer synthesis

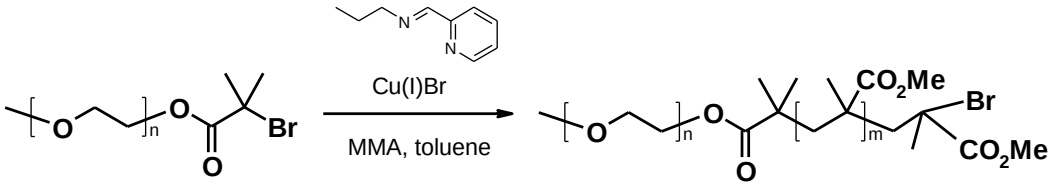

A Schlenk tube was charged with 12 g toluene, purified MMA (12 g, 0.12 mmol), PEG macroinitiator (1.05 g, 0.5 mmol), and the Cu (I) catalyst CuBr (0.07 g, 0.49 mmol). The mixture was de-aerated by three freeze- pump-thaw cycles, placed under a nitrogen gas atmosphere, and subsequently immersed into a preheated oil bath of 90 ℃. Next the ligand, PPMI was injected into the system by syringe to start the reaction. The reaction was monitored by samples taken at regular intervals which were analysed by NMR and also GPC. Once the reaction had reached the desired conversion (~70%), the schlenk tube was removed from the bath, 20 ml toluene was added to the polymer solution and the mixture was filtered by a basic alumina column to remove the copper and ligand. The polymer was purified by precipitation in methanol at -30 ℃ and further dried under vacuum. The molecular weight distribution was determined by gel permeation chromatography and the average molecular weight was calculated by NMR spectrum. M_n=19.2 kDa, PDI=1.05.

4.2.4 Polymersome formation

PBMA-PDMAEMA polymersomes were prepared as previously described (Chapter 2) using the solvent addition method with an initial concentration of 2 g L^{-1} in THF and

final solvent ratio of 90% water: 10% THF. PEG-PMMA polymersomes were prepared in a similar way but using only deionised water instead of acetic acid solution. The samples were then analysed by DLS to determine the approximate size distribution.

4.2.5 Polymersome dialysis

The polymersome solution (50 ml) at initial concentration 0.2 g L^{-1} was dialysed in tubing which had been thoroughly washed with warm water. The dialysis tubing was tied and clipped at the top and bottom and placed in a 2 L beaker of water (Acetic acid solution for PBMA-PDMAEMA). The solution was left to dialyse and the water was replaced three times a day for 5 days to encourage the maximum removal of THF.

4.2.6 Polymersome swelling

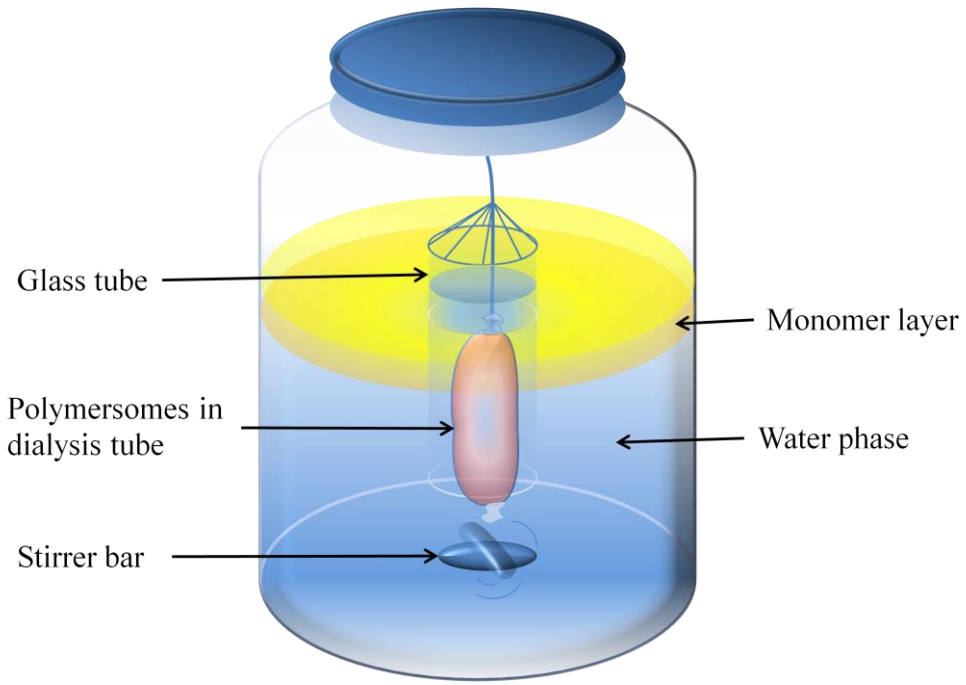

Figure 4.3 Schematic drawing of polymersomes swelling apparatus

The dialysed polymersome solution (10 ml) was properly sealed in a dialysis tube and then suspended inside a glass tube partly submerged in fresh deionised water to

prevent direct contact between the monomer layer and dialysis tubing. 20 ml monomer (methyl methacrylate and n-butyl methacrylate respectively) was added carefully by pipette down the side of the 150 ml glass jar to minimise splashing. A small amount of nitroxide TEMPO was added to the sample and the entire system was then sealed properly to avoid monomer evaporation. Gently stirring was applied to encourage homogenous distribution of dissolved monomer in the outer water phase, which then created monomer saturated aqueous environment for the polymersomes. The dialysis was allowed for a period of 5 days at ambient temperature.

4.3 Results and discussion

4.3.1 MMA swelling for both PMMA and PBMA based polymersomes

Polymer vesicles were prepared from the block copolymer solution in tetrahydrofuran (THF). with slow addition of water (being a non-solvent for the PMMA or PBMA block), to reach a final solvent composition of 80% water : 20% THF and a final blockcopolymer concentration of 0.2 g L^{-1}. The obtained polymersome dispersion was thoroughly dialyzed against water in order to remove the THF. For PMMA based polymersome, Dynamic light scattering results shows an average size of 850nm but with a PDI of 0.4, which suggests a polydisperse distribution. However, by using Multiple Narrow Modes algorithm in the instrument software, it clearly shows that the sample contains two different sized polymersomes with the average diameter of 530 nm and 3.2 μm and percentage composition of 97% and 3% respectively. Cryo-SEM investigation of waterborne dispersions of poly-((ethylene oxide)$_{45}$-block-(methyl methacrylate)$_{170}$) polymersomes showed that indeed a majority of few hundred nanometre sized polymersomes with a "smooth" surface morphology were formed. (Figure 4.4).

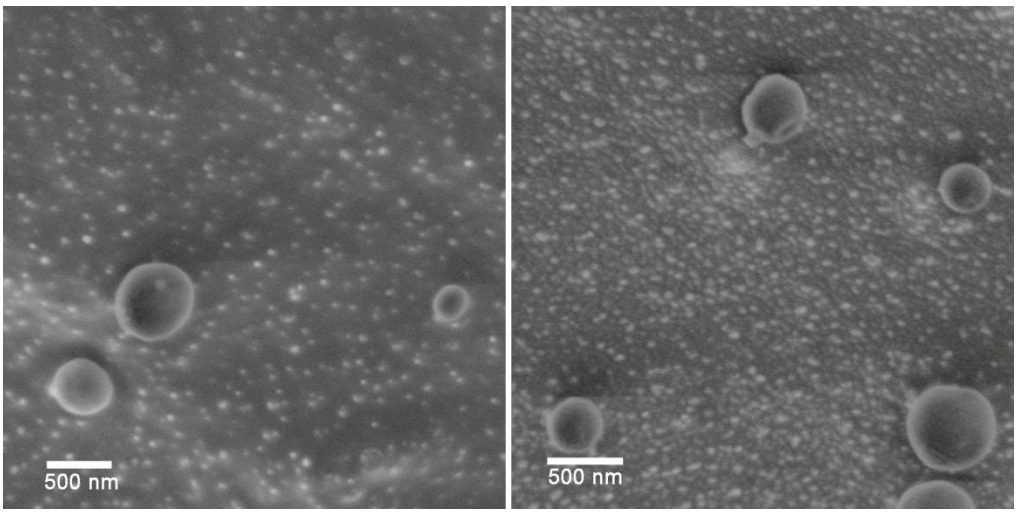

Figure 4.4 Cryo-TEM micrographs of poly((ethylene oxide)$_{45}$-block-(methyl

methacrylate)$_{170}$) polymersomes dispersed in water. Scale bar = 500 nm

During the Cryo-SEM preparation, an anti-contaminate plate was installed above the sample stage near the lens and was set 60 K lower than the stage temperature to minimise ice condensation on the sample. However, part of the sublimed water can still condense on the sample surface to form small ice crystal, which can be observed in the form of small bright dots under microscope (Figure 4.4). Moreover, Figure 4.5 shows that the smooth surface remained even after prolonged sublimation of ice upon exposure to the electron beam.

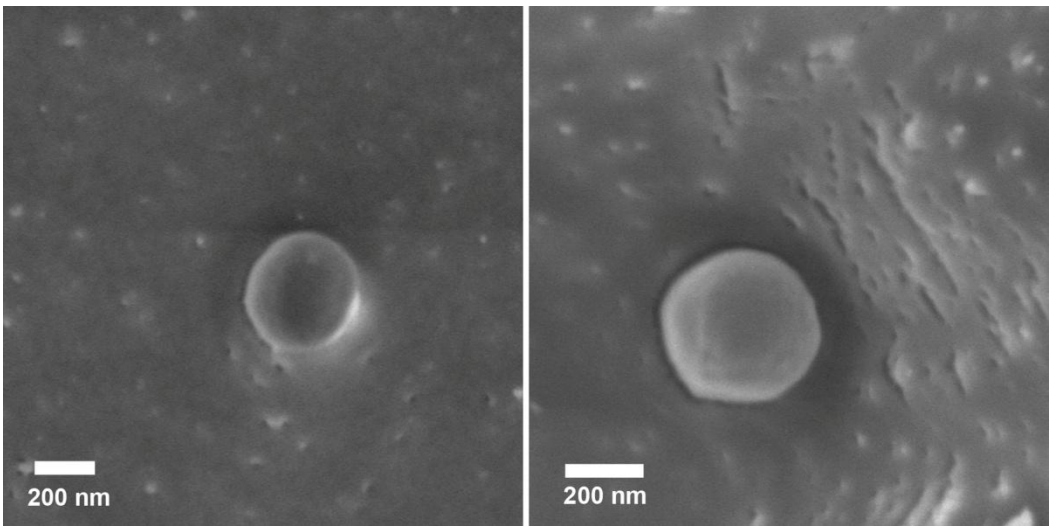

Figure 4.5 Cryo-SEM micrographs of poly((ethylene oxide)$_{45}$-block-(methyl methacrylate)$_{170}$) polymersomes after exposure under 2 kv electron beam for around 30 seconds. Comparing with figure 4.4, the potholes and the absence of the white dots suggest that the condensed ice has been sublimed by the energy of the electron beam. Scale bar = 200 nm

The same surface morphology can be observed in polymersomes made from poly(n-butyl methacrylate)$_{80}$-block-(2-(dimethylamino)ethyl methacrylate)$_{20}$ (see Figure 4.6). The polymersome dispersions prepared from this block copolymer tended to have a larger average size of around 1 μm. A potential reason for the size difference in this case is the weaker hydrophilicity of the DMAEMA block compared with PEO, which results in a smaller volume fraction in water for each block copolymer chain,

and therefore a lower curvature structure (larger radius of curvature) is required to maintain the unilamellar form. (Figure 5.7) In extreme cases, the block copolymer will self-assemble into micelles rather than vesicles in aqueous when the volume fraction of hydrophilic block is large enough.[8]

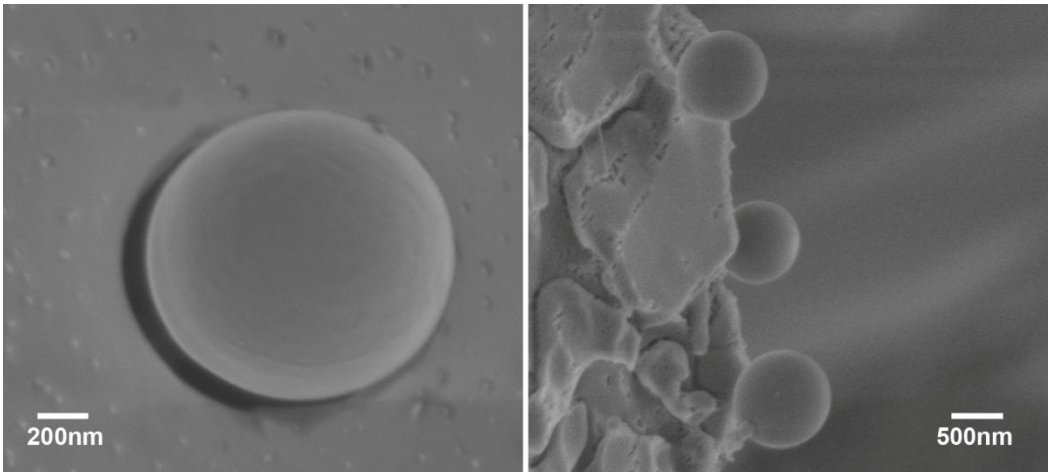

Figure 4.6. Cryo-SEM micrographs of from poly(n-butyl methacrylate)$_{80}$-block-(2-(dimethylamino)ethyl methacrylate)$_{20}$ polymersomes dispersed in pH 4.5 water. Scale bar = 200 nm (Left) and 500 nm (Right)

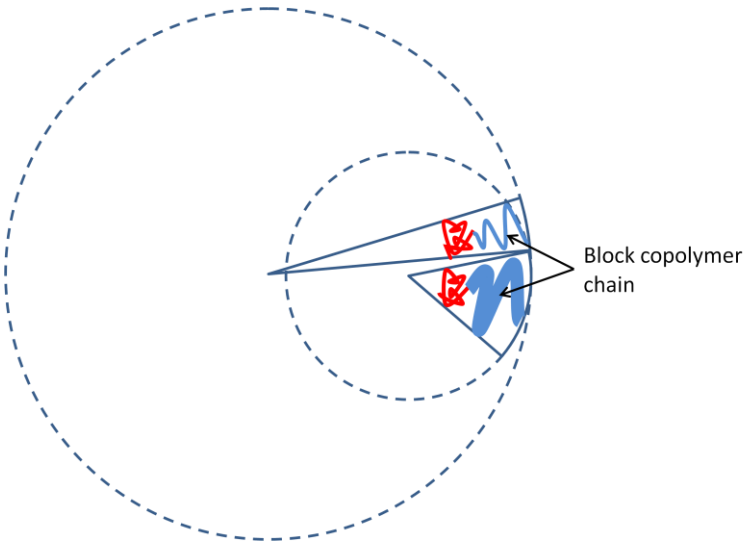

Figure 4.7. Block copolymers with different hydrophilic fractions can result in different radius of curvature.

It is worth noting that in the case of the poly((ethylene oxide)$_{45}$-block-(methyl methacrylate)$_{170}$) vesicles, a small fraction of large, that is of micron-scale dimensions,

multilamellar polymersomes were formed, which could be clearly visualised by sectioned cryo-SEM analysis. (Figure 4.8 and 4.9)

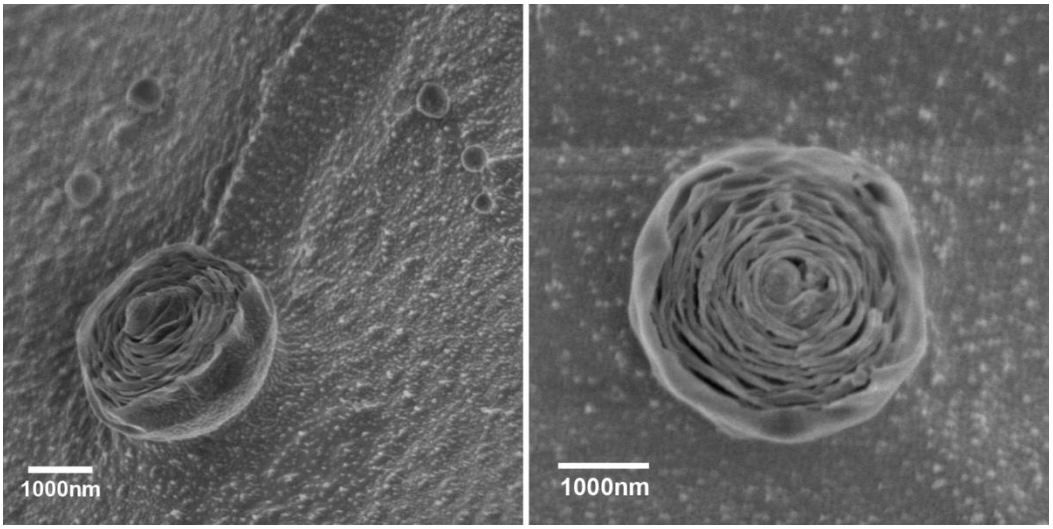

Figure 4.8 Giant multilamellar polymersomes formed from PEG_{45}-$PMMA_{170}$ with an approximate measured bilayer "thickness" of 40–45 nm, the size of these polymersomes were significantly larger than the majority ones. Scale bar = 1000 nm

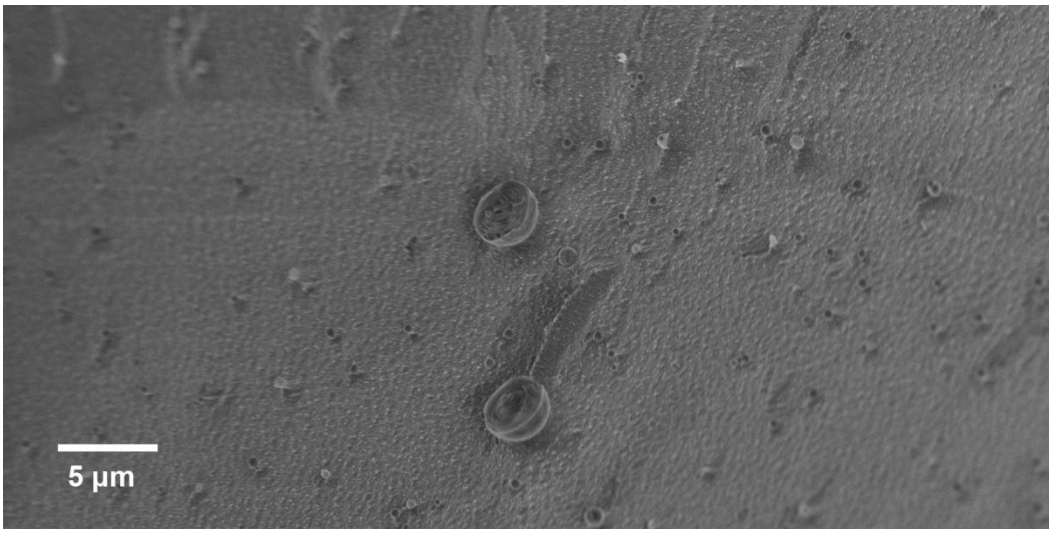

Figure 4.9 Cryo-SEM image of the overview of the PMMA based polymersome sample which consists of mostly the unilamellar polymersomes and a small fraction of multilamellar ones (two giant ones at the centre). Scale bar = 5µm

Next, the aqueous polymersome dispersions were swollen with methyl methacrylate (MMA) by exposing them to water saturated with MMA for a period of 5 days at

ambient temperature. To rule out the possibility of free radical polymerisation of MMA, a small amount of radical scavenger was added in the form of the nitroxide TEMPO. Cryogenic SEM analysis revealed the coexistence of multiple, more complex, morphologies. There were polymersomes that appeared to be “normal”, in which the monomer had swollen the bilayer (Figure 4.10). There are, in addition, more “complex” polymersomes, which show both coiled and patchy morphologies. These complex structures co-exist randomly with the unilamellar population in a roughly 50 : 50 to 60 : 40 ratio.

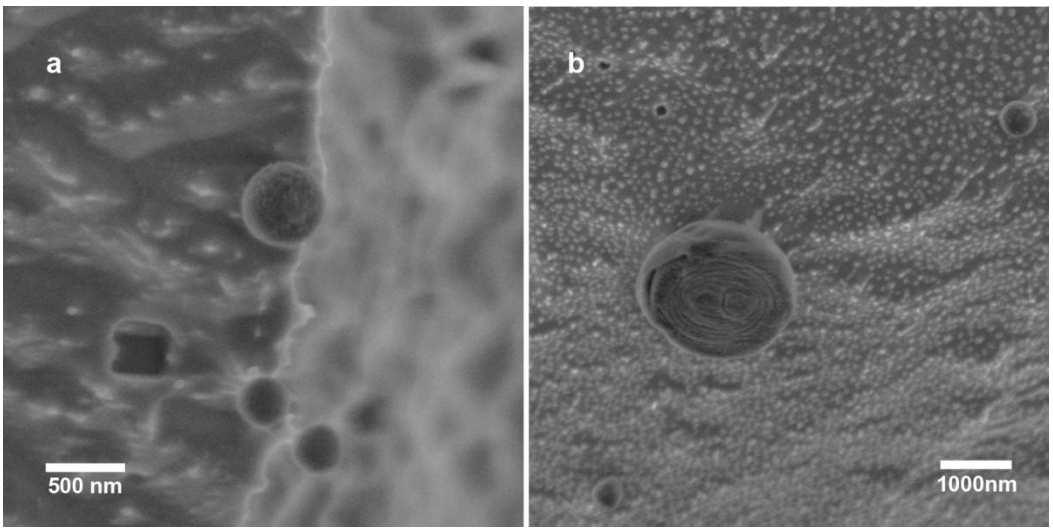

Figure 4.10 Cryo-SEM images of MMA swelling PMMA based polymersomes. (a) the larger vesicle at the top shows significant patchy morphology compared with the ones in Figure 4.4, while the bottom two look to be “normal”. (b) the giant multilamellar polymersome in the middle shows a significant less gaps between layers and the approximate measured bilayer thickness is 50–53 nm, which suggests that the thickness of each layer has increased roughly 25% percent. Scale bar = 500 nm (Left) and 1000 nm (Right)

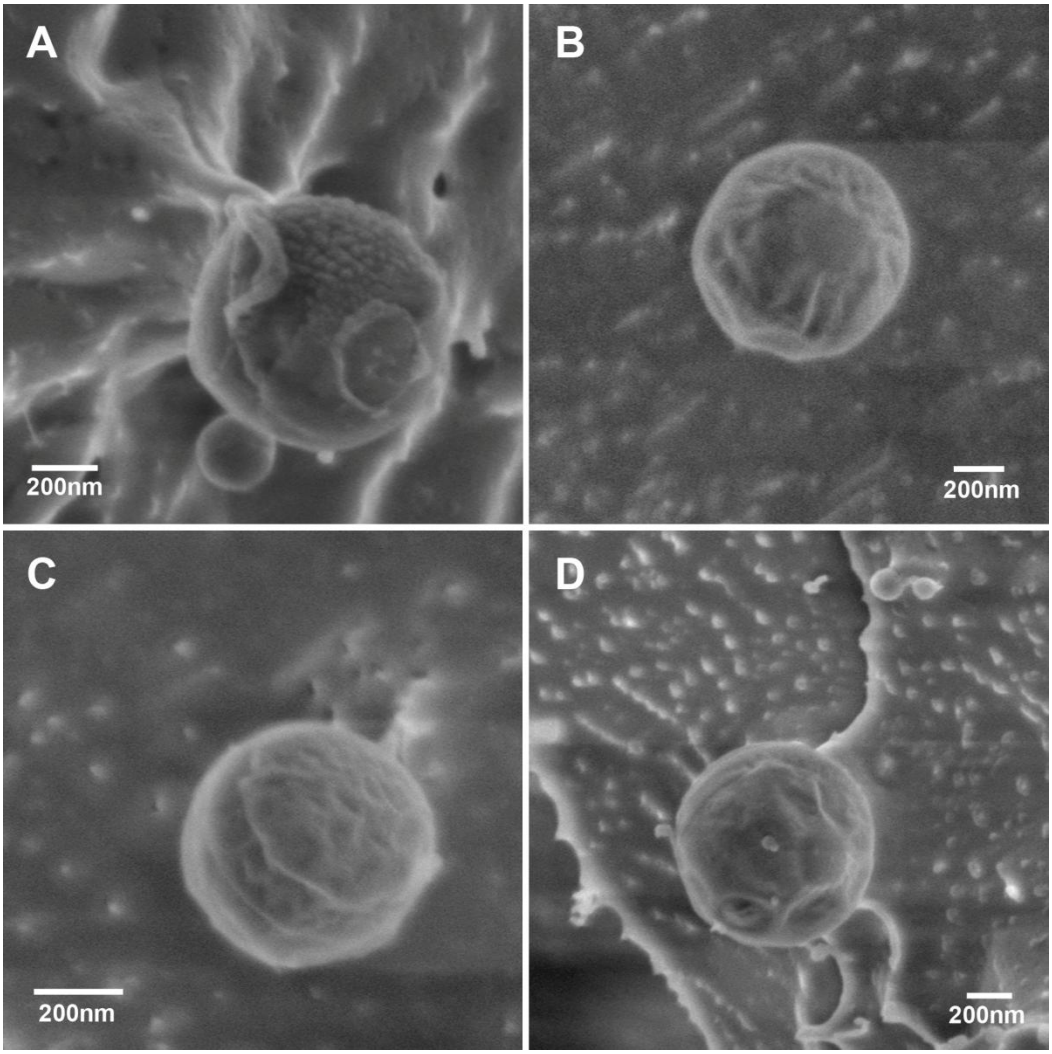

Figure 4.11 Cryo-SEM images of poly((ethylene oxide)$_{45}$-block-(methyl methacrylate)$_{170}$) polymersomes swollen with MMA. Both (A) and (C) show morphology caused by a coiled structure and (D) shows a clear globular patchy surface. Scale bar = 200 nm.

Cryo-SEM of poly((ethylene oxide)$_{45}$-block- (methyl methacrylate)$_{170}$) polymersomes swollen with MMA clearly showed that the original smooth surface morphology was no longer exclusive, but that the polymersomes now had more complex morphologies, clearly demonstrating that exposure of polymersomes to small hydrophobic molecules, in this case MMA, led to morphological transformations.(See Figure 4.11)

Swelling of the PBMA based polymersomes, with MMA and subsequent cryo-TEM analysis revealed mostly a patchy morphology in most of the vesicles (Figure 4.12). A

potential reason for the less drastic morphology changes in this case is the poorer compatibility of MMA with the hydrophobic part of the polymersome structure.

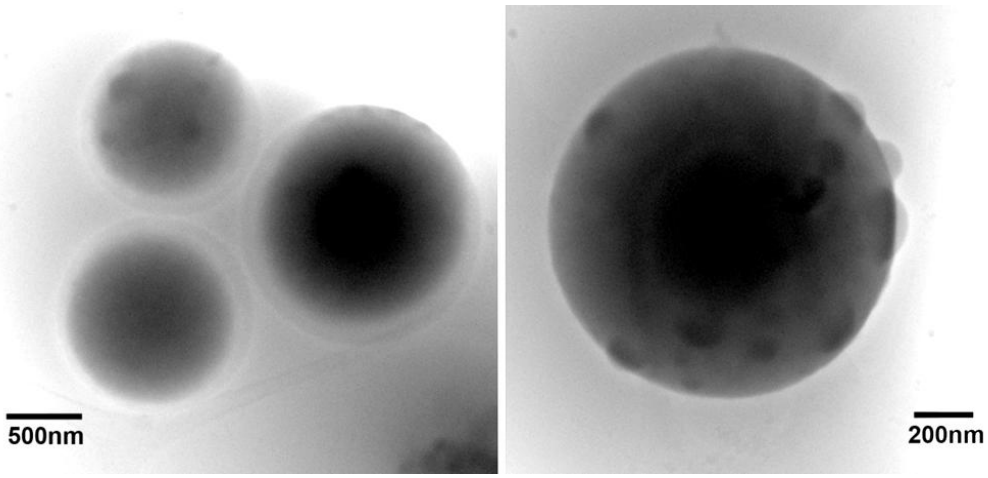

Figure 4.12 Cryo-TEM images of poly(n-butyl methacrylate)$_{80}$-block-(2-(dimethylamino) ethyl methacrylate)$_{20}$ polymersomes swollen with MMA dispersed in water. Scale bar = 500 nm (Left) and 200 nm (Right)

4.32 BMA swelling of PBMA based polymersomes

Due to the less compatibility of MMA monomer and PBMA parts of the polymersomes, the PBMA based polymersome sample was therefore exposed the to BMA monomer in order to promote swelling process and thus morphology changes. Cryo-TEM analysis of poly(n-butyl methacrylate)$_{80}$- block-(2-(dimethylamino) ethyl methacrylate)$_{20}$ polymersomes swollen with BMA monomer shows significantly different surface morphology compared with MMA swollen one (See Figure 4.13). The circular shape has maintained however the surface is no longer “smooth”, which in this case has multiple open pockets on the bilayer. Due to the size of the polymersomes and the swelling of the BMA, the electron beam could not penetrate the central part of the polymersomes, therefore shows only a solid dark core in the images.

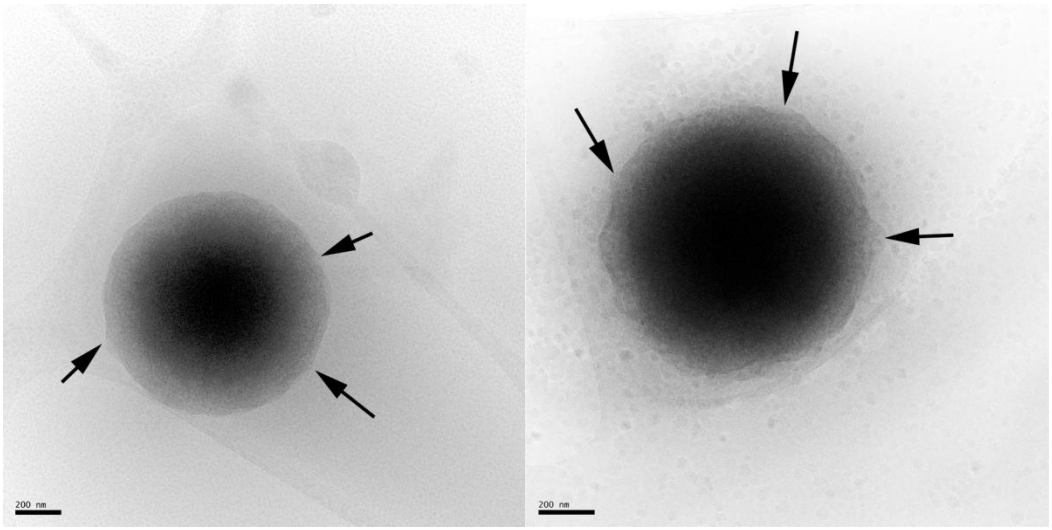

Figure 4.13 Cryo-TEM images of poly(n-butyl methacrylate)$_{80}$-block-(2-(dimethylamino) ethyl methacrylate)$_{20}$ polymersomes swollen with BMA dispersed in water. "Smooth" morphology is no longer observable and the arrow points show the open pockets area on the surface.

Cryo-SEM analysis of poly(n-butyl methacrylate)$_{80}$-block-(2-(dimethylamino) ethyl methacrylate)$_{20}$ polymersomes in water, now swollen with BMA, again shows more complex surface morphologies (Figure 4.14). Differ from PMMA based polymersomes, these PBMA based polymersomes show more brain-like surface morphology and multiple holes possibly because of the open pocket structure that was observed under cryo-TEM.

The close-up image of this structure in Figure 4.15 shows that the size of the holes is approximately 100 nm, which is consistent with the similar structure observed by Cryo-TEM. One potential explanation of the potholes formation is of the sublimation of the water or monomer reservoir from this "pocket" structure. Therefore, it is believed that the exposure to small compatible hydrophobic molecules may lead to severe morphological transitions in the bilayer.

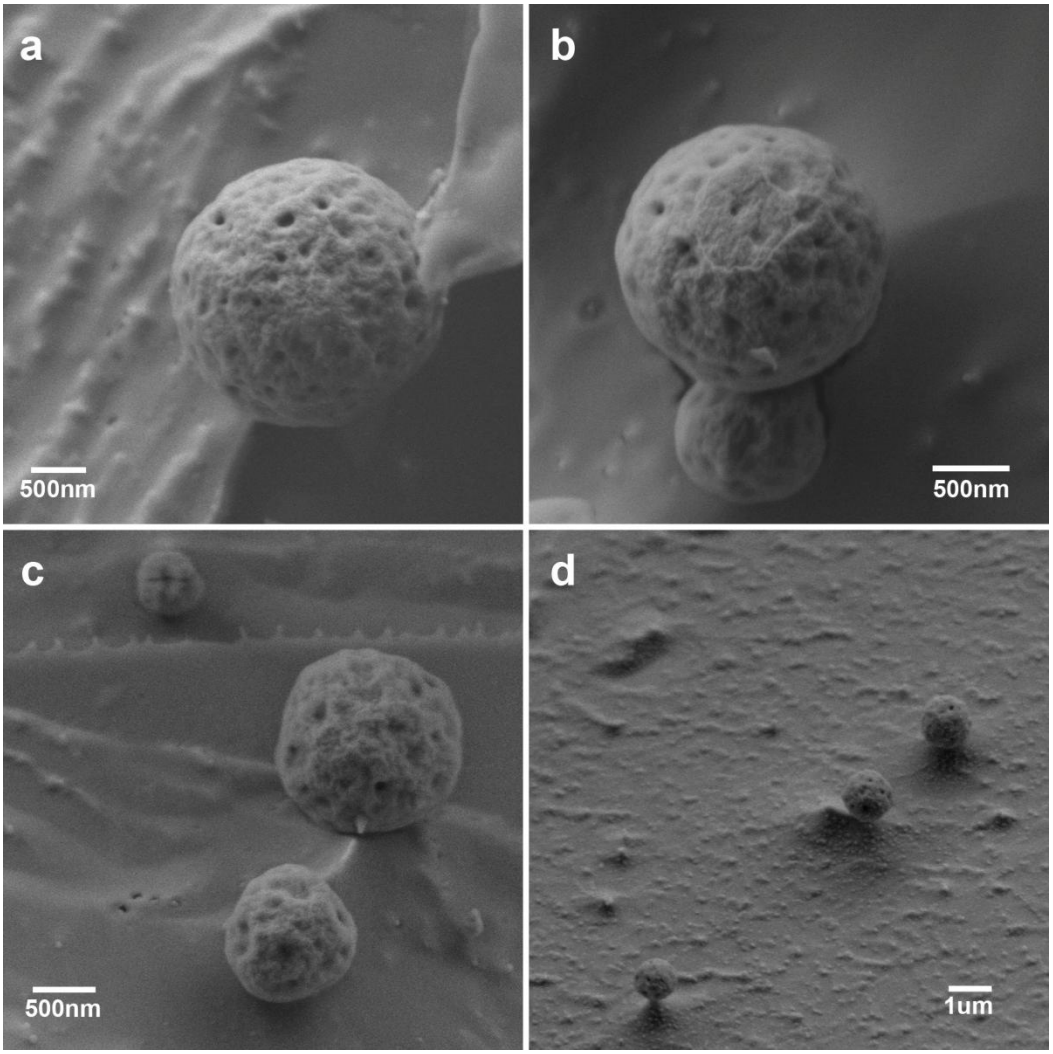

Figure 4.14 Cryo-SEM images of poly(n-butyl methacrylate)$_{80}$-block-(2-(dimethylamino) ethyl methacrylate)$_{20}$ polymersomes swollen with BMA dispersed in water.

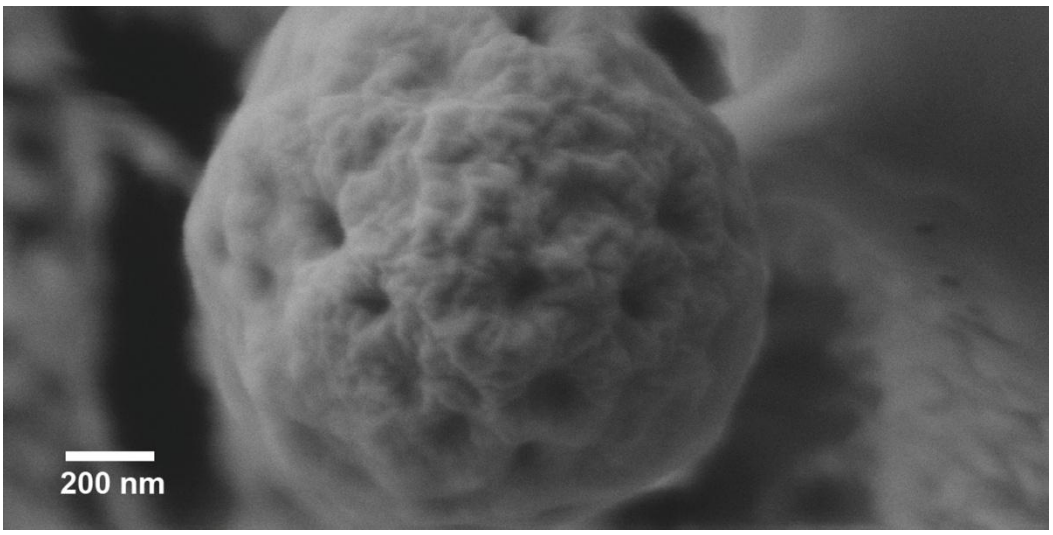

Figure 4.15 Cryo-SEM image of pBMA based polymersome after BMA swelling.

4.4 Conclusions

It is concluded that when unilamellar blockcopolymer vesicles dispersed in water are exposed to small hydrophobic molecules, they can undergo morphological transitions. Swelling of the bilayer membrane induces instability which leads to the formation of water pockets, as demonstrated by the simulations (Appendix II). One could speculate that these pockets arise due to Plateau ĆRayleigh type instability induced by interfacial tensions, or even with a Rayleigh ĆTaylor character induced by variations in densities. Coil type structures could be explained potentially through fusion of water pockets into a more cylindrical structure, which could then ripen again through coalescence into the patchy morphology. Co-existence of the various morphologies in the experiments suggests an activation barrier towards morphological changes and a possibility of multiple meta-stable states. These results may have an impact on, for example, the area of drug delivery, as polymersomes used in vivo as delivery vehicles may undergo such transitions which would lead to different drug release profiles and potentially encapsulation failure.

References

1. Israelachvili, J.N., D.J. Mitchell, and B.W. Ninham, *Theory of self-assembly of hydrocarbon amphiphiles into micelles and bilayers.* Journal of the Chemical Society, Faraday Transactions 2: Molecular and Chemical Physics, 1976. **72**(0): p. 1525-1568.
2. Fendler, J.H., *Surfactant vesicles as membrane mimetic agents: characterization and utilization.* Accounts of Chemical Research, 1980. **13**(1): p. 7-13.
3. Bangham, A.D., *Liposomes: the Babraham connection.* Chemistry and Physics of Lipids, 1993. **64**(1–3): p. 275-285.
4. Zhang, L. and A. Eisenberg, *Multiple Morphologies of "Crew-Cut" Aggregates of Polystyrene-b-poly(acrylic acid) Block Copolymers.* Science, 1995. **268**(5218): p. 1728-1731.
5. Antonietti, M. and S. Förster, *Vesicles and Liposomes: A Self-Assembly Principle Beyond Lipids.* Advanced Materials, 2003. **15**(16): p. 1323-1333.
6. Vriezema, D.M., et al., *Self-Assembled Nanoreactors.* Chemical Reviews, 2005. **105**(4): p. 1445-1490.
7. Tanner, P., et al., *Polymeric Vesicles: From Drug Carriers to Nanoreactors and Artificial Organelles.* Accounts of Chemical Research, 2011. **44**(10): p. 1039-1049.
8. Discher, D.E. and A. Eisenberg, *Polymer Vesicles.* Science, 2002. **297**(5583): p. 967-973.
9. Kita-Tokarczyk, K., et al., *Block copolymer vesicles—using concepts from polymer chemistry to mimic biomembranes.* Polymer, 2005. **46**(11): p. 3540-3563.
10. Kim, K.T., et al., *A Polymersome Nanoreactor with Controllable Permeability Induced by Stimuli-Responsive Block Copolymers.* Advanced Materials, 2009. **21**(27): p. 2787-2791.
11. Meng, F., et al., *Biodegradable Polymersomes.* Macromolecules, 2003. **36**(9): p. 3004-3006.
12. Christian, D.A., et al., *Spotted vesicles, striped micelles and Janus assemblies induced by ligand binding.* Nat Mater, 2009. **8**(10): p. 843-849.
13. Lecommandoux, S., et al., *Magnetic Nanocomposite Micelles and Vesicles.* Advanced Materials, 2005. **17**(6): p. 712-718.
14. Yu, Y. and S. Granick, *Pearling of Lipid Vesicles Induced by Nanoparticles.* Journal of the American Chemical Society, 2009. **131**(40): p. 14158-14159.
15. Chen, R., et al., *Polymer Vesicles with a Colloidal Armour of Nanoparticles.* Journal of the American Chemical Society, 2011. **133**(7): p. 2151-2153.
16. Murtagh, J. and J.K. Thomas, *Mobility and reactivity in colloidal aggregates with motion restricted by polymerization.* Faraday Discussions of the Chemical Society, 1986. **81**(0): p. 127-136.
17. Kurja, J., et al., *Free radical polymerization of styrene in dioctadecyldimethylammonium bromide vesicles.* Polymer, 1993. **34**(10): p. 2045-2049.

18. Morgan, J.D., C.A. Johnson, and E.W. Kaler, *Polymerization of Equilibrium Vesicles.* Langmuir, 1997. **13**(24): p. 6447-6451.
19. Hotz, J. and W. Meier, *Vesicle-Templated Polymer Hollow Spheres.* Langmuir, 1998. **14**(5): p. 1031-1036.
20. Krafft, M.P., et al., *Fluorinated Vesicles Allow Intrabilayer Polymerization of a Hydrophobic Monomer, Yielding Polymerized Microcapsules.* Langmuir, 2001. **17**(9): p. 2872-2877.
21. Jung, M., et al., *New Vesicle−Polymer Hybrids: The Parachute Architecture.* Langmuir, 1997. **13**(26): p. 6877-6880.
22. Hubert, D.H.W., et al., *Electrooptic Behavior and Structure of Novel Polymer−Vesicle Hybrids.* Langmuir, 1999. **15**(26): p. 8849-8855.
23. Jung, M., et al., *A Topology Map for Novel Vesicle–Polymer Hybrid Architectures.* Advanced Materials, 2000. **12**(3): p. 210-213.
24. Brückner, E. and H. Rehage, *Solubilization of toluene in phospholipid vesicles studies by video-enhanced contrast microscopy*, in *Horizons 2000 – aspects of colloid and interface science at the turn of the millenium*, G. Lagaly, Editor. 1998, Steinkopff. p. 21-28.
25. Jung, M., et al., *Interaction of Styrene with DODAB Bilayer Vesicles. Influence on Vesicle Morphology and Bilayer Properties.* Langmuir, 1999. **16**(3): p. 968-979.
26. Zhang, L., et al., *Mesosized Crystal-like Structure of Hexagonally Packed Hollow Hoops by Solution Self-Assembly of Diblock Copolymers.* Physical Review Letters, 1997. **79**(25): p. 5034-5037.
27. Kim, K.T., et al., *Polymersome Stomatocytes: Controlled Shape Transformation in Polymer Vesicles.* Journal of the American Chemical Society, 2010. **132**(36): p. 12522-12524.
28. Hoogerbrugge, P.J. and J.M.V.A. Koelman, *Simulating Microscopic Hydrodynamic Phenomena with Dissipative Particle Dynamics.* EPL (Europhysics Letters), 1992. **19**(3): p. 155.
29. Ortiz, V., et al., *Dissipative Particle Dynamics Simulations of Polymersomes.* The Journal of Physical Chemistry B, 2005. **109**(37): p. 17708-17714.
30. Groot, R.D. and P.B. Warren, *Dissipative particle dynamics: Bridging the gap between atomistic and mesoscopic simulation.* The Journal of Chemical Physics, 1997. **107**(11): p. 4423-4435.
31. Español, P. and P. Warren, *Statistical Mechanics of Dissipative Particle Dynamics.* EPL (Europhysics Letters), 1995. **30**(4): p. 191.
32. Plimpton, S., *Fast Parallel Algorithms for Short-Range Molecular Dynamics.* Journal of Computational Physics, 1995. **117**(1): p. 1-19.
33. Lindahl, E. and O. Edholm, *Mesoscopic Undulations and Thickness Fluctuations in Lipid Bilayers from Molecular Dynamics Simulations.* Biophysical Journal. **79**(1): p. 426-433.

Appendix

Simulation of the packing pattern of spherical particles on the vesicle surface

The effect of the surface charge density σ on the packing patterns of a mixture of two different sized spherical particles on a spherical vesicle was studied with the collaboration of Sara Fortuna & David L. Cheung. The vesicle diameter is 1 μm, and the small and the big spherical particle's diameters are 120nm and 200nm, respectively.

The particles interact with a total pair potential given by:

$$E_{ij} = E_{ij}^{LJ\alpha-2\alpha} + E_{ij}^{\text{Yukawa}} \quad \text{(A.1)}$$

where

$$E_{ij}^{LJ\alpha-2\alpha} = \epsilon_0 \left[\left(\frac{r_{\text{eq}}}{r_{ij}} \right)^{2\alpha} - 2 \cdot \left(\frac{r_{\text{eq}}}{r_{ij}} \right)^{\alpha} \right] \quad \text{(A.2)}$$

and

$$E_{ij}^{\text{Yukawa}} = \frac{A\prime \cdot \exp(-r_{ij}/\xi)}{(r_{ij}/\xi)} \quad \text{(A.3)}$$

$E_{ij}^{LJ\alpha-2\alpha}$ is a Lennard-Jones (LJ) like potential where ϵ_0 is the depth of the potential well, r_{eq} is the equilibrium distance between the two particles ij, and α is a parameter describing the "softness" of the potential. Larger α harder the potential, in which particles are less likely to overlap. It has been shown in the previous report [29] that silica nanoparticles are well described by a LJ potential with α = 12.

E_{ij}^{Yukawa} is a Yukawa potential [33] (or screened Coulomb potential), used in the description of colloidal particles to take into account the electrostatic interactions between colloids. In this potential, ξ is the screening length parameter, which accounts for the screening of the Coulomb interactions between charged particles by counter-ions in solution, and $A' = \frac{q_i q_j}{4\pi\varepsilon}$ where q_i and q_j are the charges on the particles i and j, respectively. The charge on each particle can be calculated from the surface charge density σ which is the same for all the particles (they all have the

same chemical composition): $q_i = 4\pi r_i^2 \sigma$. It is then possible to write $A' = r_i^2 r_j^2 \cdot A$, with $A = \frac{4\pi}{\varepsilon}\sigma^2$.

For each chosen value of surface charge density σ, a chain of MC simulations has been performed. Each simulation runs for 10,000,000 Monte Carlo (MC) steps. The MC steps follow the Metropolis algorithm. At each simulation step, a particle is chosen at random and displaced, generating a new configurations'. s' is accepted or rejected with probability:

$$P(s \to s') = \min\left[1, e^{-\frac{E_{s'} - E_s}{k_B T}}\right] \quad \text{(A.4)}$$

where E_s is the energy associated with the old configuration s, $E_{s'}$ is the energy associated with the new configuration s', k_B is the Boltzmann constant, and T is the system temperature.

For each N, the starting configuration corresponds to the final configuration of a simulation with $N-1$ particles, therefore each simulation is linked to the previous one by addition of one particle to the equilibrated system.

Particles are added to the system following a Grand-Canonical-like acceptance probability, under the assumption that the particles, once adsorbed on the surface, cannot be released. A particle is added to the system with probability:

$$P(N \to N+1) = \min\left[1, \frac{1}{(N+1)} e^{-\frac{\tilde{\mu} - E_{N+1} + E_N}{k_B T}}\right] \quad \text{(A.5)}$$

where $\tilde{\mu}$ is an effective chemical potential of the form: $\tilde{\mu} = \mu + k_B T \cdot \ln\frac{V}{\Lambda^3}$, where μ is the chemical potential, V the system constant volume, and $\Lambda = \sqrt{\frac{h^2}{2\pi m k_B T}}$ the thermal de Broglie wavelength, with h Plank's constant, m mass of the particle.

At the beginning of each simulation of the chain, an attempt to add a particle is performed. If not accepted, 1000MC moves are performed and another insertion is attempted. The particle to insert is chosen with a selection probability that corresponds to the experimental encounter probability. As we are describing the non-equilibrium process of particle absorption on a vesicle surface, particle removals

are never attempted and the overall procedure does not obey detailed balance. The simulation chain stops when 10000 attempts to insert a particle fail.

All the simulations have been run at $k_{\mathrm{B}}T = 0.1$ and $\tilde{\mu} = 0$. All the energies are expresses in units of ϵ_0.

The encounter probability that the vesicle collides with a particle is linked to its number density and its velocity. According to the Stokes Einstein equation, particles with a smaller radius will have a higher diffusion coefficient and so move faster in the solution.

Fick's first law states that the flux of particles, J, in a diffusion limited system is directly proportional to the concentration gradient. For small particles diffusing through the surface of a large sphere, radius R and surface area A, the total steady state collision rate, will be:

$$AJ = -4\pi R^2 D \frac{dN}{dR} \qquad \text{(A.6)}$$

Let the central sphere be a particle, radius c, far larger than the diffusion particles; this leads to the assumption that the central particle is motionless.

The diffusion coefficient for a particle with radius r, in a solution of viscosity η at temperature T, is given by the Stokes Einstein equation:

$$D = \frac{K_B T}{6\pi\eta r} \qquad \text{(A.7)}$$

Inserting Eq. A.7 into Eq. A.6 and integrating over R from the surface of the central sphere gives the collision frequency:

$$AJ = \frac{4ck_bTN}{6\eta r} \quad \text{(A.8)}$$

Here c and A are the radius and area of the central particle, respectively, and N is the total number of small particles. It has been assumed that c >> r.

For two populations of monodisperse spheres with number densities N_a and N_b and radii r_a and r_b, respectively, colliding with a large vesicle, the flux of particles, J_a and J_b respectively, onto the surface will abide by the ratio:

$$\frac{J_a}{J_b} = \frac{N_a r_b}{N_b r_a} \quad \text{(A.9)}$$

This assumes that both latices feel the same effect on their diffusion rates due to the

other latex, and $r_a \approx r_b$.

The polymersomes analysed under the Cryo-SEM were made of block co-polymers consisting of 9.7 KDa PBMA and ~4 KDa DMAEMA. These formed vesicles of ~1μm diameter according to DLS results.

Added to these were 120 nm and 200 nm latex beads in different ratios. By measuring the exact weight percentage of the latices and accounting for the different aggregation rates of the different size beads (given by Eq. A.9), the vesicles were expected to collide with the latices in the following ratios.

120 nm Latex solution (0.9%wt) Added /g	200 nm Latex Solution (0.4%wt) Added /g	Relative probability of meeting 120 nm bead	Relative probability of meeting a 200 nm bead
1	0	1	0
0.3974	0.6541	0.56	0.44
0.1888	0.8298	0.79	0.21
0.075	0.9567	0.91	0.09
0	1	0	1

Table A.1 Different ratios of mixed latex samples and their encounter probabilities when added to the polymersome solution.

Three different particle densities with encounter probabilities of small beads corresponding to 56%, 78% and 91% respectively were then studied. The simulated packing paterns are shown in Figure A.1. The ratios of beads observed in the electron micrographs most closely resemble the simulations with a medium strength Yukawa potential of A = 10 000, implying that Coulombic interactions play a role showing a long-range repulsion between the large particles, and to a lesser extent between the large and small ones. The interactions between the small particles are dominated by the Lennard-Jones potential. In effect the large particles distort the organized packing of the small ones.

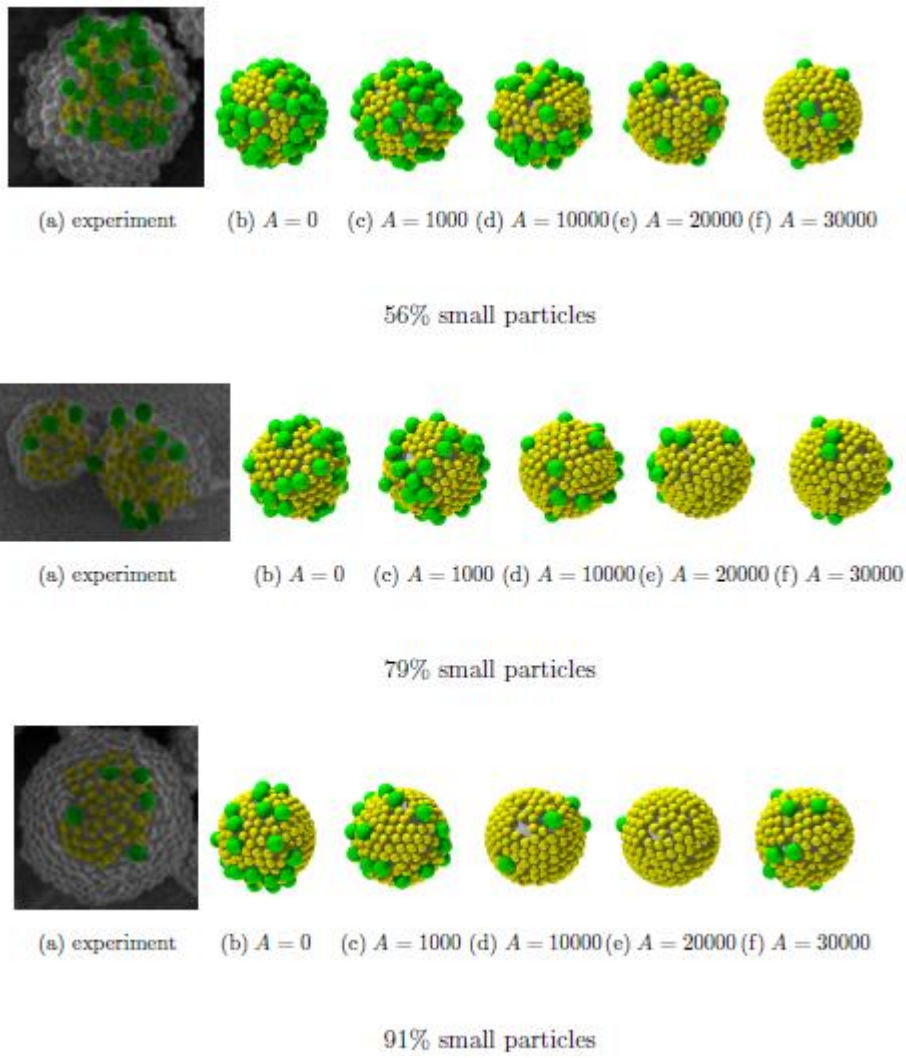

Figure A.1: simulation output, selected snapshots. Different surface charge densities give different packing patterns. The experimental system is well represented by a value of A of about 10 000.

Simulation of the polymersome bilayer swelling using dissipative particle dynamics (DPD).

In order to gain insight into the initial swelling of polymer vesicles, DPD simulations of a model bilayer have been performed

The individual polymer chains consisted of 10 DPD beads, 4 hydrophilic and 6 hydrophobic; as the hydrophobic ratio f=0.6 such chains would be expected to form stable bilayer in solution. A pre-assembled bilayer, consisting of 100 polymer chains

(3000 polymer beads in total), was initially placed in 21000 solvent beads (type S). To mimic the effect of exposure of the bilayer to hydrophobic monomers at regular intervals a number of solvent beads are changed to hydrophobic beads. The density of the system was set to $\rho = 3r_c^{-3}$, where r_c is the non-bonded interaction range, giving a total volume $V = 8000r_c$. The cross-sectional area was set to $A=383.7r_c$, the area for which the initial bilayer had zero surface tension.

	A	B	S	M
A	78	86.7	79.3	86.7
B	86.7	78	100	78
S	79.3	100	78	100
M	86.7	78	100	78

Table A.2 Non-Bonded interaction parameters (in k_BT)

In discussion of the simulation results, quantities are given in reduced units, i.e. lengths in units of r_c , mass in units of bead mass m, energies in k_BT , and time in units $\tau=(mr_c^2/k_BT)^{1/2}$, with other units derived from these.

The system was simulated using dissipative particle dynamics (DPD)[28]. The interaction between beads was given by $F_{ij} = F_{ij}^C + F_{ij}^D + F_{ij}^R$ where the terms on the right hand side are the conservative, dissipative, and random forces respectively. The conservative force has two components; the first is the non-bonded interaction, which has the usual soft, repulsive form $F_{ij} = a_{ij} (1- r_{ij}/r_c)r_{ij}$ where $r_{ij} = |r_i - r_j| = |r_{ij}|$ is the separation between i and j, rij = rij /rij , and r_c is the interaction range (which defines the length unit for the simulations). The interaction parameters (See Table A.2) were taken from the research that reported by V. Ortiz *et.al* [29].

In addition to the non-bonded interaction, neighbouring beads in the polymers are bound together via a harmonic potential $F_{ij} = -k_{bond} r_{ij}$ where $k_{bond}=4k_BT$[30].

The dissipative and random forces are given by $F_{ij} = -\lambda w_{ij}^2 (r_{ij})^2 (r_{ij} .v) r_{ij}$ and $F_{ij} =\sigma w(r_{ij})\xi\delta t^{-1/2} r_{ij}$ where $w(r) = (1-r_{ij} /r_c)$, $\lambda=3k_BT \tau r_c^{-2}$ is the damping parameter, σ is

the random noise strength (related to λ by $\sigma^2 = 2k_BT\lambda$), ξ is a Gaussian random number of zero mean and unit variance and δt is the integration time step[31].

The simulations were performed using LAMMPS simulation package[32]. All simulations were performed at $k_BT=1$ with a time step of $\delta_t=0.02\tau$. The initial simulation configuration consisted of a polymer bilayer in a pure W solvent, which was simulated for 1.5 × 106 time steps (106 time steps for equilibration and 5×105 time steps for data gathering). Successive cycles of hydrophobic particle addition were then performed. For each cycle 500 W beads (chosen at random) were exchanged for M beads. The system was then simulated 1.5 × 106 time steps at each loading.

The changes in the bilayer rigidity may be quantified by studying the undulation motions of the bilayer. Considering the bilayer as a thin sheet with position *u(x,y)[33]*, the two-dimensional Fourier transform of this can be written as:

$$[u_{und}{}^2(q)] = \frac{k_BT}{A} \times \begin{cases} (K_c q^4 + \gamma q^2)^{-1} & q < q_0 \\ (\gamma_p q^2)^{-1} & q > q_0 \end{cases} \qquad \text{(A.10)}$$

where *A* is the (projected) area of the bilayer, k_c is the bending modulus, γ is the surface tension, and γ_p is the tension due to protrusion models. q_0 denotes the wave vector at which the large-scale undulation motions are replaced by small-scale protrusion modes.

The fluctuations in the bilayer thickness may be considered through the peristaltic fluctuations, $u_{per}(x, y) = (w(x, y) - w_0)/2$, where $w(x, y)$ is the bilayer thickness at *x* and *y* and w_0 is the average thickness. The power-spectrum for the peristaltic modes is then:

$$[u_{per}{}^2(q)] = \frac{k_BT}{A} \times \begin{cases} (K_c q^4 + \gamma q^2 + k_e)^{-1} & q < q_0 \\ (\gamma_p q^2)^{-1} & q > q_0 \end{cases} \qquad \text{(A.11)}$$

Where k_d is the peristaltic bending modulus (which may be different to k_c) and k_e is the force constant keeping the bilayer leaflets at their equilibrium separation. At

large-q the data for all N_M falls, as for the undulatory modes, onto a single curve.

The Snapshots in Figure A.2 shows how the bilayer structures changes with increasing number of the hydrophobic molecules (N_m). When N_m=0 particles, the entire system was stable and forms a well defined bilayer with relatively smooth surface. When hydrophobic beads were introduced into the system, these molecules rapidly diffuse into the bilayer. This initially leads to both a swelling in the bilayer and a decreasing in the rigidity. Large undulatory motions can be observed at this stage. Once the density of the hydrophobic molecules $\rho_M > \rho_M^c \approx 0.3125$ (N_m=3000) these large undulatory fluctuations are replaced by a large bud of hydrophilic head groups forms within the bilayer, enclosing a small number of solvent molecules. This is consistent with the experiment results above.

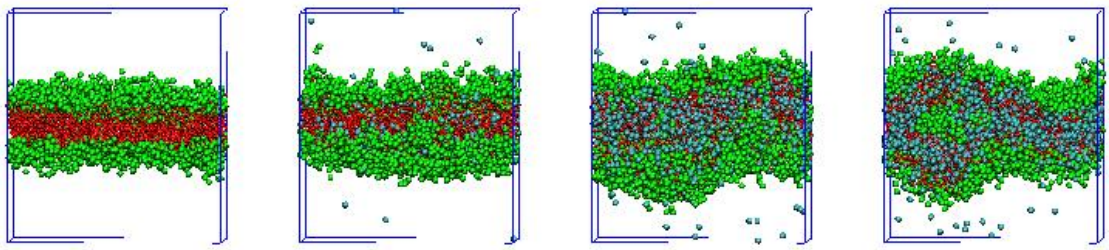

Figure A.2 Simulation snapshots for $\rho_M r_c^3$=0, 0.0675, 0.25, 0.325 (left to right). Head group beads shown in green, tail groups in red and hydrophobic monomers in blue (for clarity solvent beads not shown)

While the simulation result shown above explains the formation of budded vesicles, both swollen and budded vesicles are seen experimentally. The formation of different vesicle types may be because of the budding transition being kinetically driven by the rate of hydrophobic molecules entering the vesicle bilayer or due to the existence of different metastable states. In order to minimise their energy, vesicles generally exist in the zero-surface tension state. By calculating the bilayer surface tension as a function of the area-per-polymer this may be investigated. For the bilayer in pure solvent this is an almost linear function with $\gamma = 0$ for $A_m \approx 0.64\ r_c^2$. For loadings below the budding transition the zero surface tension state moves towards higher A_m ,

indicating that the bilayer is under compression. Above the budding transition γ shows a more complex dependence on A_m , in particular there are a number of values of A_m for which $\gamma = 0$, indicating that the vesicle may exist in a number of metastable states.

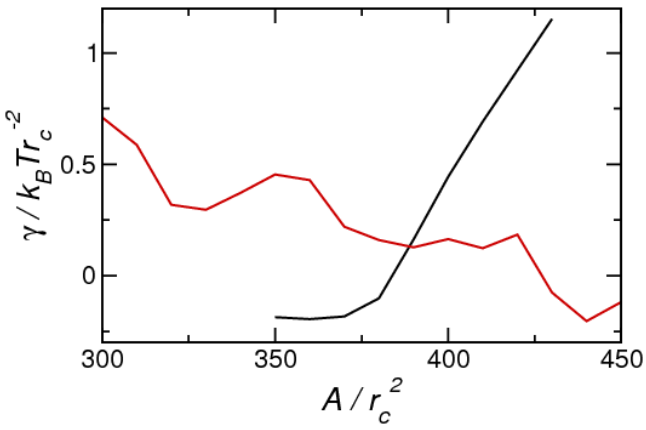

Figure A.3 Plot of Surface tension against bilayer area for ρMrc3=0 (black) and ρMrc3=0.375 (red)